CIVIL ENGINEERING STUDIES
Illinois Center for Transportation Series No. 09-040
UILU-ENG-2009-2011
ISSN: 0197-9191

MECHANISTIC-EMPIRICAL DESIGN CONCEPTS FOR CONTINUOUSLY REINFORCED CONCRETE PAVEMENTS IN ILLINOIS

Prepared By

Matthew Beyer
Jeffery Roesler
University of Illinois at Urbana-Champaign

Research Report ICT-09-040

A report of the findings of

ICT-R57
Evaluation and Implementation of Improved CRCP and JPCP Design Methods for Illinois

Illinois Center for Transportation

April 2009

Technical Report Documentation Page

1. Report No.	2. Government Accession No.	3. Recipient's Catalog No.
FHWA-ICT-09-040		

4. Title and Subtitle

Mechanistic-Empirical Design Concepts for Continuously Reinforced Concrete Pavements in Illinois

5. Report Date
April 2009

6. Performing Organization Code

7. Author(s)
Matthew Beyer and Jeffery Roesler

8. Performing Organization Report N o.
ICT-09-040
UILU-ENG-2009-2011

9. Performing Organization Name and Address
Illinois Center for Transportation
University of Illinois at Urbana-Champaign
Department of Civil and Environmental Engineering
205 North Matthews Ave.
Urbana, IL 61801

10. Work Unit (TRAIS)

11. Contract or Grant No.
ICT-R57

13. Type of Report and Period Covered
Final Report
July 2005 to December 2008

12. Sponsoring Agency Name and Address
Illinois Department of Transportation
Bureau of Materials and Physical Research
126 East Ash Street
Springfield, IL 62704-4766

14. Sponsoring Agency Code

15. Supplementary Notes

16. Abstract

The Illinois Department of Transportation (IDOT) currently has an existing jointed plain concrete pavement (JPCP) design based on mechanistic-empirical (M-E) principles. However, their continuously reinforced concrete pavement (CRCP) design procedure is empirical and based on a modified AASHTO nomograph for jointed reinforced concrete pavement. The objective of this study was to develop and implement an M-E design procedure that IDOT could use for routine CRCP design. The proposed procedure is based on mechanistic-empirical design principles taken largely from the models presented in NCHRP 1-37A and on work completed by Dr. Dan Zollinger of Texas A&M University. The equations for calculating the mean crack spacing and the number of punchouts per mile at the end of the design life for a given traffic volume, pavement layer and CRC slab geometry, shoulder type, and layer material properties have been implemented in a user-friendly spreadsheet. Several new developments in the proposed design process are fatigue damage accumulations at the critical top and bottom location in the CRCP slab, equations for calculating the equivalent damage ratio for several shoulder types and crack stiffness values, application of a strength reduction factor to the concrete stress ratio calculated at the surface of the CRCP, and a new logistic-type punchout prediction model. Due to the numerous measured and assumed input variables in this CRCP design framework, the mechanistic analysis was calibrated against CRCP field performance data from Illinois and CRCP accelerated pavement test data completed at the University of Illinois.

17. Key Words	18. Distribution Statement
Continuously Reinforced Concrete Pavement, CRCP, Design, Steel, slab thickness	No restrictions. This document is available to the public through the National Technical Information Service, Springfield, Virginia 22161.

19. Security Classif. (of this report)	20. Security Classif. (of this page)	21. No. of Pages	22. Price
Unclassified	Unclassified	83	

ACKNOWLEDGEMENTS

This publication is based on the CRCP results of ICT-R57, **Evaluation and Implementation of Improved CRCP and JPCP Design Methods for Illinois**. ICT-R57 was conducted in cooperation with the Illinois Center for Transportation; the Illinois Department of Transportation; and the U.S. Department of Transportation, Federal Highway Administration.

Members of the Technical Review Panel are the following:

Amy Schutzbach, IDOT (TRP chair)
David Lippert, IDOT
Paul Niedernhofer, IDOT
LaDonna Rowden, IDOT
Hal Wakefield, FHWA
Charles Wienrank, IDOT
Mark Gawedzinski, IDOT

The authors would also like to thank Dr. Dan Zollinger for sharing his CRCP design program and fruitful discussions. His original design program was the basis for the proposed CRCP design concepts presented in this report along with published information from the NCHRP 1-37A project.

DISCLAIMER

EXECUTIVE SUMMARY

The Illinois Department of Transportation (IDOT) currently has an existing jointed plain concrete pavement (JPCP) design based on mechanistic-empirical (M-E) principles. However, their continuously reinforced concrete pavement (CRCP) design procedure is empirical and based on a modified AASHTO nomograph for jointed reinforced concrete pavement. The objective of this study was to develop and implement an M-E design procedure that IDOT could use for routine CRCP design. The proposed procedure is based on mechanistic-empirical design principles taken largely from the models presented in NCHRP 1-37A and on work completed by Dr. Dan Zollinger of Texas A&M University. The equations for calculating the mean crack spacing and the number of punchouts per mile at the end of the design life for a given traffic volume, pavement layer and CRC slab geometry, shoulder type, and layer material properties have been implemented in a user-friendly spreadsheet. Several new developments in the proposed design process are fatigue damage accumulations at the critical top and bottom location in the CRCP slab, equations for calculating the equivalent damage ratio for several shoulder types and crack stiffness values, application of a strength reduction factor to the concrete stress ratio calculated at the surface of the CRCP, and a new logistic-type punchout prediction model. Due to the numerous measured and assumed input variables in this CRCP design framework, the mechanistic analysis was calibrated against CRCP field performance data from Illinois and CRCP accelerated pavement test data completed at the University of Illinois.

CONTENTS

CHAPTER 1. INTRODUCTION

A continuously reinforced concrete pavement (CRCP) is constructed without man-made transverse contraction or expansion joints and contains spliced longitudinal reinforcing steel bars. This type of pavement is characterized by the development of transverse cracks spaced roughly 2 to 6 ft apart. The steel reinforcement is designed to promote regularly spaced cracks and to hold these transverse cracks tightly together. Illinois has extensive experience with CRCP, as this type of pavement has been widely used in the state since the mid-1950s (Gharaibeh et al., 1999).

Punchouts have been the most serious structural performance problems for CRCP in Illinois (Zollinger and Barenberg, 1990). A punchout is an isolated piece of concrete that settles into a depression or void at the edge of the concrete slab as shown in Figure 1. This type of distress is a structural failure and develops at a location bounded by two transverse cracks, a longitudinal fatigue crack, and the edge of the pavement. They can also occur at the intersection of Y cracks. Erosion of the subbase and subsequent loss of support under the slab has been identified as a primary cause of punchout formation (Zollinger and Barenberg, 1990).

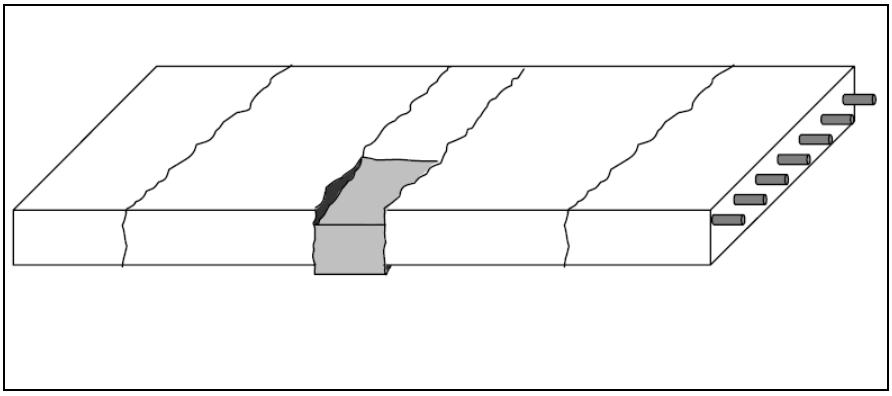

Figure 1. Punchout in CRCP between two closely spaced transverse cracks (from Kohler 2005).

1.1 CRCP DESIGN PROCEDURES

A number of CRCP design procedures have been developed over the years to determine thickness and/or longitudinal steel requirements. The Portland Cement Association method (PCA, 1984) determined from a finite element study with JSLAB that CRCP bending stresses were smaller with short crack spacing, but had higher corner deflections. Based on these analyses, the PCA design method recommended using the same thickness for CRCP as calculated from their jointed plain concrete pavement (JPCP) design method. The 1993 AASHTO design method provides for CRCP thickness and longitudinal steel design. The AASHTO CRCP thickness requirement is based on the AASHTO thickness design equations for jointed concrete pavements, with the use of slightly different load transfer coefficients. The AASHTO (1993) design method is based on empirical equations derived from testing of doweled-jointed plain and reinforced concrete pavements sections at the AASHO Road Test. The AASHTO procedure for CRCP also determines the longitudinal reinforcing steel content to limit crack spacing, crack width, and allowable steel stress (Huang, 2004). Neither the PCA nor the AASHTO design methods design the slab thickness to resist the development of punchouts in CRCP.

The Illinois Department of Transportation (IDOT) currently has an existing JPCP design based on mechanistic-empirical (M-E) principles (Zollinger and Barenberg, 1989). IDOT does not have an M-E based CRCP design procedure. The current CRCP design procedure used by IDOT is based on a modified AASHTO nomograph for a jointed reinforced concrete pavement (JRCP). For CRCP design, the required thickness is taken as 80% of the required thickness for a JRCP with the same expected traffic volume and subgrade support (IDOT, 2002).

The most recent proposed design procedure for CRCP is the mechanistic-empirical design procedure contained within the Mechanistic-Empirical Pavement Design Guide (M-E PDG) that was developed by Applied Research Associates, Inc. (2003b) under NCHRP 1-37A. The M-E PDG procedure for CRCP calculates the mean crack spacing and the required slab thickness based on the expected traffic, pavement layer geometry, layer properties, and local climate conditions. The primary structural failure criterion is the number of punchouts per mile. The CRCP models contained in the M-E PDG were calibrated using national CRCP performance data (ARA, 2003a).

1.2 IMPROVED CRCP DESIGN PROCEDURE IN ILLINOIS

The objective of this study was to develop and implement an M-E design procedure that IDOT can use for routine CRCP design. When considering improvements to the CRCP design procedure in Illinois, two options were considered. The first was to use the M-E PDG (NCHRP, 2007) and calibrate its performance prediction models against a range of Illinois design inputs. The second was to develop a new mechanistic-empirical design procedure for Illinois based on the M-E PDG performance prediction models. The second option was selected because it allows for the modification or exclusion of specific models and inputs now and in the future. This report proposes CRCP design concepts for Illinois based on mechanistic-empirical design principles taken largely from the models contained in the M-E PDG.

CHAPTER 2. CRCP DESIGN CONCEPTS

This chapter lists equations and concepts used in the proposed CRCP design procedure relating to climate, concrete properties, traffic, transverse crack spacing, crack width, load transfer, tensile stresses, fatigue damage, and punchout prediction. The majority of these parameters change continuously during the design life, and a seasonal approach is used to describe this time-dependent behavior.

2.1 CLIMATE

The temperature differential between the top and bottom of a concrete slab (ΔT) is critical to the calculation of curling stresses and subsequent pavement damage. Ambient (air) temperatures and the temperature at the depth of reinforcing steel are also used in the calculation of mean crack spacing and average crack width. The Enhanced Integrated Climatic Model (EICM) version 3.4 (Larson and Dempsey, 2008) was run to obtain slab temperature differential frequencies, as well as the temperature at the depth of steel for Illinois.

The model was run for four concrete thicknesses (8, 10, 12, and 14 in.) located in Champaign, Illinois. This location was chosen because past work with the EICM has found that Champaign provides a representative climate for Illinois (Roesler et al., 2008). The concrete pavements were assumed to have a 4-in. asphalt concrete base and a concrete short-wave absorptivity value of 0.65. This value can vary depending on the color of the concrete and may be as high as 0.85. Temperature differentials through the concrete and at the depth of steel temperatures were obtained for every hour over a seven-year period (December 1997 to November 2003) for each of the four concrete thicknesses. The climatic data were also used to determine the minimum and average seasonal ambient temperatures that were needed for the crack spacing calculation. The climate and temperature data were organized on a seasonal basis as described in Table 1.

Table 1. Months of the Year by Season

Season	Months
Spring	March, April, May
Summer	June, July, August
Fall	September, October, November
Winter	December, January, February

2.1.1 Temperature Differential Frequency Distributions

For the purposes of this design procedure, a temperature differential (ΔT) is defined as the temperature at the top of the concrete slab minus the temperature at the bottom of the slab. Using this sign convention, a positive temperature differential means the temperature at the top of the concrete slab is greater than the temperature at the bottom of the slab. The temperature differentials obtained from the EICM were separated into bins of 2.5°F. Figure 2 shows a sample yearly frequency distribution.

Seasonal frequency distributions were produced for each of the four concrete thicknesses for use in calculating temperature curling stress (described in Section 2.7.2). From these distributions, only those temperature differentials falling between -20 and 20°F were considered for the calculation of temperature curling stress. This was done to avoid using extreme temperature events (i.e., events that occur one time), since they may cause extremely high stresses that have an extremely low probability of occurring simultaneously

with critical loads. Greater than 99% of all seasonal temperature differentials occurred within this range. The Champaign seasonal frequency distributions for the four concrete thicknesses can be found in Appendix A.

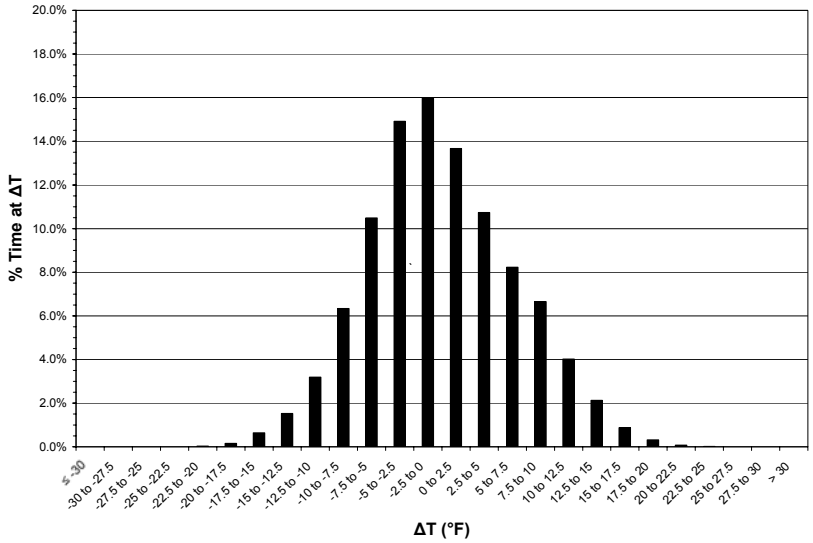

Figure 2. Yearly temperature differential frequency distribution for concrete pavement with 10-in.slab thickness in Champaign, Illinois.

2.1.2 Ambient Temperature

The ambient temperature is a function of time of year and geographic location. The average and minimum seasonal ambient temperatures for Champaign are shown in Table 3. These values were calculated using average and minimum monthly ambient temperature data from the seven-year period examined with the EICM.

2.1.3 Temperature at the Depth of Steel

Depth to steel (ζ) is defined as the depth from the surface of the concrete slab to the top of the reinforcing steel. Current IDOT standards put the depth of the longitudinal reinforcing steel at 3 in. when the pavement thickness is less than or equal to 8 in., and at 3.5 in. when the pavement thickness is greater than 8 in. The new proposed depth to steel as a function of slab thickness is presented in Table 2, which is approximately one-third of the concrete slab thickness. For the purposes of this climatic analysis, the steel depth was taken as 4 in., regardless of design life. The overall thickness of the concrete slab had a negligible effect on the temperature at the depth of steel. The average seasonal temperatures at the steel depth for Champaign are shown in Table 3. These values were calculated using hourly temperature data from the seven-year period examined with the EICM.

Table 2. Required Depth of Steel from the Concrete Surface

Slab thickness (in.)	Depth of steel (in.)
8	3.5
10	3.5
12	4.0
14	4.5

Table 3. Seasonal Climatic Data for Champaign, Illinois based on EICM Results

Season	Average Seasonal Ambient Temperature (°F)	Minimum Seasonal Ambient Temperature (°F)	Average Seasonal Temperature at the Depth of Steel (ζ = 4") (°F)
Spring	52.4	25.3	52.5
Summer	72.6	51.0	71.8
Fall	53.8	26.8	54.6
Winter	30.1	1.0	30.7

2.2 CONCRETE PROPERTIES

The following time-dependent concrete properties are needed for the calculation of crack spacing and in the fatigue damage calculations.

2.2.1 Compressive Strength

The compressive strength of the concrete at 28 days (f'_{c28}) is used in the calculation of the peak bond stress. This parameter is a user-defined input.

2.2.2 Tensile Strength

The concrete tensile strength or indirect tensile strength at 28 days (f'_{t28}) is used in the mean crack spacing calculation and is given as:

$$f'_{t28} = 0.7 * MOR_{28} \tag{1}$$

where MOR_{28} is the concrete modulus of rupture at 28 days (psi).

2.2.3 Modulus of Rupture

The concrete modulus of rupture (MOR) using the third-point loading configuration is used in the calculation of the concrete tensile strength and elastic modulus. The modulus of rupture for seasonal increment *i* (MOR_i) is calculated as follows (ARA, 2004a):

$$MOR_i = STRRATIO * MOR_{28} \tag{2}$$

$$STRRATIO = a_1 + a_2 \log(A/0.0767) - a_3[\log(A/0.0767)]^2 \tag{3}$$

where,

$STRRATIO$ = the ratio of MOR at a given age to MOR at 28 days;
A = the age of the concrete (years); and
a_1, a_2, a_3 are coefficients (1.0, 0.12, 0.01566, respectively).

The modulus of rupture at 90 days (MOR_{90}) is a user-defined input for the software and is approximately equal to the center-point loading configuration MOR at 14 days, which is IDOT's current testing age and flexural strength standard. The modulus of rupture at 28 days (MOR_{28}) can then be estimated as:

$$MOR_{28} = 0.9 * MOR_{90} . \quad (4)$$

2.2.4 Elastic Modulus

The concrete elastic modulus (E_{PCC}) is used in the calculation of mean crack spacing, average crack width, and curling and loading stresses. The elastic modulus at 28 days (E_{PCC28}) is a user-defined input, while the elastic modulus for seasonal increment *i* ($E_{PCC,i}$) is calculated as follows (ARA, 2004a):

$$E_{PCC,i} = \frac{MOR_i}{MOR_{28}} E_{PCC28} . \quad (5)$$

The concrete elastic modulus can be estimated from the following ACI 318 equation:

$$\mathrm{E_{PCC,i}} = 57{,}000\sqrt{\mathrm{f'_{c,i}}} . \quad (6)$$

2.3 TRAFFIC

The level of traffic is quantified as the total number of 18-kip equivalent single-axle loads (ESALs) in the design lane and has a significant effect on the required slab thickness. The cumulative number of ESALs in the design lane through seasonal increment *i* ($ESAL_i$) is calculated as:

$$ESAL_i = \frac{GF_i}{GF_m}\left(ESAL_m\right)\left(TM\right) \quad (7)$$

where,

GF_i = the cumulative traffic growth factor for seasonal increment *i*;
GF_m = the cumulative traffic growth factor at the end of the design life;
$ESAL_m$ = the total number of 18-kip equivalent single-axle loads (ESALs) in the design lane during the design life of the pavement ; and
TM = the traffic multiplier for reliability.

Load spectra was not used in this CRCP design procedure, since a traffic analysis revealed similar required slab thickness whether ESAL or load spectra was used (Bordelon et al., 2009).

2.3.1 Cumulative Traffic Growth Factor

The cumulative traffic growth factor is used to account for annual increases in the amount of expected traffic. The cumulative traffic growth factor for seasonal increment *i* (GF_i) is calculated as follows (Huang, 2004):

$$GF_i = \left[(1+r)^A - 1\right]\left(\frac{1}{r}\right) \tag{8}$$

where r is the annual growth factor as a fraction and A is the age of the concrete (in years). When the annual growth factor is zero, the cumulative number of ESALs is assumed to increase linearly over the design life.

2.4 CRACK SPACING

The mean crack spacing is the average distance between the transverse cracks. This value is used in the calculations of crack width and influences the magnitude of bending stresses in the slab. The mean crack spacing for seasonal increment *i* ($\overline{L_i}$) is calculated as follows (ARA, 2003b):

$$\overline{L_i} = \frac{f'_{t28} - C_i \sigma_{0,i}\left(1 - \frac{2\zeta}{h_{PCC}}\right)}{\frac{f}{2} + \frac{U_m P_b}{c_{1,i} d_b}} \tag{9}$$

where,

f'_{t28} = the concrete tensile strength at 28 days (psi);
C_i = the Bradbury coefficient for seasonal increment *i*;
$\sigma_{0,i}$ = Westergaard's nominal stress factor for seasonal increment *i* (psi);
ζ = the depth to steel (in.);
h_{PCC} = the concrete slab thickness (in.);
f = the base friction coefficient;
U_m = the peak bond stress (psi);
P_b = the percent steel as a fraction;
$c_{1,i}$ = the first bond stress coefficient for seasonal increment *i*; and
d_b = the reinforcing steel bar diameter (in.).

These variables are discussed later in greater detail.

2.4.1 Bradbury Coefficient

The Bradbury coefficient is used to correct the curling stress for finite slab sizes. The Bradbury coefficient at the center of the slab or mid-slab edge for seasonal increment *i* (C_i) is calculated as follows (Westergaard, 1927; Bradbury, 1938):

$$C_i = 1 - \frac{2\cos\lambda_i \cosh\lambda_i \left(\tan\lambda_i + \tanh\lambda_i\right)}{\sin 2\lambda_i + \sinh 2\lambda_i} \tag{10}$$

$$\lambda_i = \frac{L}{\ell_i \sqrt{8}} \tag{11}$$

where L is the length of the slab (in.) and ℓ_i is the radius of relative stiffness for seasonal increment *i* (in.). In the M-E PDG, the length of the slab is assumed to be calibrated to 144 in. for the crack spacing equation.

2.4.1.1 Radius of Relative Stiffness (curling)

The curling radius of relative stiffness for seasonal increment *i* (ℓ_i) is calculated as:

$$\ell_i = \left[\frac{E_{PCC,i} {h_{PCC}}^3}{12(1 - {\mu_{PCC}}^2) k_s} \right]^{1/4} \tag{12}$$

where,

$E_{PCC,i}$ = the concrete modulus of elasticity for seasonal increment *i* (psi),
h_{PCC} = the concrete slab thickness (in.),
μ_{PCC} = the concrete Poisson's ratio, and
k_s = the modulus of subgrade reaction for curling (psi/in.).

The *k*-value of the soil is kept constant for all curling analyses. Because this analysis considers only the unbonded base condition, the base thickness and modulus of elasticity are ignored in the calculation of the radius of relative stiffness.

2.4.2 Westergaard's Nominal Stress Factor

Westergaard's nominal stress factor for seasonal increment *i* ($\sigma_{0,i}$) is calculated as follows (ARA , 2003b):

$$\sigma_{0,i} = \frac{E_{PCC,i} \varepsilon_{tot-\Delta,i}}{2(1 - \mu_{PCC})} \tag{13}$$

where,

$E_{PCC,i}$ = the concrete modulus of elasticity for seasonal increment *i* (psi);
$\varepsilon_{tot-\Delta,i}$ = the equivalent total strain difference between the pavement surface and slab bottom for seasonal increment *i*; and
μ_{PCC} = the concrete Poisson's ratio.

2.4.2.1 Equivalent Total Strain

The equivalent total strain difference between the pavement surface and slab bottom for seasonal increment *i* ($\varepsilon_{tot-\Delta,i}$) is calculated as follows (ARA, 2003b):

$$\varepsilon_{tot-\Delta,i} = \alpha_{PCC}\Delta t_{eqv,i} + \varepsilon_{\infty}\Delta\left(1 - rh_{PCC}{}^{3}\right)_{eqv} \quad (14)$$

where,

α_{PCC} = the concrete coefficient of thermal expansion (1/°F);
$\Delta t_{eqv,i}$ = the equivalent temperature for seasonal increment *i* (°F);
ε_{∞} = the concrete ultimate shrinkage (strains); and
$\Delta\left(1 - rh_{PCC}{}^{3}\right)_{eqv}$ = the relative humidity difference between the pavement surface and bottom.

2.4.2.2 Equivalent Temperature

The equivalent temperature for seasonal increment *i* ($\Delta t_{eqv,i}$) is calculated as follows (ARA, 2003b):

$$\Delta t_{eqv,i} = \frac{R_{0,i}}{2CF}\left(1 - e^{-\frac{h_{PCC}}{12}\sqrt{\frac{2\pi}{(\gamma_{PCC})^2}}}\right) \quad (15)$$

$$CF = 1.000 + 0.1116h_{PCC}{}^{3/2} - 0.565h_{PCC} + 0.685h_{PCC}{}^{1/2} \quad (16)$$

where,

$R_{0,i}$ = the effective range in temperature for seasonal increment *i* (see Table 4);
h_{PCC} = the concrete slab thickness (in.); and
γ_{PCC} = the concrete thermal diffusivity (ft^2/day).

Table 4. Effective Temperature Ranges (ARA, 2003b)

Minimum Seasonal Ambient Temperature (°F)	Effective Range in Temperature (R_0)
< 40	21.5
40 to 60	23.4
60 to 80	25.7
> 80	30.1

2.4.2.3 Relative Humidity Difference between the Pavement Surface and Bottom

The relative humidity difference between the pavement surface and bottom $\left(\Delta(1-rh_{PCC}{}^{3})_{eqv}\right)$ is calculated as follows (ARA, 2003b):

$$\Delta\left(1-rh_{PCC}{}^{3}\right)_{eqv} = 0.2*\left(0.0028h_{PCC}{}^{2} - 0.107h_{PCC} + 1.4292\right) \tag{17}$$

where h_{PCC} is the concrete slab thickness (in.). The use of this equation assumes a wet, freezing climatic zone with a minimum ambient humidity range of 50 to 95%.

2.4.3 Peak Bond Stress

The peak bond stress (U_m) is calculated as follows (ARA, 2003b):

$$U_m = 0.0020k_1 \tag{18}$$

$$k_1 = 0.1172 * f'_{c28} * 1000 \tag{19}$$

where k_1 is the bond slip coefficient and f'_{c28} is the concrete compressive strength at 28 days (psi).

2.4.4 First Bond Stress Coefficient

The first bond stress coefficient for seasonal increment *i* ($c_{1,i}$) is calculated iteratively as follows (ARA , 2003b):

$$c_{1,i} = \begin{cases} IF & \overline{L_i} - L_{seed} < 0.01 \quad , \quad c_{1,i} = c_{1seed} \\ ELSE & c_{1seed} = 0.577 - 9.499\times10^{-9}\dfrac{\ln\varepsilon_{tot-\zeta\max}}{\left(\varepsilon_{tot-\zeta\max}\right)^2} + 0.00502L_{seed}\left(\ln L_{seed}\right) \end{cases} \tag{20}$$

where L_{seed} is a seed crack spacing value (in.) and $\varepsilon_{tot-\zeta\max}$ is the total maximum strain at the depth of the steel (strains).

2.4.4.1 Total Maximum Strain at the Depth of Steel

The total maximum strain at the depth of the steel ($\varepsilon_{tot-\zeta\max}$) is calculated as follows (ARA, 2003b):

$$\varepsilon_{tot-\zeta\max} = \Delta T_{\zeta\max}\alpha_{PCC} + \varepsilon_{shr} \tag{21}$$

where,

$\Delta T_{\zeta\max}$ = the maximum concrete temperature difference from the concrete set temperature at the steel depth (°F);
α_{PCC} = the concrete coefficient of thermal expansion (1/°F); and
ε_{shr} = the unrestrained concrete drying shrinkage at the steel depth (strains).

2.4.4.2 Maximum Concrete Temperature Difference

The maximum concrete temperature difference from the concrete set temperature at the steel depth ($\Delta T_{\zeta\max}$) is calculated as follows (ARA, 2003b):

$$\Delta T_{\zeta\max} = \begin{cases} IF & T_{set} > T_{steel,\min} \quad , \quad T_{set} - T_{steel,\min} \\ ELSE & 0 \end{cases} \tag{22}$$

where T_{set} is the concrete set temperature at the depth of steel (°F) and $T_{steel,\min}$ is the minimum—or lowest—average seasonal temperature at the depth of the steel (°F). For Champaign, Illinois, the minimum average seasonal temperature at the depth of steel occurs during the winter season (from Table 3, $T_{steel,\min}$ = 30.7°F).

2.4.4.3 Concrete Set Temperature at the Depth of Steel

The concrete set temperature at the depth of steel (T_{set}) is the temperature at which the concrete layer exhibits zero thermal stress. This value is calculated as follows (ARA, 2004a):

$$T_{set} = CC * 0.59328 * H * 0.5 * 1000 * \frac{1.8}{1.1 * 2400} + T_{air} \tag{23}$$

$$H = -0.0787 + 0.007 * T_{air} - 0.00003 * T_{air}^{\ 2} \tag{24}$$

where,

CC = the cement content of the concrete mixture (lb/yd^3);
H = the heat of hydration (KJ/g); and
T_{air} = the average seasonal ambient temperature for the season of construction (°F).

The allowable temperature range for this equation is 60 to 120°F.

2.4.4.4 Unrestrained Concrete Drying Shrinkage at the Depth of Steel

The unrestrained concrete drying shrinkage at the depth of steel (ε_{shr}) is calculated as follows (ARA, 2003b):

$$\varepsilon_{shr} = \varepsilon_{\infty}\left[1-\left(\frac{rh_{PCC,\zeta}}{100}\right)^3\right] \tag{25}$$

where ε_{∞} is the concrete ultimate shrinkage (strains) and $rh_{PCC,\zeta}$ is the relative humidity in the concrete at the depth of steel (%).

2.5 CRACK WIDTH

Crack width is a function of shrinkage, thermal contraction, and restraint from the reinforcing steel and subbase friction, and is used in calculations of crack shear capacity. The average crack width at the depth of steel for seasonal increment *i* (cw_i) is calculated as follows (ARA, 2003b):

$$cw_i = \max\left(\overline{L_i}\left(\varepsilon_{shr} + \alpha_{PCC}\Delta T_{\zeta,i} - \frac{c_{2,i} f_{\sigma,i}}{E_{PCC,i}}\right)\cdot 1000\cdot \overline{C} \quad , \quad 0.001\right) \tag{26}$$

where,

$\overline{L_i}$ = the mean crack spacing for seasonal increment *i* (in.);
ε_{shr} = the unrestrained concrete drying shrinkage at the steel depth (strains);
α_{PCC} = the concrete coefficient of thermal expansion (1/°F);
$\Delta T_{\zeta,i}$ = the average concrete temperature difference from the concrete set temperature at the steel depth for seasonal increment *i* (°F);
$c_{2,i}$ = the second bond stress coefficient for seasonal increment *i*;
$f_{\sigma,i}$ = the maximum longitudinal tensile stress in the concrete at the depth of steel for seasonal increment *i* (psi);
$E_{PCC,i}$ = the concrete modulus of elasticity for seasonal increment *i* (psi); and
$\overline{C}$ = the crack width calibration constant (1.0).

This equation gives the average crack width in terms of mils.

2.5.1 Average Concrete Temperature Difference

The average concrete temperature difference from the concrete set temperature at the steel depth for seasonal increment *i* ($\Delta T_{\zeta,i}$) is calculated as follows (ARA, 2003b):

$$\Delta T_{\zeta,i} = \begin{cases} IF & T_{set} > T_{steel,i} \quad , \quad T_{set} - T_{steel,i} \\ ELSE & 0 \end{cases} \tag{27}$$

where T_{set} is the concrete set temperature at the depth of steel (°F) and $T_{steel,i}$ is the average seasonal temperature at the depth of the steel for seasonal increment *i* (°F).

2.5.2 Second Bond Slip Coefficient

The second bond slip coefficient for seasonal increment *i* ($c_{2,i}$) is calculated as follows (ARA, 2003b):

$$c_{2,i} = a_i + \frac{b_i}{k_1} + \frac{c_i}{\overline{L_i}^2} \tag{28}$$

$$a_i = 0.7606 + 1772.5\left(\varepsilon_{tot-\zeta,i}\right) - 2\times10^6\left(\varepsilon_{tot-\zeta,i}\right)^2 \tag{29}$$

$$b_i = 9\times10^8\left(\varepsilon_{tot-\zeta,i}\right) + 149486 \tag{30}$$

$$c_i = 3\times10^9\left(\varepsilon_{tot-\zeta,i}\right)^2 - 5\times10^6\left(\varepsilon_{tot-\zeta,i}\right) + 2020.4 \tag{31}$$

where,

k_1 = the bond slip coefficient;
$\overline{L_i}$ = the mean crack spacing for each seasonal increment *i* (in.); and
$\varepsilon_{tot-\zeta,i}$ = the total strain at the depth of the steel.

2.5.2.1 Total Strain at the Depth of Steel

The total strain at the depth of the steel ($\varepsilon_{tot-\zeta,i}$) is calculated as follows (ARA, 2003b):

$$\varepsilon_{tot-\zeta,i} = \Delta T_{\zeta,i}\alpha_{PCC} + \varepsilon_{shr} \tag{32}$$

where,

$\Delta T_{\zeta,i}$ = the average concrete temperature difference from the concrete set temperature at the steel depth for seasonal increment *i* (°F);
α_{PCC} = the concrete coefficient of thermal expansion (1/°F); and
ε_{shr} = the unrestrained concrete drying shrinkage at the steel depth (strains).

2.5.3 Maximum Longitudinal Tensile Stress in the Concrete at the Depth of Steel

The maximum longitudinal tensile stress in the concrete at the depth of steel for seasonal increment *i* ($f_{\sigma,i}$) is calculated as follows (ARA 2003b):

$$f_{\sigma,i} = \frac{\overline{L}_i U_m P_b}{c_{1,i} d_b} + \sigma_{env,i} + \frac{\overline{L}_i}{2} f \tag{33}$$

where,

$\overline{L}_i$ = the mean crack spacing for each seasonal increment *i* (in.);
U_m = the peak bond stress (psi);
P_b = the percent steel as a fraction;
$c_{1,i}$ = the second bond slip coefficient for seasonal increment *i*;
d_b = the reinforcing steel bar diameter (in.);
$\sigma_{env,i}$ = the environmental tensile stress in the concrete for seasonal increment *i* (psi); and
f = the base friction coefficient, which generally varies between 0.5 (unstabilized) to 10 (stabilized materials) and is shown in Table 8.

2.5.3.1 Environmental Tensile Stress in the Concrete

The environmental tensile stress in the concrete for seasonal increment *i* ($\sigma_{env,i}$) is calculated as follows (ARA, 2003b):

$$\sigma_{env,i} = C_i \sigma_{0,i} \left(1 - \frac{2\zeta}{h_{PCC}} \right) \tag{34}$$

where,

C_i is the Bradbury coefficient for seasonal increment *i*;
$\sigma_{0,i}$ is Westergaard's nominal stress factor for seasonal increment *i* (psi);
ζ is the depth to steel (in.); and
h_{PCC} is the concrete slab thickness (in.).

2.6 LOAD TRANSFER

The amount of load transfer at the transverse crack plays an important role the structural response of the slab and is a function of aggregate interlock, steel reinforcement, and base support. The transverse crack load transfer efficiency for seasonal increment *i* ($LTE_{c,i}$) is calculated as follows (ARA, 2007):

$$LTE_{c,i} = 100 * \left(1 - \left(1 - \frac{1}{1 + \log^{-1}\left[(0.214 - 0.183\frac{a}{\ell_i} - \log(J_{c,i}) - r_d)/1.18 \right]} \right) \left(1 - \frac{LTE_{base}}{100} \right) \right) \quad (35)$$

$$r_d = 2.5P_b - 1.25 \quad (36)$$

where,

a = the radius for a loaded area (6 in.);
ℓ_i = the loading radius of relative stiffness for seasonal increment *i* (in.);
$J_{c,i}$ = the transverse crack stiffness for seasonal increment *i* $\left((AGG/k\ell)_c\right)$;
r_d = the residual factor to account for residual load transfer provided by the steel reinforcement;
P_b = the percent steel as a fraction; and
LTE_{base} = the load transfer efficiency contributed by the base layer (%).

2.6.1 Radius of Relative Stiffness (loading)

The radius of relative stiffness for seasonal increment *i* (ℓ_i) based on a soil stiffness value for loading is calculated as follows:

$$\ell_i = \left[\frac{E_{PCC,i} h_{PCC}^{\ 3}}{12(1 - \mu_{PCC}^{\ 2})k_d} \right]^{1/4} \quad (37)$$

where,

$E_{PCC,i}$ = the concrete modulus of elasticity for seasonal increment *i* (psi);
h_{PCC} = the concrete slab thickness (in.);
μ_{PCC} = the concrete Poisson's ratio; and
k_d = the modulus of subgrade reaction for loading (psi/in.).

2.6.2 Transverse Crack Stiffness

Stiffness is a means of describing aggregate interlock at a crack or joint. The transverse crack stiffness of seasonal increment *i* ($J_{c,i}$) is calculated as follows (ARA, 2003b):

$$Log\left(J_{c,i}\right) = ae^{-e^{-\left(\frac{J_s-b}{c}\right)}} + de^{-e^{-\left(\frac{s_{0,i}-f}{g}\right)}} + he^{-e^{-\left(\frac{J_s-b}{c}\right)}} \cdot e^{-e^{-\left(\frac{s_{0,i}-f}{g}\right)}} \quad (38)$$

where,

J_s = the stiffness of the shoulder/lane joint $\left((AGG/k\ell)_s\right)$;

$s_{0,i}$ is the crack shear capacity for seasonal increment *I*; and

a, b, c, d, f, g, h are coefficients (-2.20, -11.26, 7.56, -28.85, 0.35, 0.38, 49.80, respectively).

2.6.2.1 Stiffness of the Shoulder/Lane Joint

The stiffness of the shoulder/lane joint (J_s) is estimated as follows (Crovetti, 1994):

$$J_s = \left[\frac{\frac{1}{LTE_s} - 0.01}{0.012}\right]^{-\frac{1}{0.849}} \quad (39)$$

where LTE_s is the shoulder load transfer efficiency (%).

2.6.2.2 Crack Shear Capacity

Crack shear capacity is a measure of the ability of the crack to transfer shear loads across the transverse crack. The crack shear capacity for seasonal increment *i* ($s_{0,i}$) is calculated as follows (ARA, 2003b):

$$s_{0,i} = 0.05 \cdot h_{PCC} \cdot e^{-0.032 cw_i} \quad (40)$$

where h_{PCC} is the concrete slab thickness (in.) and cw_i is the average crack width at the depth of steel for seasonal increment *i* (mils).

2.6.2.2.1 Shear capacity loss

The design procedure implemented in the M-E PDG includes a routine for calculating a loss in shear capacity due to aggregate wear-out (ARA, 2003b). This series of calculations is an attempt to account for deterioration in transverse crack stiffness and subsequent loss in transverse crack LTE over the life of the pavement. However, there was limited evidence that load transfer at the transverse crack progressively and systematically decreases with time; or at least, in a manner that can be easily modeled.

Falling-weight deflectometer (FWD) deflection data from the Long-Term Pavement Performance (LTPP) database were analyzed by Khazanovich and Gotlif (2003) to determine deflection LTE of in-service pavements and the variability of these values with time. Their evaluation of nearly 40 years of LTE data found no significant decrease in

transverse crack LTE with time. For the data set examined, more than 98% of transverse cracks had LTE greater than 80%, with more than 60% of transverse cracks having LTE greater than 90%. These results are an indication that LTE remains high over time. Kohler (2005) also found little loss in LTE over time under accelerated load testing of CRCP. In the loading testing, temperature had the major role in affecting the fluctuation in transverse crack LTE. For this reason, the shear capacity loss calculation routine is not included in this CRCP analysis.

2.7 TENSILE STRESSES AND FATIGUE DAMAGE

For each temperature frequency bin *j* of seasonal increment *i*, loading and curling stresses are calculated separately to estimate the total tensile stress in the concrete slab. Although this approach introduces an error due to the superposition assumption, there were no published CRCP correction factors (R) for combined load and curling stresses which are available for jointed plain concrete pavement (e.g., Salsilli, 1991; Lee and Darter, 1994). Since calibration of the mechanistic-empirical CRCP method was expected, it was deemed expedient to not develop any further more theoretically accurate stress prediction algorithms at this time for combined mechanical and temperature loading. The approach developed in NCHRP 1-37A for calculating critical tensile stresses in CRCP is ideal, but was not publicly available for implementation. The total tensile bending stress (load plus temperature stress) is now used to determine a stress ratio, and then the number of allowable load repetitions-to-failure can be estimated. Finally, fatigue damage is calculated as the ratio of expected load repetitions to allowable load repetitions.

2.7.1 Loading Stress

Punchouts are the result of a longitudinal crack forming between two adjacent transverse cracks. These longitudinal cracks are fatigue cracks which have developed by repeated loading of the slab. Two types of slab bending can occur as a result of traffic loading: transverse bending and longitudinal bending. Transverse bending can produce tensile stresses at both the top and bottom of the slab. For CRCP, high transverse tensile stresses typically occur between the wheel loads, away from the longitudinal edge of the slab. Longitudinal bending produces high tensile stresses at the edge of the slab and is more typical of JPCP. If the transverse crack spacings are small, then the transverse bending stresses are greater than the longitudinal stresses. These stresses are even higher when erosion, permanent deformation of the underlying layers, or negative curling exists. This analysis considers only the two transverse bending stresses shown in Figure 3.

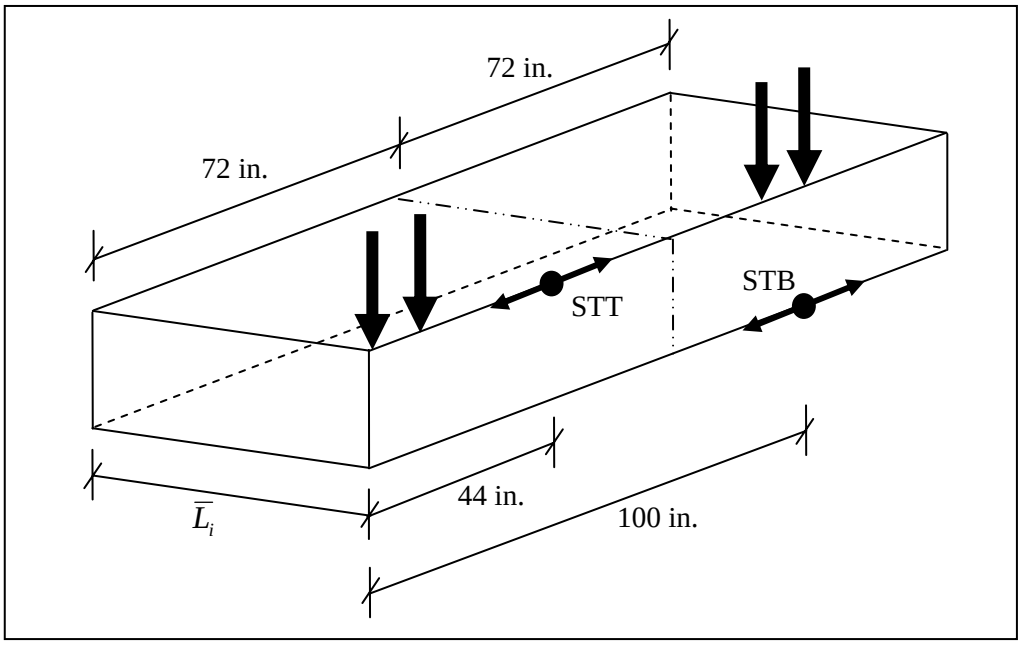

Figure 3. Location of the critical top and bottom tensile bending stresses in a CRCP slab.

ISLAB2000, a finite element analysis program for rigid pavement analysis (ERES, 1999), was used to create a catalogue of tensile stresses for the two critical bending stress locations shown in Figure 3. The ISLAB2000 analysis simulated the behavior of a concrete slab ($\overline{L}$ = 48 in., E_{PCC} = 4 x 10^6 psi, μ_{PCC} = 0.15) with a subgrade modulus (k) of 200 psi/in. loaded by a dual wheel 18-kip single axle. This behavior is a function of shoulder load transfer efficiency (LTE_s), transverse crack load transfer efficiency (LTE_c), and the nondimensional slab size ratio ($\overline{L}/\ell$), where ℓ is the loading radius of relative stiffness. Shoulder and crack load transfer efficiencies were varied from 1 to 99%, and the nondimensional slab size ratio was varied from 0.6187 to 3.7126. The critical top stresses were found to be located at approximately 44 in. from the edge of the slab, while the critical bottom stresses were located approximately 100 in. from the edge of the slab, as shown in Figure 3.

Because the loading stresses calculated by ISLAB2000 are based on a single pavement thickness (11 in.), elastic properties (E = 4,000 ksi and Poisson's Ratio = 0.15), and soil *k*-value (200 psi/in), the catalogued results are normalized to allow for results to be applicable to other slab thicknesses, properties, and sizes. The CRCP nondimensional tensile stresses in the transverse direction are calculated as follows:

$$STT = \frac{\sigma_T \overline{h}_{PCC}^{\,2}}{P} \tag{41}$$

$$STB = \frac{\sigma_B \overline{h}_{PCC}^{\,2}}{P} \tag{42}$$

where,

STT = the nondimensional tensile stress at the top of the slab;

STB = the nondimensional tensile stress at the bottom of the slab;
σ_T = the critical top tensile stress corresponding to a given shoulder load transfer efficiency, crack load transfer efficiency, and nondimensional slab size ratio;
σ_B = the critical bottom tensile stress;
$\overline{h}_{PCC}$ = the concrete slab thickness corresponding to the critical stress; and
P = the applied half-axle load (9,000 lbs).

An interpolation scheme is used in the design methodology to obtain the nondimensional stresses from the catalogued results for any set of shoulder load transfer efficiency, crack load transfer efficiency, and nondimensional slab size ratio. The catalogued critical and nondimensional tensile loading stresses and details of the ISLAB2000 analysis can be found in Appendix B.

For any shoulder and transverse crack LTE and concrete thickness, the loading stresses due to an 18-kip single-axle load are calculated for seasonal increment *i* ($\sigma_{LOAD,i}$) as follows:

$$\sigma_{LOAD-STT,i} = STT_i \frac{P}{h_{PCC}^{\ 2}} \tag{43}$$

$$\sigma_{LOAD-STB,i} = STB_i \frac{P}{h_{PCC}^{\ 2}} \tag{44}$$

where,

STT_i = the nondimensional top tensile stress for seasonal increment *i*;
STB_i = the nondimensional bottom tensile stress for seasonal increment *i ;*
h_{PCC} = the concrete slab thickness (in.); and
P = the applied half-axle load (9,000 lbs).

As previously mentioned, the load stress is independently calculated from the temperature curling stress.

2.7.2 Temperature Curling Stress

The seasonal temperature differential frequency distributions are used to calculate curling stresses in the slabs for each temperature frequency bin *j* of seasonal increment *i*. Pavement thicknesses are assigned to a specific set of seasonal frequency distributions according to the scheme in Table 5.

Table 5. Seasonal Frequency Distributions by Pavement Thickness

Pavement Thickness	ΔT Frequency Distribution Set (in.)
$h_{PCC} \leq 9$ in.	8
9 in. < $h_{PCC} \leq 11$ in.	10
11in. < $h_{PCC} \leq 13$ in.	12
$h_{PCC} > 13$ in.	14

Temperature curling stress calculations are calculated at the critical top and bottom tensile stress locations determined from the load stress analysis. The curling stresses along the joint at the critical load stress location for each temperature frequency bin *j* of seasonal increment *i* ($\sigma_{CURL,ij}$) can be calculated as follows (Westergaard, 1927):

$$\sigma_{CURL-STT,ij} = C_{STT,i} \frac{E_{PCC,i}\alpha_{PCC}\Delta T_{ave,j}}{2} \tag{45}$$

$$\sigma_{CURL-STB,ij} = C_{STB,i} \frac{E_{PCC,i}\alpha_{PCC}\Delta T_{ave,j}}{2} \tag{46}$$

where,

$C_{STT,i}$ = the slab size correction coefficient for the top tensile stress case;
$C_{STB,i}$ = the coefficient for the bottom tensile stress case;
$E_{PCC,i}$ = the concrete modulus of elasticity for seasonal increment *i* (psi);
α_{PCC} = the concrete coefficient of thermal expansion (1/°F);
$\Delta T_{ave,j}$ = the mean temperature differential for frequency bin *j* (°F)

2.7.2.1 Slab Size Correction Coefficient

Traditionally the slab size correction coefficient (C) has been evaluated at the middle of the slab. However, the original Westergaard (1927) equations enable evaluation of the curling stresses in a finite-sized slab at any location from the edge of the slab ($y = L/2$) and the middle of the slab ($y = 0$). The slab size correction coefficient evaluated at the mid-slab is given in Equation (10). The generalized equation for the nondimensional slab size correction coefficient at any offset from the middle of the slab is given as follows (Westergaard, 1927):

$$C_i = 1 - C_{1,i}\left(C_{2,i} + C_{3,i}\right) \tag{47}$$

$$C_{1,i} = \frac{2\cos\lambda_i \cosh\lambda_i}{\sin 2\lambda_i + \sinh 2\lambda_i} \tag{48}$$

$$C_{2,i} = \left(\tan\lambda_i + \tanh\lambda_i\right)\cos y_i' \cosh y_i' \tag{49}$$

$$C_{3,i} = \left(\tan\lambda_i - \tanh\lambda_i\right)\sin y_i' \sinh y_i' \tag{50}$$

$$\lambda_i = \frac{L}{\ell_i\sqrt{8}} \tag{51}$$

$$y_i' = \frac{y}{\ell_i\sqrt{2}} \tag{52}$$

where,

L = the width of the slab (which is set to 144 in. for CRCP without widened lanes);
ℓ_i = the radius of relative stiffness for seasonal increment *i* (in.); and
y = the distance from the center line of the slab to the location of the curling stress of interest (in.);
μ_{PCC} = the concrete Poisson's ratio.

The curling radius of relative stiffness should be used for curling stress calculations. The load stress analyses revealed that the critical tensile stresses at the top and bottom of the slab are located 28 in. from the slab's center line. The critical bottom tensile stresses are 28 in. toward the inside lane and the top tensile stresses are 28 in. toward the edge of the slab.

2.7.3 Total Stress

The total tensile stress ($\sigma_{TOT,ij}$) at each critical location is calculated as the sum of the load stress of seasonal increment *i* and the curling stress for each temperature frequency bin *j* as follows:

$$\sigma_{TOT-STT,ij} = \sigma_{LOAD-STT,i} - R_{ij} \cdot \sigma_{CURL-STT,ij} \quad (53)$$

$$\sigma_{TOT-STB,ij} = \sigma_{LOAD-STB,i} + R_{ij} \cdot \sigma_{CURL-STB,ij} \quad (54)$$

where,

$\sigma_{CURL,ij}$ = the curling stress for each temperature frequency bin *j* of seasonal increment *i*;
$\sigma_{LOAD,i}$ = the loading stress for seasonal increment *i*; and
R_{ij} = the total stress adjustment factor for each temperature frequency bin *j* of seasonal increment *i*.

At the top of slab location (STT), the temperature curling stress is subtracted from the loading stress because of the sign convention employed in this procedure. Recall that a temperature differential (ΔT) is defined as the temperature at the top of the concrete slab minus the temperature at the bottom of the slab (Section 2.1.1) and that tensile stresses are positive (Appendix B). Negative temperature differentials result in upward curling of the slabs and tensile stresses at the top of the slab. Therefore, a negative temperature differential should be additive to the critical top tensile stresses.

Curling of the slabs negates one of the assumptions used when applying superposition. As a result, the total stress using superposition will not be the same as a finite element analysis, which considers load and temperature simultaneously. Previous researchers on JPCP have employed superposition with the use of a correction factor to compensate for the error introduced (e.g., Zollinger and Barenberg, 1989; Salsilli, 1991). As stated previously, no adjustment factors R_{ij} exist for CRCP and thus, 1.0 was used for this research along with calibration for field performance.

2.7.4 Allowable Load Repetitions

The number of allowable load repetitions for each temperature frequency bin *j* of seasonal increment *i* (N_{ij}) are calculated using one of two concrete fatigue equations. The fatigue equation to be used is a user-defined input. The allowable repetition calculations are made for both of the transverse bending stress cases.

2.7.4.1 Fatigue Equations

2.7.4.1.1 Stress ratio

Both concrete fatigue equations are functions of the slab stress ratio. The stress ratio for each temperature frequency bin *j* of seasonal increment *i* (SR_{ij}) is calculated as:

$$SR_{STT,ij} = \begin{cases} IF & \sigma_{TOT,ij} \Big/ \left(\hat{R} \cdot MOR_i\right) > 0.02 \quad , \quad \sigma_{TOT,ij} \Big/ \left(\hat{R} \cdot MOR_i\right) \\ ELSE & 0.02 \end{cases} \tag{55}$$

$$SR_{STB,ij} = \begin{cases} IF & \sigma_{TOT,ij} \Big/ MOR_i > 0.02 \quad , \quad \sigma_{TOT,ij} \Big/ MOR_i \\ ELSE & 0.02 \end{cases} \tag{56}$$

where,

$\sigma_{TOT,ij}$ = the total stress for temperature frequency bin *j* of seasonal increment *i* (psi);
$\hat{R}$ = the top of slab tensile strength reduction factor; and
MOR_i = the concrete modulus of rupture for seasonal increment *i* (psi).

2.7.4.1.2 M-E PDG fatigue equation

The concrete fatigue equation used for the CRCP design in the M-E PDG is given as follows (ARA, 2007):

$$LogN_{ij} = 2.0 * \left(1 / SR_{ij}\right)^{1.22} - 1. \tag{57}$$

This fatigue equation was originally developed from U.S. Army Corps of Engineers full-scale airfield slab tests. It has been adjusted based on LTPP and other highway performance databases, with failure defined as 50% slab cracking. One note is that this fatigue equation is similar to the fatigue equation used for JPCP fatigue in the M-E PDG, except for the (-1) term at the end. This adjustment to the equation translates to one log cycle less of allowable repetitions for CRCP relative to JPCP for the same stress ratio. This fatigue equation represents JPCP slab tests and has been adjusted by the M-E PDG researchers to account for the observed performance of CRCP, which could not be accurately predicted by the JPCP fatigue algorithm. One disadvantage of this equation is that it predicts the allowable repetitions to 50% slab cracking, and this doesn't necessarily translate directly to a certain number of punchouts per mile.

2.7.4.1.3 Zero-maintenance fatigue equation

The zero-maintenance concrete fatigue equation (Darter, 1977) which is employed in the current IDOT JPCP design method (Zollinger and Barenberg, 1989) is given as follows:

$$LogN_{ij} = 17.61 - 17.61(SR_{ij}). \quad (58)$$

This equation was developed from concrete beam fatigue results, with failure defined as complete fracture of the beams. The zero-maintenance fatigue equation has a reliability of 50% (Darter, 1977). The advantage of this fatigue equation is that it is based on laboratory fatigue testing of concrete beams and is used in the current IDOT JPCP design method. This fatigue equation represents fatigue failure of concrete beams, and thus, is a conservative estimate of concrete slab fatigue (Roesler, 1998).

2.7.5 Expected Load Repetitions

The number of expected load repetitions producing the critical stress levels is a function of the cumulative number of ESALs in the design lane. The number of expected load repetitions for seasonal increment *i* (n_i) is calculated as:

$$n_{STT,i} = (EDR_{STT,i})(ESAL_i - ESAL_{i-1}) \quad (59)$$

$$n_{STB,i} = (EDR_{STB,i})(ESAL_i - ESAL_{i-1}) \quad (60)$$

where,

EDR_i = the equivalent damage ratio (Zollinger and Barenberg, 1989) for seasonal increment *i*;
$ESAL_i$ = the cumulative number of 18-kip equivalent single-axle loads in the design lane through seasonal increment *i* (ESALs); and
$ESAL_{i-1}$ = the cumulative number of 18-kip equivalent single-axle loads in the design lane through the previous seasonal increment *i* -1 (ESALs).

2.7.5.1 Equivalent Damage Ratio

An equivalent damage ratio (EDR) is "the ratio of the traffic applied at a critical location that will produce the same accumulated fatigue damage as the total traffic distributed over all locations" (Huang, 2004). It is a means of accounting for wander of vehicular traffic within the driving lane. This value must be considered in rigid pavement design because the location of the applied load greatly influences the magnitude of the resulting stress. If all traffic is considered channelized, fatigue damage and required slab thicknesses would be much greater. For this analysis, the critical load position that produces the highest stresses at the top and bottom of the slab is zero offset from the edge at the transverse crack.

Since no equations for EDR were found in the literature, an analysis was conducted with ISLAB2000 to obtain the equations for the top and bottom of the slab. The total fatigue damage accumulated at the critical location on the top or bottom of the CRCP slab was calculated using the damage produced at offset positions and Gauss quadrature weighting

factors. It was found that the equivalent damage ratio is a function of the nondimensional slab size ratio ($\overline{L}/\ell$), and that the shoulder load transfer efficiency (LTE_s) influences the EDR for the top of the slab. Based on this analysis, the equivalent damage ratio for seasonal increment *i* (EDR_i) is calculated as:

$$EDR_{STT,i} = \begin{cases} IF \quad LTE_s \le 60 & , \quad -0.1424\left(\overline{L}_i/\ell_i\right)+0.2806 \\ IF \quad 60 < LTE_s \le 85 & , \quad -0.1138\left(\overline{L}_i/\ell_i\right)+0.2688 \\ IF \quad 85 < LTE_s \le 98 & , \quad -0.0965\left(\overline{L}_i/\ell_i\right)+0.3064 \\ IF \quad LTE_s > 98 & , \quad -0.0933\left(\overline{L}_i/\ell_i\right)+0.3414 \end{cases} \tag{61}$$

$$EDR_{STB,i} = -0.2264\left(\overline{L}_i/\ell_i\right)+0.5533 \tag{62}$$

where ($\overline{L}_i/\ell_i$) is the nondimensional slab size ratio for seasonal increment *i* (in.). Note that ℓ_i is the loading radius of relative stiffness for seasonal increment *i*. Appendix C contains additional information regarding the determination of these wander adjustment equations.

2.7.6 Cumulative Fatigue Damage

The fatigue damage concept proposed by Miner (1945) is a method for combining damage due to different loading levels over time. Miner's hypothesis states that accumulated fatigue damage for a given stress level is the summation of the number of expected load repetitions divided by the number of allowable load repetitions, and assumes that damage accumulates linearly. Failure of the pavement should occur when the accumulated fatigue damage equals 1.0, although failure can occur at other accumulated fatigue damage values because of variations in materials, traffic loading, load sequencing, environmental conditions, and base/subgrade support (Smith and Roesler, 2003).

The fatigue damage for each temperature frequency bin *j* of seasonal increment *i* (D_{ij}) is calculated as:

$$D_{STT,ij} = F_j \cdot \frac{n_{STT,i}}{N_{STT,ij}} \tag{63}$$

$$D_{STB,ij} = F_j \cdot \frac{n_{STB,i}}{N_{STB,ij}} \tag{64}$$

where,

F_j = the frequency of occurrence for temperature frequency bin *j*;

n_i = the number of expected load repetitions for seasonal increment *i*; and

N_{ij} = the number of allowable load repetitions for each temperature frequency bin *j* of seasonal increment *i*.

The total summation of the fatigue damage for each seasonal increment *i* is computed separately for the critical top and bottom position in the CRCP slab. The fatigue damage for seasonal increment *i* (D_i) is calculated as:

$$D_{STT,i} = \sum D_{STT,ij} \tag{65}$$

$$D_{STB,i} = \sum D_{STT,ij} \ . \tag{66}$$

The total fatigue damage through seasonal increment *i* ($D_{TOT,i}$) is then calculated as:

$$D_{TOT-STT,i} = \sum_{i=1}^{m} D_{STT,i} \tag{67}$$

$$D_{TOT-STB,i} = \sum_{i=1}^{m} D_{STB,i} \tag{68}$$

$$m = 4 \cdot LIFE \tag{69}$$

where m is the total number of seasons in the design life and $LIFE$ is the design life (years).

2.8 PUNCHOUT PREDICTION

The number of punchouts per mile can be predicted as a function of accumulated fatigue damage. Two such functional forms to describe the evolution of punchouts have been identified from the literature. These calibrated punchout functions each plot the mean number of punchouts per mile and provide 50% design reliability. Since there are two critical positions that accumulate fatigue damage, the larger damage is used to predict the number of expected punchouts as follows:

$$\overline{D}_{TOT,i} = \begin{cases} \text{IF} \quad D_{TOT-STT,i} > D_{TOT-STB,i} \quad , \quad D_{STT-TOT,i} \\ \text{IF} \quad D_{TOT-STT,i} \le D_{TOT-STB,i} \quad , \quad D_{STB-TOT,i} \end{cases} \tag{70}$$

where m is the total number of seasons in the design life.

2.8.1 Power Function Punchout Model

The first punchout functional form below is used in the M-E PDG (ARA, 2003b) and is adapted to have an upper limit so that it does not oscillate:

$$PO_i = \begin{cases} \text{IF} \quad D_{TOT,i} < 2.42 \text{x} 10^{-7} \quad , \quad \sum_{i=1}^{m} \dfrac{a}{1 + b \cdot \overline{D}_{TOT,i}^{c}} \\ \text{ELSE} \quad 50 \end{cases} \tag{71}$$

where,

PO_i = the total predicted number of punchouts per mile at the end of seasonal increment *i*;

$\overline{D}_{TOT,i}$ = the accumulated fatigue damage at either the top or bottom tensile stress location at the end of seasonal increment *i*;

m = the total number of seasons in the design life (4 times the number of years); and

a, b, c are calibration constants for punchout function (-6.515, -1.600 x 10^{-5}, -0.733, respectively).

The calibration constants presented assume the use of the zero-maintenance fatigue equation. For the given calibration, the accumulated fatigue damage is bound at 2.42 x 10^{-7} in./in. (50 punchouts per mile) to prevent the calculation of an excessively high number of punchouts per mile and negative punchouts at even larger damage values.

2.8.2 S-Curve Punchout Model

The second punchout function has the same functional form used successfully by IDOT to determine the percent cracking level in jointed plain concrete pavements (Barenberg, 1991), and is given as:

$$PO_i = \sum_{i=1}^{m} \frac{1}{a + b \cdot c^{-\log \overline{D}_{TOT,i}}} \tag{72}$$

where,

PO_i = the total predicted number of punchouts per mile at the end of seasonal increment *i*;

$\overline{D}_{TOT,i}$ = the accumulated fatigue damage at either the top or bottom tensile stress location at the end of seasonal increment *i*;

m = the total number of seasons in the design life (4 times the number of years); and

a, b, c are calibration constants for punchout function (0.02, 1.00 x 10^{-32}, 32386, respectively).

The calibration constants are derived with the application of the zero-maintenance fatigue equation. This is a logistic-type function which produces an s-curve which saturates at 50 punchouts per mile for the given calibration constants. The 50 punchouts-per-mile saturation level was chosen since almost all performance data suggest that repairs would be completed before this level of accumulated distress. The nature of this function does not require the use of boundaries on the amount of accumulated fatigue damage.

CHAPTER 3. ILLINOIS INPUTS AND DESIGN CHARTS

The previous chapter laid out the framework for a CRCP design using M-E design concepts. This chapter defines the inputs required to perform a CRCP design for Illinois conditions. It also presents the procedure used to calibrate the punchout prediction models, CRCP design charts for Illinois, and a discussion of the limitations of the CRCP models and input data.

3.1 DESIGN INPUTS

The following are suggested design inputs for Illinois.

3.1.1 General Information

3.1.1.1 Slab Thickness

The thickness of the concrete slab (h_{PCC}) is a user-defined input. This analysis considers slab thicknesses between 8 and 14 in.. The slab thickness greatly influences the stresses and subsequent damage in the pavement. Temperature and loading stresses are reduced as the thickness of the slab increases.

3.1.1.2 Design Life

The Illinois Department of Transportation Bureau of Design and Environment Manual (2002) defines design life as "the number of years that a pavement is to carry a specific traffic volume and retain a serviceability level at or above a designated value." A 20-year design life is usually used by IDOT for rigid pavement designs, although the use of a 30-year design life has been used more recently in certain high-volume traffic corridors.

3.1.1.2.1 Percent steel

Percent steel (P_b) is equal to the area of steel reinforcement per area of concrete expressed as a percent. For this report and subsequent design charts, a 20-year design life assumes that 0.7% steel is specified. For a 30-year extended life design, the steel percentage is assumed to increase to 0.8%.

3.1.1.2.2 Reinforcing steel bar diameter

IDOT allows the use of No. 6 (0.75-in.) or No. 7 (0.875-in.) reinforcing steel bars. Other bar diameters may be used to ensure that spacing between the longitudinal reinforcing is not too small or large.

3.1.1.2.3 Depth to steel

Depth to steel is defined as the depth from the surface of the concrete slab to the top of the reinforcing steel. Current IDOT standards put the depth of the longitudinal reinforcing steel at 3 in. when the pavement thickness is less than or equal to 8 in., and at 3.5 in. when the pavement thickness is greater than 8 in. The new proposed depth to steel as a function

of slab thickness is presented in Table 2, which is approximately one-third of the concrete slab thickness. The use of two-layer reinforcement is not recommended at this time.

3.1.1.3 Aggregate Type

The type of coarse aggregate greatly influences the concrete coefficient of thermal expansion and the concrete thermal diffusivity. Limestone and dolomite have both been used as coarse aggregate in Illinois. Limestone is assumed to be the default coarse aggregate used in CRCP designs.

3.1.1.4 Shoulder Type

Shoulders provide edge support for the pavement and a degree of load transfer across the longitudinal shoulder/lane joint which reduces the tensile stresses in the CRCP. Two shoulder types are associated with CRCP: tied and untied. Tied shoulders are constructed of concrete and are physically connected to the mainline pavement with evenly spaced steel tie bars. Tied shoulders can be monolithically paved with the driving and passing lanes or can be added separately after the mainline paving is completed. The main difference is that monolithic tied concrete shoulders are tied contraction joints which have aggregate interlock, while separated PCC shoulders are tied construction joints. Untied shoulders are not connected to the mainline pavement and offer limited edge support. Untied shoulders are typically made from asphalt concrete or granular materials. Table 6 shows load transfer efficiencies for these shoulder types and the corresponding stiffness of the shoulder/lane joint. Current IDOT pavement design procedures state that tied concrete shoulders should be used for nearly all rigid pavement designs (IDOT, 2002).

Table 6. Recommended Shoulder Load Transfer Efficiency and Stiffness of the Shoulder/Lane Joint (ARA 2003b)

Shoulder Type	LTE_s **(%)**	J_s
Tied concrete (monolithic)	73	4.00
Tied concrete (separate)	40	0.77
Asphalt	5	0.04
Granular	5	0.04

3.1.2 Traffic

3.1.2.1 Total 18k ESALs in Design Lane

The amount of expected traffic over the design life of the pavement is quantified as the total number of 18-kip equivalent single-axle loads (ESALs) in the design lane. For Illinois, with existing load limits and a 30-year design, this value has a practical upper bound of roughly 230 million ESALs based on current legal axle loads (Bordelon et al., 2009). Current IDOT pavement design policy states that CRCP should be used primarily when greater than 35 million ESALs are expected during the design life (IDOT, 2002).

3.1.2.2 Annual Growth Factor

An annual growth factor (r) can be used to account for expected annual growth in the amount of traffic in the design lane. When the annual growth factor is equal to zero, the total number of 18-kip ESALs in the design lane is evenly distributed over the design life.

3.1.3 Concrete Properties

3.1.3.1 Elastic Modulus

The concrete elastic modulus, or stiffness, typically varies between 3 and 6 x 10^6 psi. A typical concrete elastic modulus at 28 days (E_{PCC28}) is 4.4 x 10^6 psi.

3.1.3.2 Poisson's Ratio

Poisson's ratio (μ_{PCC}) for concrete is taken as 0.15 even though this value may vary between 0.15 and 0.25. This value is typically assumed and not determined from actual testing.

3.1.3.3 Coefficient of Thermal Expansion

The coefficient of thermal expansion (α_{PCC}) for concrete is heavily influenced by the type of coarse aggregate. For a concrete using limestone as a coarse aggregate, a typical coefficient of thermal expansion is 5.50 x 10^{-6} /°F based on tests conducted by the Federal Highway Administration (FHWA) for the LTPP sections in Illinois.

3.1.3.4 Compressive Strength

Compressive strength is determined from testing on cylinder specimens. A typical mean concrete compressive strength at 28 days (f'_{c28}) is 4,500 psi for Illinois concrete.

3.1.3.5 Modulus of Rupture

Modulus or rupture, or flexural strength, is a measure of the concrete's tensile strength in bending. A typical concrete modulus of rupture at 90 days (MOR_{90}) is 750 psi using a third-point loading configuration, which is equivalent to a mean flexural strength at 14 days using a center point loading configuration (Zollinger and Barenberg, 1989). Although IDOT requires a minimum flexural strength at 14 days to be 650 psi (center point), the mean value for design must be greater than this due to the normal variation in testing and materials.

3.1.3.6 Top of Slab Strength Reduction Factor

Microcracking at the surface of concrete slabs can result in a reduction in slab strength at the surface and a decrease in the overall load carrying capacity of the slab. McCullough and Dossey (1999), Roesler et al. (2003), and Rao (2005) observed that the strength of concrete at the top of the slab can be less than the strength at the bottom of the slab due to moisture loss (higher evaporation rates). This early-age surface microcracking has also been shown to be a contributing factor to top-down cracking (Heath and Roesler, 2000). The majority of this cracking is the result of shrinkage stresses caused by drying shrinkage gradients and slab restraint.

To account for reduced strength at the top of the slab, a strength reduction factor ($\hat{R}$) is applied to the concrete modulus of rupture for the top of slab tensile stress case.

Altoubat and Lange (2001) suggested a strength reduction factor of 0.8 for restrained concrete subjected to drying shrinkage. Beyer and Roesler (2008a) reported a reduction in peak load (directly correlated to modulus of rupture) of 19% in laboratory concrete beam specimens with surface microcracking compared to beams without microcracking. Based on these results, the strength reduction factor for the top of slab location is taken as 0.8.

3.1.3.7 Ultimate Shrinkage

Concrete ultimate shrinkage (ε_∞) values typically vary between 415 x 10^{-6} and 1070 x 10^{-6} in./in. When specific shrinkage data is unavailable, the ultimate shrinkage can be taken as 780 x 10^{-6} in./in. per ACI 209 (1992) recommendations.

3.1.3.8 Thermal Diffusivity

Thermal diffusivity of concrete (γ_{PCC}) is a function of coarse aggregate type, as shown in Table 7. For a concrete using limestone as a coarse aggregate, the concrete thermal diffusivity is 1.22 ft^2/day.

Table 7. Concrete Thermal Diffusivity (ARA, 2003b)

Coarse Aggregate Type	Concrete Thermal Diffusivity (ft^2/day)
Quartzite	1.39
Limestone	1.22
Dolomite	1.20
Granite	1.03
Rhyolite	0.84
Basalt	0.77
Syenite	1.00
Gabbro	1.00
Chert	1.39

3.1.3.9 Cement Content

The cement content of the concrete mixture (CC) is the amount of cement per cubic yard. This value does not include contributions from mineral admixtures such as fly ash and slag (ARA, 2004a). For a typical IDOT mixture design, the cement content of the concrete mixture is taken as 600 lb/yd^3.

3.1.2 Base Properties

3.1.4.1 Base/Subbase Type

The type of base/subbase determines the base friction coefficient and base load transfer efficiency. An asphalt-treated base (ATB), also known as a bituminous aggregate mixture (BAM), is currently used by IDOT when constructing CRCP (IDOT, 2002).

3.1.4.1.1 Base friction coefficient

The base friction coefficients (f) shown in Table 8 were used in the calibration of the M-E PDG to obtain proper crack spacings. For this analysis, the mean friction coefficient is used for a given subbase/base type. For an ATB, the mean base friction coefficient is 7.5.

Table 8. Base Friction Coefficients (ARA, 2003b)

Subbase/Base Type	**Friction Coefficient (low – mean – high)**
Fine grained soil	0.5 – 1.1 – 2.0
Sand**	0.5 – 0.8 – 1.0
Aggregate	0.5 – 2.5 – 4.0
Lime-stabilized clay**	3.0 – 4.1 – 5.3
ATB	2.5 – 7.5 – 15
CTB	3.5 – 8.9 – 13
Soil cement	6.0 – 7.9* – 23
LCB	1.0 – 6.6* – 20
LCB not cured**	> 36 (higher than LCB cured)
* Trimmed mean values used in the M-E PDG calibration ** Base type did not exist or not considered in sections used to calibrate the M-E PDG	

3.1.4.1.2 Base load transfer efficiency

The load transfer efficiency contributed by the base layer (LTE_{base}) is shown in Table 9. For an ATB, the base load transfer efficiency is 30%.

Table 9. Load Transfer Efficiency Contributed by the Base Layer (ARA, 2003b)

Base Type	***LTE*$_{base}$ (%)**
Aggregate	20
ATB or CTB	30
Lean Concrete Base	40

3.1.3 Environmental Properties

3.1.3.1 Construction Season

The construction season determines the concrete set temperature at the depth of steel (T_{set}), the temperature at which the concrete layer exhibits zero thermal stress. The specific months in each season were previously defined in Table 1. For the spring, summer, and fall seasons, Equation (23) is used to calculate the concrete set temperature at the depth of steel. Calculations for the winter season result in T_{set} values that fall outside the allowable temperature range of Equation (23). As a result, the concrete set temperature during the winter season is set at 65°F based on measurements by Kohler (2005) for zero stress and zero crack width temperatures.

3.1.3.2 Relative Humidity in the Concrete at the Depth of Steel

The relative humidity in the concrete at the depth of steel ($rh_{PCC,\zeta}$) is used in the calculation of unrestrained concrete drying shrinkage at the depth of steel. Laboratory testing by Rodden (2006) on concrete cubes (12 in. x. 12 in. x 15 in.) indicated relative humidity values between 85 and 95% at depths of 3 to 5 in. below the surface of the concrete, with an ambient relative humidity of 50%. During full-scale testing on concrete slabs conducted at the Advanced Transportation Research and Engineering Laboratory (ATREL) in Rantoul, Illinois, Kohler (2005) measured relative humidity values between 90 and 100% at depths of 3 and 4.5 in. Based on these results, the relative humidity in the concrete at the depth of steel is taken conservatively as 85%, the lower boundary of the reported values.

3.1.3.3 Total Stress Correction Factor

A number of regression equations have been developed for jointed plain concrete pavements (JPCP) to determine the total stress correction factor (R) needed when adding curling and loading stresses to calculate total stress (Salsilli, 1991; Lee and Darter, 1994). These equations are based on a number of inputs, including the concrete modulus of elasticity, temperature differential through the slab, slab thickness, slab length, slab width, etc. Regression coefficients for these equations were obtained by using existing databases of results from the finite element program ILLISLAB.

Because the slab lengths typically associated with CRCP are smaller than those for JPCP and critical stress locations are at a different position than JPCP, these equations cannot be used to determine the total stress correction factor for CRCP. A limited analysis was conducted with ISLAB2000 to determine the value of R for CRCP total stress calculations. Two methods were used to calculate stress. In the first, loading and temperature stresses were calculated together over a range of temperature differentials. In the second, loading stress without a temperature differential was added to temperature stress calculated at a given temperature differential using the principle of superposition. Maximum errors of up to 30% were observed for the majority of expected temperature differentials. However, significantly higher errors were observed at the top of the slab for extreme temperature differentials (-20°F). In these extreme cases, the total stress was underestimated by up to 200%, although these cases occur much less than 1% of the time. In the absence of other estimates, the total stress correction factor is taken as 1.0 for all stress calculations and a design method can still be developed if calibration to field data is utilized.

3.1.4 Subgrade Properties

3.14.1 Modulus of Subgrade Reaction

The modulus of subgrade reaction, or *k*-value, is a measure of the support provided by the subbase and subgrade. Seasonal variations of *k*-values for loading are not considered for this analysis. As a result, summer or fall dynamic *k*-values should be used as inputs. Typical dynamic *k*-values for Illinois are 50, 100, and 200 psi/in. The *k*-values for all temperature curling analyses are set at 100 psi/in.

3.1.5 Punchout Prediction

3.1.5.1 Fatigue Equation

Concrete fatigue equations are used to calculate the number of allowable load repetitions from the ratio of total stress to the concrete modulus of rupture. The M-E PDG and zero-maintenance fatigue equations have been identified from the literature. The zero-maintenance equation is the one currently used by IDOT in their procedure for the design of jointed plain concrete pavements (Zollinger and Barenberg, 1989; Roesler et al., 2005a).

3.1.5.2 Reliability

A traffic multiplier (TM) is used to account for variability within the design procedure in terms of uncertainty in inputs, testing variability, and inherent material variability. For 50% reliability, the traffic multiplier is equal to 1.0. Based on past experience, 95% reliability has been used for high-type rigid and flexible pavement systems (Thompson and Cation, 1986; Zollinger and Barenberg, 1989). For full-depth HMA pavement, a traffic multiplier of 4.0 is used to account for the design uncertainties. IDOT's current JPCP method doesn't directly use a traffic multiplier, but it can be calculated, and it is approximately 2.5 for a failure criteria of 20% slabs cracked. AASHTO (1993) also uses a traffic multiplier concept and it is approximately 3.0 for high-type rigid pavements. For this design framework, a traffic multiplier of 4.0 is used at 95% reliability. There is not a quantitative way to tie this traffic multiplier into a reliability level, but it does fit between the 2.5 traffic multiplier for the current JPCP design and 4.0 for the current full-depth HMA design. The traffic multiplier of 4.0 can also be thought as a high level of confidence in the design.

3.1.5.3 Failure Criterion

The goal of this design procedure is to limit the development of punchouts over the design life of the pavement. Failure of the pavement occurs when the number of punchouts per mile exceeds a given limit. The failure criterion is set at 10 punchouts per mile.

3.2 CALIBRATION

3.2.1 Punchout Prediction

To obtain realistic thickness values from the punchout prediction models, and to account for unknown factors and current model limitations, a calibration procedure is used to correlate calculated fatigue damage with respect to CRCP field performance data.

3.2.1.1 CRCP Calibration Database

Three sources of data used by the NCHRP 1-37A team (ARA, 2003a) and accelerated pavement testing data of CRCP (Kohler and Roesler, 2006) were used to calibrate the punchout prediction models. The data sets include LTPP General Pavement Experimental Study number 5 (GPS-5); Vandalia (US 40) experimental CRCP sections; heavily trafficked CRCP sections on I-80 and I-94 (Edens expressway) near Chicago, Illinois; and four accelerated pavement test sections of CRCP tested at the University of Illinois ATREL facility from 2001 to 2005. From the NCHRP 1-37A database, only test sections in Illinois constructed with asphalt-treated bases (ATB) were extracted for use in calibration of the power function and S-curve punchout prediction models. Of these test

sections, those constructed during the winter season or with greater than 50 observed punchouts per mile were excluded. Fifty punchouts per mile was used as a limiting criterion because it is believed that rehabilitation of the pavement would occur for levels of distress greater than this value. The resulting data set contained a total of 15 test sections: eight from I-80, three from I-94 (Edens expressway), and four from accelerated pavement testing. Design inputs and field performance data for these test sections are presented in Appendix D.

Typical Illinois design inputs were used to complete the data set for those parameters for which values were unavailable. The base friction coefficients (f) for all test sections were set at 7.5, the mean value for ATB as shown in Table 8. In addition, a 30-year design life was assumed for all test sections, because a number of distress surveys occurred at pavement ages greater than 20 years. The total number of design ESALs was estimated so that for a given test section, the appropriate number of cumulative ESALs reported in the data set would correspond to the age of the pavement at the time of the distress survey.

The NCHRP 1-37A team reviewed field survey data sheets to obtain the number of observed punchouts per mile. Punchouts and patches occurring at the driving lane/shoulder edge were identified from this review. Clustered punchouts—those formed by a longitudinal crack propagating over several transverse cracks—were counted as one punchout (ARA, 2003b). A linear extrapolation was used to estimate the number of punchouts per mile, because each test section was only 528 feet in length (Rao et al., 2004). A total of 32 data points were obtained for the calibration procedure, because the majority of test sections had two or more distress surveys conducted over time.

3.2.1.2 Method of Least Squares

The method of least squares was used to determine calibration coefficients for the power function and S-curve punchout prediction models. This method seeks to provide a fitted regression model to a set of data by minimizing the residual or error in the model. A residual is defined as the vertical deviation of an observed value from the fitted model. The residual sum of squares or the sum of squares of the errors about the regression model (SSE) is given as follows (Walpole et al., 2002):

$$SSE = \sum_{i=1}^{n} \bar{e}_i^2 = \sum_{i=1}^{n} (\bar{y}_i - \hat{y}_i)^2 \tag{73}$$

where,

$\bar{e}_i$ = the residual;

$\bar{y}_i$ = the observed value;

$\hat{y}_i$ = the value given by the fitted regression model; and

n = the number of data points.

The goal of the method of least-squares regression is to minimize the SSE parameter.

The mean squared error (s^2) is calculated as follows (Walpole et al., 2002):

$$s^2 = \sum_{i=1}^{n} (y_i - \hat{y}_i)^2 / (n-2) = \frac{SSE}{n-2} \quad (74)$$

where the standard deviation (s) or standard error of the estimate (SEE) is the square root of the mean squared error.

3.2.1.3 Power Function Punchout Model

Recall that the power function punchout model takes the following functional form:

$$y_i = \frac{a}{1 + b \cdot x_i^c} \quad (75)$$

Calibration of this model using the zero-maintenance fatigue equation with only the I-80 and I-94 (Edens expressway) CRCP data set resulted in the following calibration constants:

- a = -6.515
- b = -1.600 x 10^{-5}
- c = -0.733

The accelerated CRCP test data from the University of Illinois (ATREL) was not considered in this calibration, since it could not be fitted with this functional form. The relationship between accumulated fatigue damage and observed punchouts is shown in Figure 4 along with the calibrated power function punchout model. The relationship between the predicted and observed number of punchouts per mile is shown in Figure 5. The slope of a linear correlation forced to fit though the origin has an R^2 of 79% and an SEE of 4.4 punchouts per mile. Recall that for this punchout function, the accumulated fatigue damage is bound at 2.42 x 10^{-7} in./in. (50 punchouts per mile) to prevent the calculation of an excessively high number of punchouts per mile or negative punchouts as damage approaches infinity.

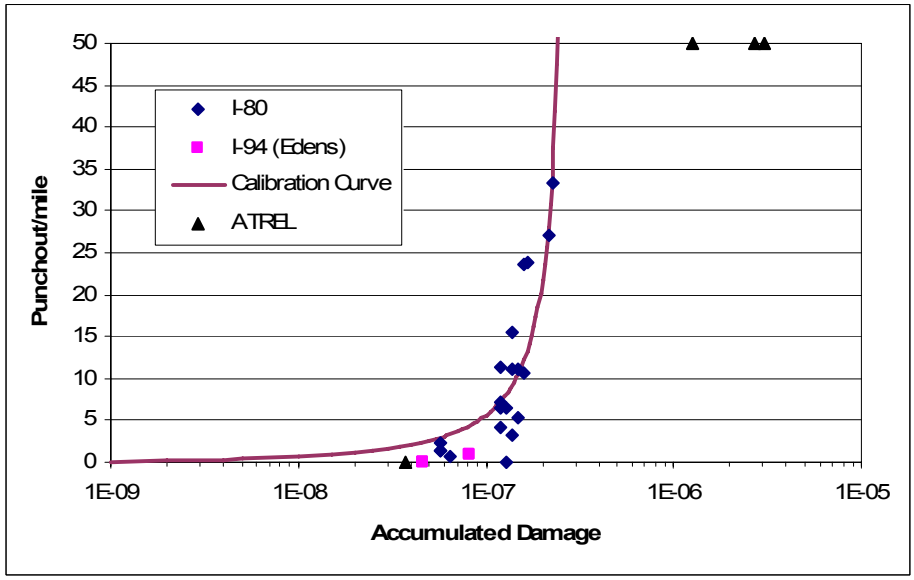

Figure 4. Relationship between accumulated fatigue damage and observed punchouts per mile for Illinois CRCP calibration data set (power function punchout model).

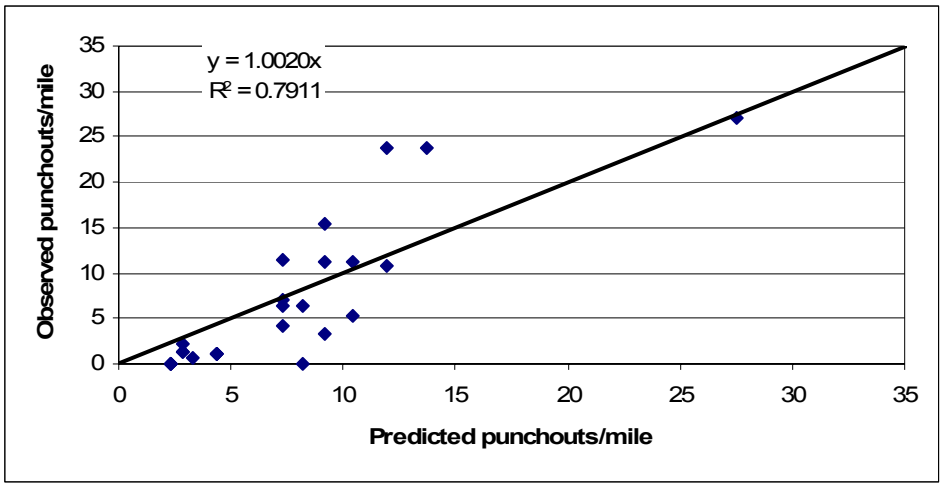

Figure 5. Predicted punchouts per mile versus observed punchouts per mile for Illinois CRCP calibration data set (power function punchout model).

3.2.1.4 S-Curve Punchout Model

Recall that the S-curve punchout model takes the following functional form:

$$y_i = \frac{1}{a + b \cdot c^{-\log x_i}} \tag{76}$$

Calibration of this model using the zero-maintenance fatigue equation with CRCP data from I-80, I-94 (Edens expressway), and the University of Illinois (ATREL) accelerated pavement test sections of CRCP resulted in the following calibration constants:

- a = 0.02
- b = 1.00 x 10^{-32}
- c = 32386

The calibration constant a was manually set equal to 0.02 so that saturation of the function would occur at 50 punchouts per mile. The relationship between accumulated fatigue damage and observed punchouts is shown in Figure 6. The relationship between the predicted and observed number of punchouts per mile is shown in Figure 7. The slope of a linear correlation forced to fit though the origin has an R^2 of 95% and an SEE of 3.78 punchouts per mile.

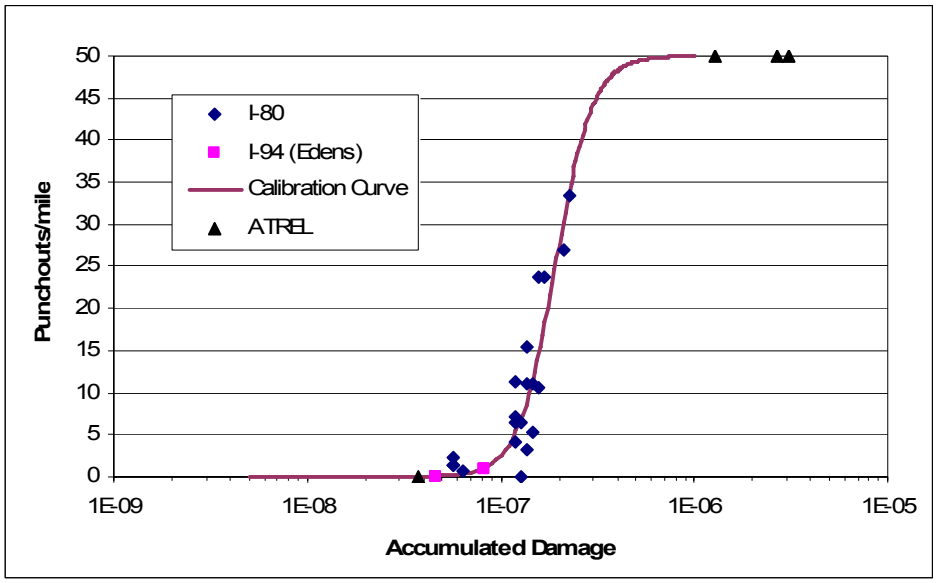

Figure 6. Relationship between accumulated fatigue damage and observed punchouts per mile for Illinois CRCP calibration data set (S-curve punchout model).

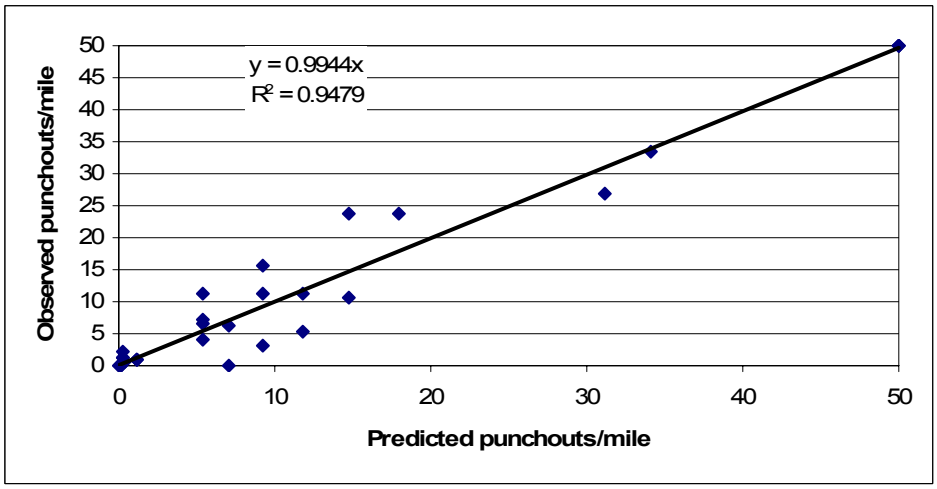

Figure 7. Predicted punchouts per mile versus observed punchouts per mile for Illinois CRCP calibration data set (S-curve punchout model).

3.2.2 Crack Spacing and Punchouts

Visual surveys of in-service pavements were used to determine typical mean crack spacings and punchouts per mile in Illinois. In June 2007, IDOT conducted a visual survey of Interstate 39 (I-39) just north of Normal, Illinois with a video survey van. Overhead images of the pavement surface were made using two cameras mounted on the front of the van. For this analysis, the northbound and southbound driving lanes of I-39 from milepost 2.580 to milepost 5.370 were examined.

3.2.2.1 Crack Spacing

Four northbound and four southbound segments of I-39 were examined to determine their respective mean crack spacing. The segments were selected such that regions near bridges and merging ramps were excluded. The spacings were found by dividing the length of each segment (501.60 ft) by the number of individual slabs (number of cracks plus one). The observed crack spacings and segment locations are shown in Table 10.

For all segments examined, the average observed crack spacing was 4.54 ft. This value falls within the 2-to-6-ft range that is typically associated with CRCP (ARA, 2003b). The average observed crack spacing also falls near the upper bound of the 3.5-to-4.5-ft crack spacings calculated by this design software for typical Illinois design inputs (Beyer and Roesler, 2009).

Table 10. Observed Crack Spacing and Location on I-39 CRCP Sections

Segment			**Observed Crack Spacing**	
Direction of Travel	**Starting Milepost**	**Ending Milepost**	**(ft)**	**(in.)**
North	2.678	2.773	3.66	43.9
	3.354	3.449	4.78	57.3
	4.076	4.171	5.34	64.0
	5.218	5.313	5.34	64.0
South	5.201	5.106	4.40	52.8
	4.609	4.514	4.82	57.9
	3.460	3.365	4.08	48.9
	2.758	2.663	3.92	47.0
North average			4.78	57.3
South average			4.30	51.7
Overall average			4.54	54.5

3.2.2.2 Punchouts

The entire length of the northbound and southbound driving lanes within the surveyed area were examined for punchouts. For this analysis, punchouts were specifically defined as those locations bounded by two closely spaced transverse cracks, a longitudinal crack, and the edge of the pavement. In addition, locations with asphalt patches at the edge of the pavement and concrete patches the entire width of the driving lane were counted as punchouts because it is assumed that these maintenance activities were done because of earlier punchouts at these locations. Figure 8(a)-(c) shows examples of each type of CRCP punchout distress.

Shown in Figure 8(d) is an example of extended longitudinal cracking that was observed in the surveyed area. Previous work by Roesler et al (2005b) found thin, closely spaced longitudinal cracking on sections of I-39 and I-57 in Illinois. Most of this cracking ranged from 2 to 10 ft in length and had small crack widths. It was determined that settlement of the reinforcing steel in the concrete was the cause of the longitudinal cracking.

The longitudinal cracking observed in the surveyed area of I-39 had an average length of 90 ft per occurrence and appears to have wide crack widths. It is unclear whether this behavior is due to settlement of the reinforcing steel or some other mechanism, but mechanical loading is not suspected, and it is not believed that this type of longitudinal cracking is related to traditional punchouts. Punchouts and patches located within areas with extended longitudinal cracking were not considered for this analysis.

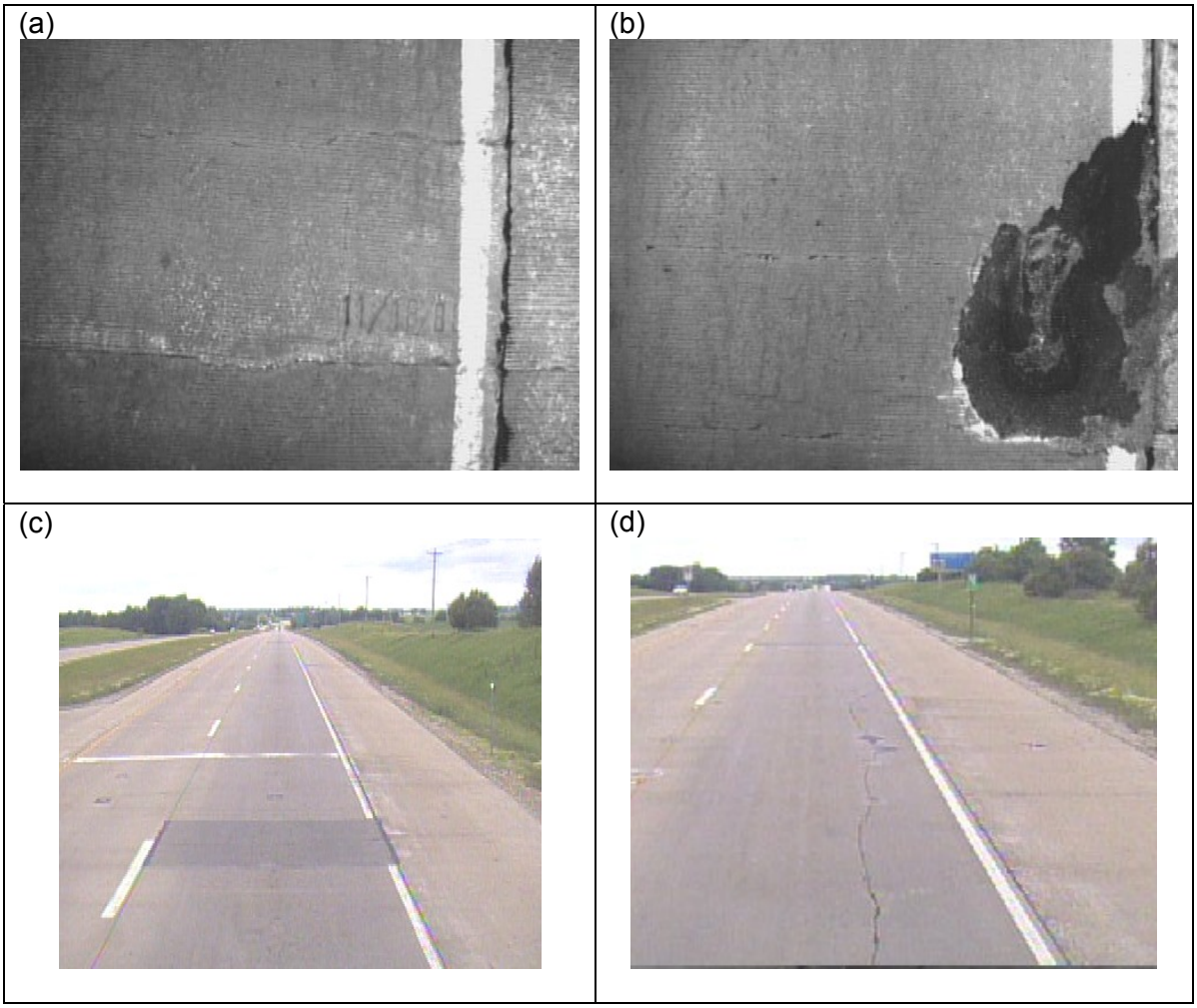

Figure 8. Observed CRCP distresses, including (a) traditional punchout, (b) asphalt patching, (c) concrete patching, and (d) extended longitudinal cracking.

The number of observed punchouts/patches and longitudinal cracking are shown in Table 11. Only two traditional punchouts were observed over the length of the surveyed area, with both occurring in the northbound driving lane. The majority of the observed patches (sixteen out of nineteen) were concrete patches.

Table 11. Observed Punchouts/Patches and Longitudinal Cracking on I-39

Segment			Observed Punchouts/ Patches	Observed Longitudinal Cracking (ft)
Direction of Travel	Starting Milepost	Ending Milepost		
North	2.580	5.370	16	750
South	5.367	2.600	5	954
North average distress / mile			5.8	270.8
South average distress / mile			1.8	344.8
Overall average distress / mile			3.8	307.8

These crack spacing and punchout results for I-39 provide insight into the performance of Illinois CRCP built in the last 20 years. The cumulative ESALs for this

section at the end of 2006 was approximately 24×10^6. This punchout information was not used in the initial calibration of the punchout prediction models, since the base was cement treated.

3.3 DESIGN CHARTS

The design equations and algorithms presented in Chapter 2 and CRCP inputs in this chapter were implemented in an MS EXCEL spreadsheet with the use of *Visual Basic* (Beyer and Roesler, 2009). CRCP design charts were generated using the design inputs shown in Table 12. Figure 9 and Figure 10 show the evolution of punchouts per mile with time for both the power and S-curve punchout prediction models, respectively. Since much of the performance data is weighted toward the end of the CRCP design life, the performance at intermediate ages is less reliable than at the end of the design life.

Table 12. Inputs for CRCP Design Charts

Design Input		**Design Input**	
Design life	variable	γ_{PCC}	1.22 ft^2/day
Aggregate type	limestone	CC	600 lb/yd^3
Shoulder type	variable	*Base type*	ATB
Design ESALs	variable	f	7.5
Annual growth factor	0%	LTE_{base}	30%
E_{PCC28}	4.40 x 10^6 psi	*Construction season*	summer
μ_{PCC}	0.15	$rh_{PCC,\zeta}$	85%
α_{PCC}	5.50 x 10^{-6} 1/°F	R	1.0
f'_{c28}	4,500 psi	*k-value*	100 psi/in.
MOR_{90}	750 psi	*Fatigue equation*	zero-maintenance
$\hat{R}$	0.8	*Reliability*	variable
ε_{∞}	780 x 10^{-6} in./in.	*Failure criterion*	10 PO/mile

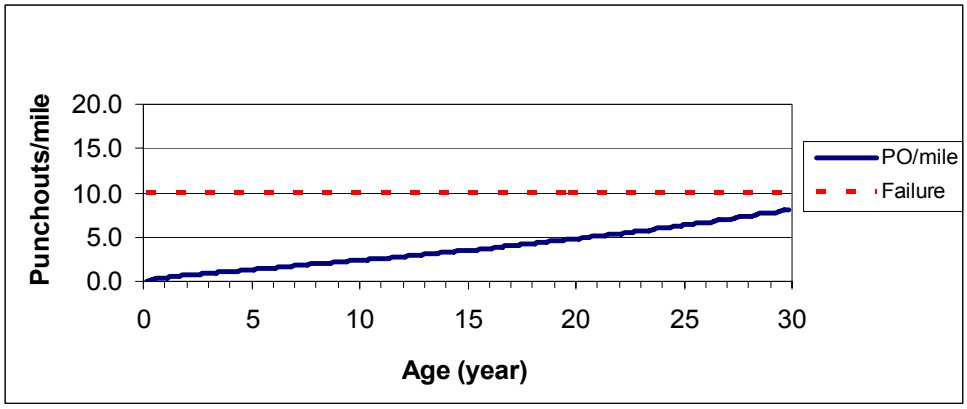

Figure 9. Relationship between number of punchouts per mile and age for 30-year design life, h_{PCC} = 11 in., k_d = 100 psi/in., tied concrete (separated) shoulders, 70 million ESALs, and 95% reliability (power function punchout model).

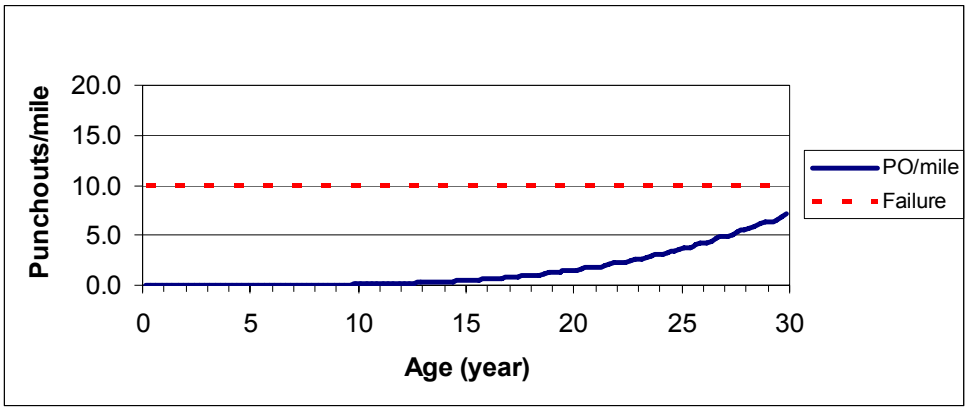

Figure 10. Relationship between number of punchouts per mile and age for 30-year design life, h_{PCC} = 11 in., k_d = 100 psi/in., tied concrete (separated) shoulders, 70 million ESALs, and 95% reliability (S-curve punchout model).

The design charts were developed based on the S-curve punchout model. For these design charts, CRCP failure was defined as 10 punchouts per mile. Figures 11 through 22 show the required concrete thicknesses (in 0.5-in. increments) for different design lives (20 and 30 years), loading *k*-values (50, 100, and 200 psi/in.), reliabilities (50 and 95%), and shoulder type (tied concrete [monolithic], tied concrete [separate], and asphalt/granular). For the design charts plotted below, a 20-year design assumed 0.7% steel, No. 6 bar, and 3.5-in. depth to steel. For the 30-year design charts, 0.8% steel, No. 7 bar, and 4.5-in. depth to steel were assumed.

3.3.1 Modulus of Subgrade Reaction (k_d = 50 psi/in.)

Figures 11 through 14 show the required concrete thicknesses for 50 psi/in. modulus of subgrade reaction and several levels of traffic and shoulder types.

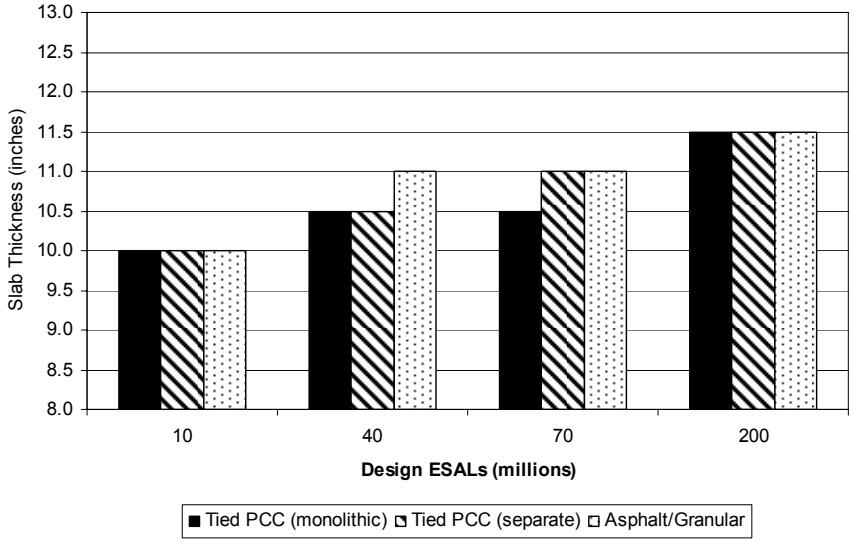

Figure 11. Design chart for 20-year design life, 50% reliability, and 50 psi/in. modulus of subgrade reaction.

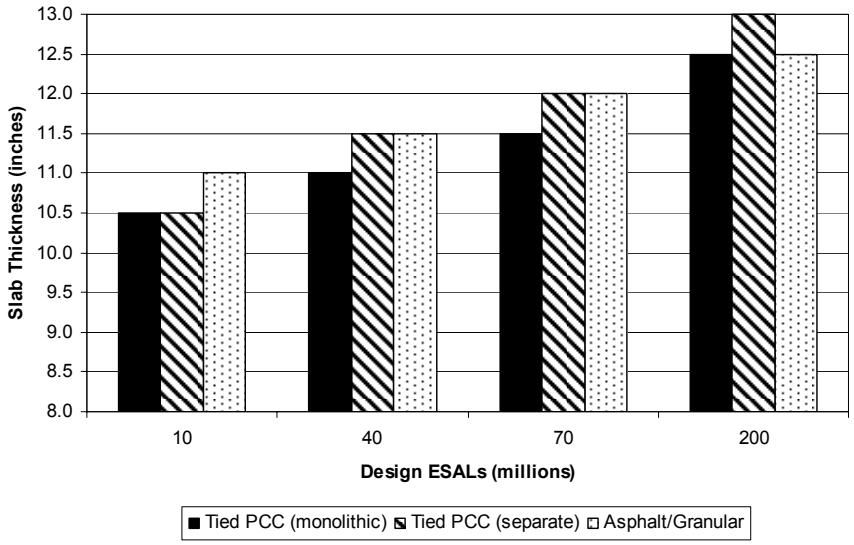

Figure 12. Design chart for 20-year design life, 95% reliability, and 50 psi/in. modulus of subgrade reaction.

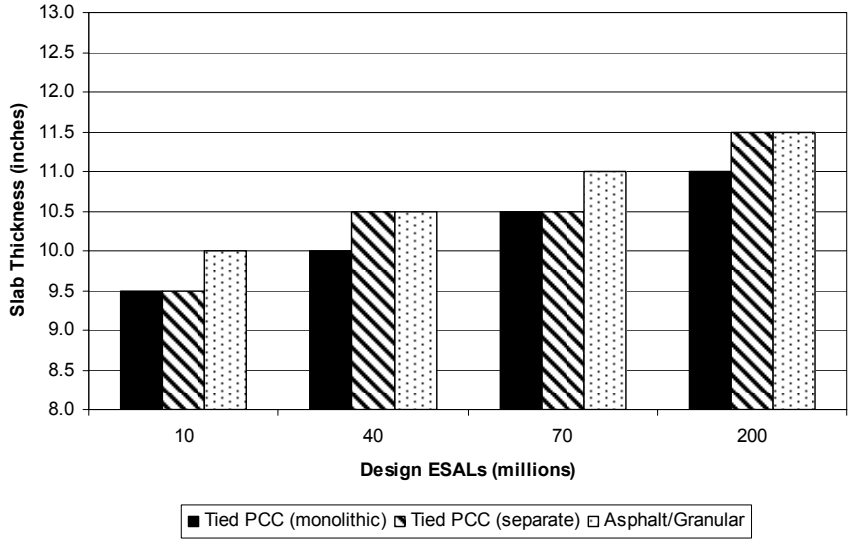

Figure 13. Design chart for 30-year design life, 50% reliability, and 50 psi/in. modulus of subgrade reaction.

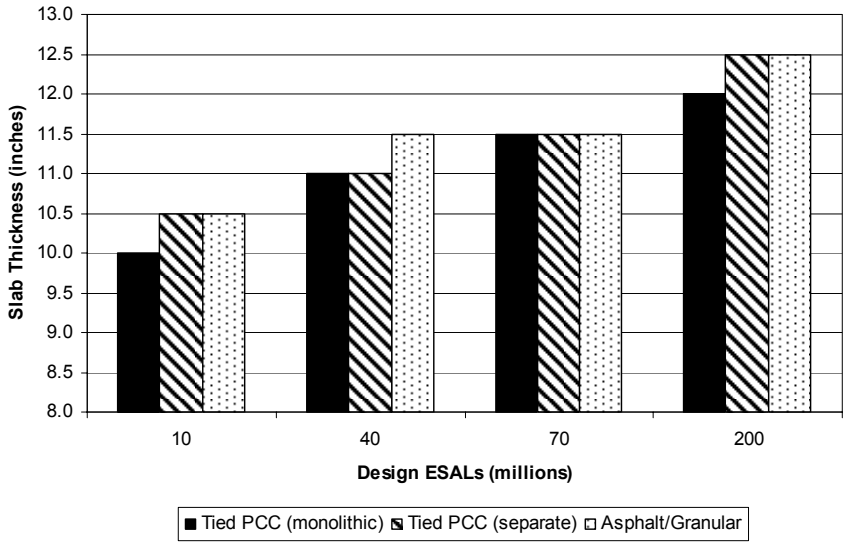

Figure 14. Design chart for 30-year design life, 95% reliability, and 50 psi/in. modulus of subgrade reaction.

3.3.2 Modulus of Subgrade Reaction (k_d = 100 psi/in.)

Figures 15 through 18 show the required concrete thicknesses for 100 psi/in. modulus of subgrade reaction and several levels of traffic and shoulder types.

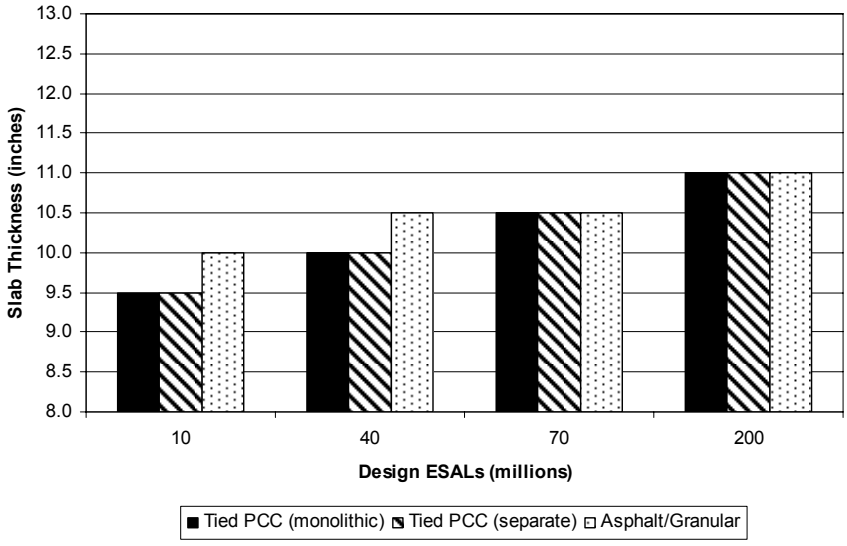

Figure 15. Design chart for 20-year design life, 50% reliability, and 100 psi/in. modulus of subgrade reaction.

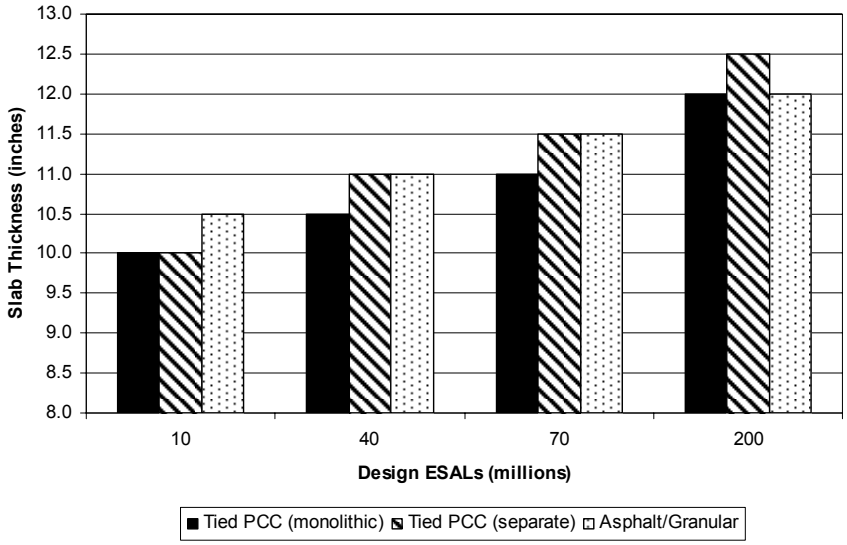

Figure 16. Design chart for 20-year design life, 95% reliability, and 100 psi/in. modulus of subgrade reaction.

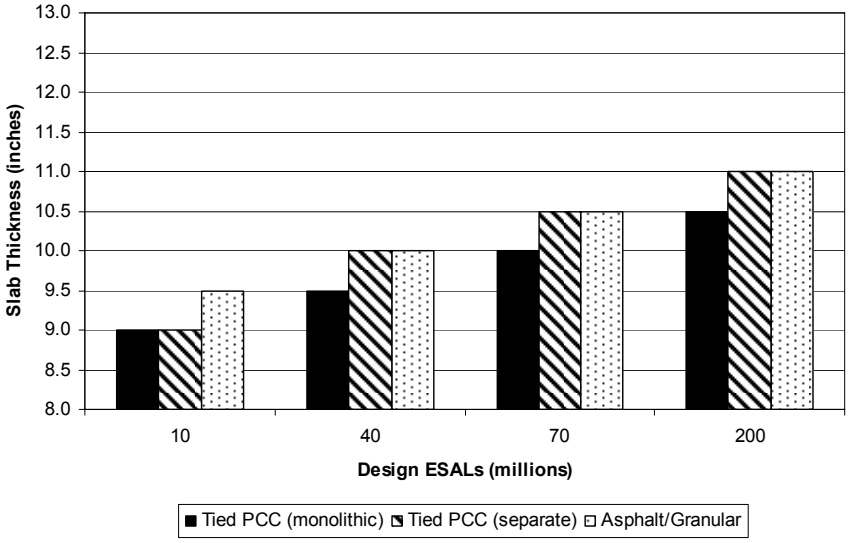

Figure 17. Design chart for 30-year design life, 50% reliability, and 100 psi/in. modulus of subgrade reaction.

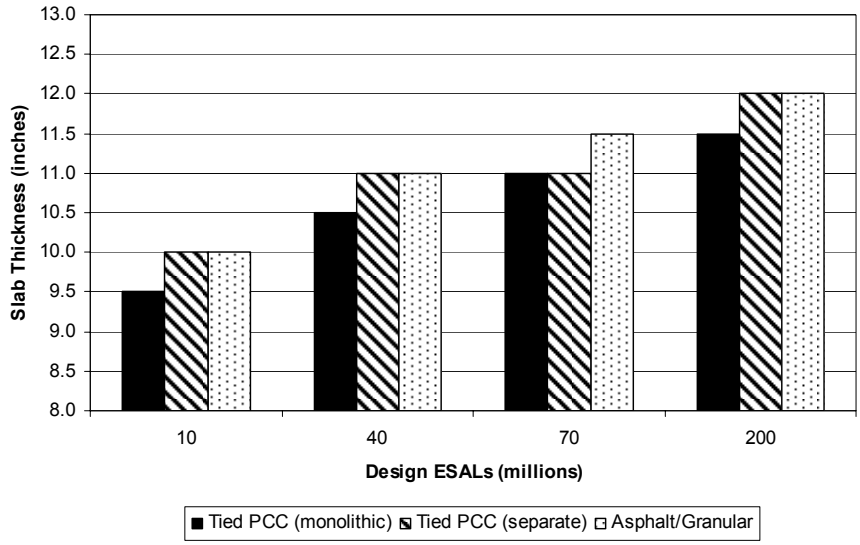

Figure 18. Design chart for 30-year design life, 95% reliability, and 100 psi/in. modulus of subgrade reaction.

3.3.3 Modulus of Subgrade Reaction (k_d = 200 psi/in.)

Figures 19 through 22 show the required concrete thicknesses for 200 psi/in. modulus of subgrade reaction and several levels of traffic and shoulder types.

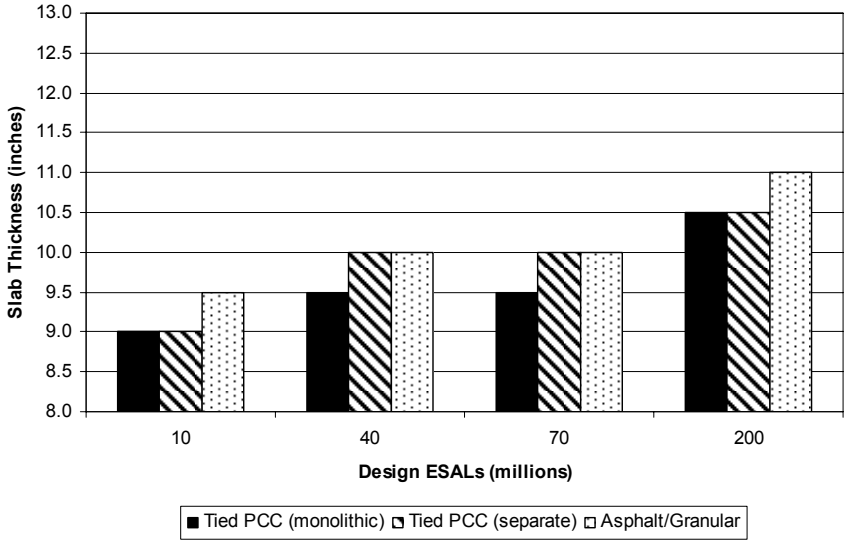

Figure 19. Design chart for 20-year design life, 50% reliability, and 200 psi/in. modulus of subgrade reaction.

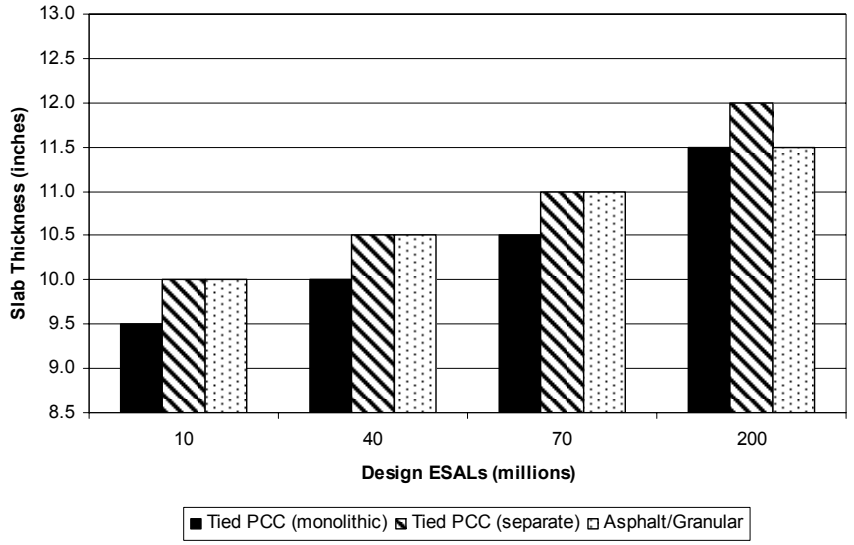

Figure 20. Design chart for 20-year design life, 95% reliability, and 200 psi/in. modulus of subgrade reaction.

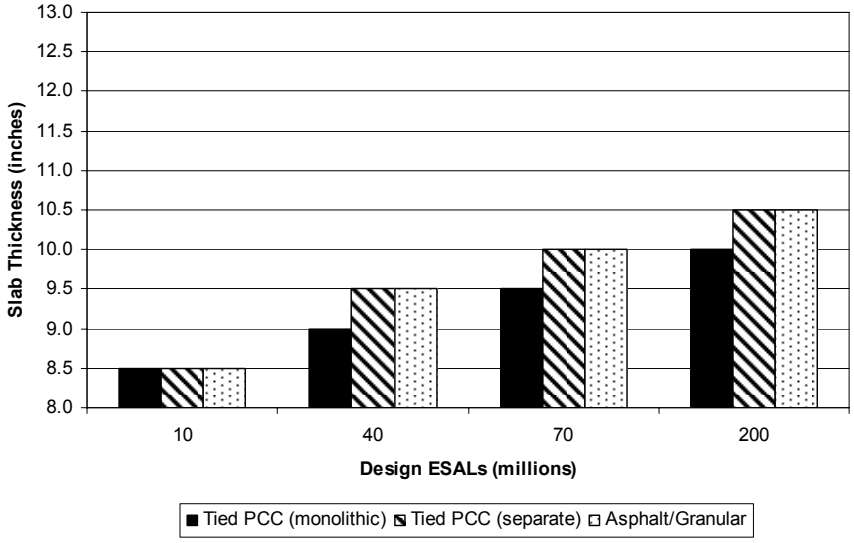

Figure 21. Design chart for 30-year design life, 50% reliability, and 200 psi/in. modulus of subgrade reaction.

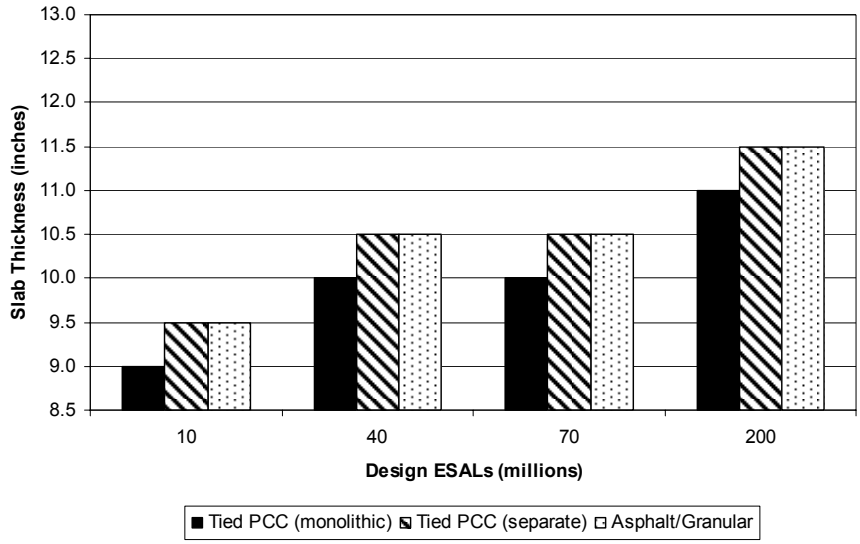

Figure 22. Design chart for 30-year design life, 95% reliability, and 200 psi/in. modulus of subgrade reaction.

3.3.4 Current IDOT CRCP Thicknesses

For comparison purposes, the required slab thicknesses for the current IDOT and proposed M-E CRCP design procedures are shown in Table 13. Note that both design procedures only consider 20-year designs and tied concrete shoulders. The M-E design procedure thicknesses are for 95% reliability. The thicknesses derived for 10 million ESALs shown in Table 13 for the proposed M-E CRCP procedure are overly conservative due to most of the performance data being obtained on sections with 20 to 50 million ESALs. In the future, increasing the failure criteria for CRCP to 20 punchouts per mile may be warranted for designs with only 10 million ESALs. The percent slabs cracked is also increased for IDOT's JPCP design for total ESALs less than 10 million (Zollinger and Barenberg, 1989).

Table 13. CRCP Thicknesses from Current IDOT and Proposed M-E Design Procedures

***k*-value (psi/in.)**	**Design ESALs (millions)**							
	10		**40**		**70**		**200**	
	IDOT	**M-E**	**IDOT**	**M-E**	**IDOT**	**M-E**	**IDOT**	**M-E**
50	9.5	10.5	11.0	11.0	12.0	11.5	13.5	12.5
100	9.0	10.0	11.0	10.5	12.0	11.0	13.5	12.0
200	9.0	9.5	11.0	10.0	12.0	10.5	13.5	11.5
NOTE: Both design procedures assume 20-year designs and tied concrete shoulders (monolithic). M-E design procedure assumes 95% reliability								

3.3.5 Design Input Sensitivity

3.3.5.1 Shoulder Type

Shoulder type has limited effect on required slab thickness. For a given traffic level, CRCP with tied concrete (separate) and asphalt/granular shoulders typically have the same slab thickness. These thicknesses are either equal to or 0.5 in.greater than the thicknesses for tied concrete (monolithic) shoulders. For 95% reliability, asphalt/granular shoulders can

result in slab thicknesses less than the thicknesses required for tied concrete (separate) shoulders. This result is counterintuitive, because asphalt/granular shoulders have much less shoulder load transfer than tied concrete (separate) shoulders.

Calculations of tensile stress and fatigue damage indicate that the stresses at the bottom of the slab control for tied concrete shoulders, resulting in bottom-up cracking. For asphalt/granular shoulders, stresses at the top of the slab control, resulting in top-down cracking. This change in cracking type (top-down to bottom-up) is one reason that the use of asphalt/granular shoulders can result in slab thicknesses less than those for tied concrete (separate) shoulders. The use of the same load transfer efficiencies (40%) at the tied shoulder (separated) joint and longitudinal contraction joint for the ISLAB2000 stress analysis was also a significant contributing factor.

3.3.5.2 Subgrade Modulus of Reaction

An increase in the subgrade modulus of reaction (*k*-value) results in a decrease in required slab thickness. Decreases in thickness of 1.0 in. occur typically when the *k*-value is changed from 50 psi/in. to 200 psi/in. for a given shoulder type, reliability, and traffic level.

3.3.5.3 Traffic Level

The traffic level appears to be the controlling variable. For a given shoulder type, reliability, and subgrade modulus, an increase in traffic from 10 million to 200 million ESALs results in increases of 2.0 in. in required slab thickness.

3.3.5.4 Reliability

An increase in reliability from 50 to 95% typically results in an increase of 0.5 to 1.5 in. in the required slab thickness, depending on the shoulder type, traffic, and soil type.

3.3.5.5 Strength Reduction Factor

The design charts presented above include a strength reduction factor ($\hat{R}$) of 0.8 to account for differences in the strength of the concrete at the top and bottom of the slab. When no strength difference is assumed ($\hat{R} = 1.0$), the majority of stresses at the bottom of the slab control for asphalt/granular shoulders. This change from top-down to bottom-up cracking results in a reduction of 0.5 to 1.0 in. in required thicknesses. Twenty-year design charts using asphalt/granular shoulders and no reduction in strength are shown in Figure 23 and Figure 24. A change in the strength reduction factor from 0.8 to 1.0 has no effect on the required thicknesses for tied concrete shoulders.

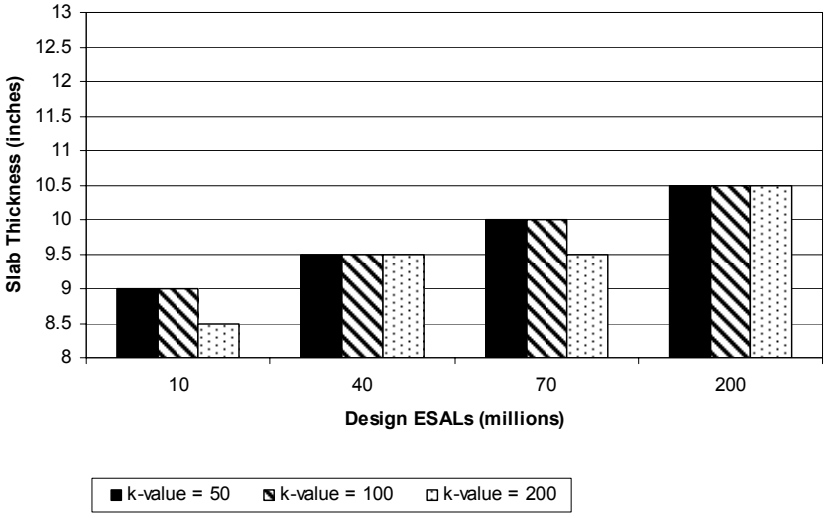

Figure 23. Design chart for 20-year design life, 50% reliability, asphalt concrete shoulders, and $\hat{R}$ = 1.0.

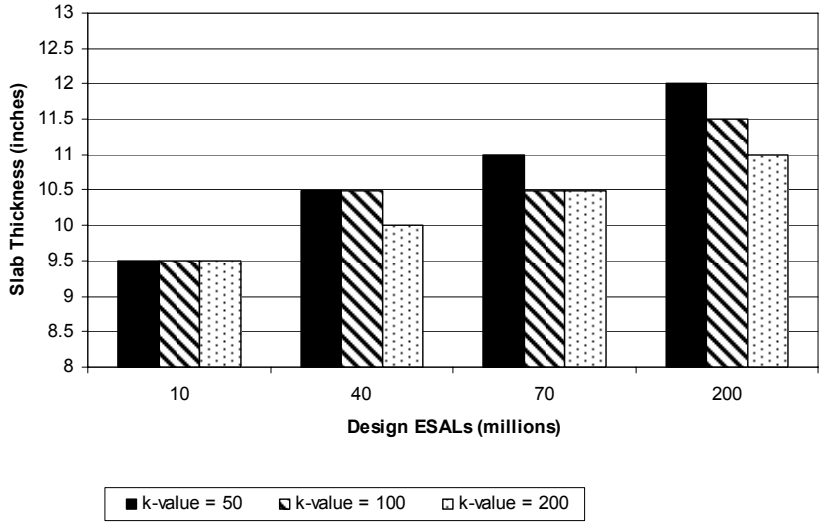

Figure 24. Design chart for 20-year design life, 95% reliability, asphalt concrete shoulders, and $\hat{R}$ = 1.0.

3.4 LIMITATIONS

The CRCP design procedure as presented in this report is subject to the following design limitations.

3.4.1 Calculation of Total Tensile Stress

The use of a total stress correction factor (R) of 1.0 assumes that the principle of superposition is valid. However, extensive literature and a limited analysis with ISLAB2000 both indicate that error is introduced into the calculation of total stress when using superposition. In the proposed design framework, it is assumed that any error is accounted for by calibration with field data.

3.4.2 Erosion and Loss of Support

Erosion of the subbase and subsequent loss of support under the slab has been identified as a primary cause of punchout formation. Erosion and permanent deformation of the support layers increase the stresses in the slab, but are not explicitly accounted for in this design procedure because of the difficulty in defining support loss. The M-E PDG considers permanent loss of support due to erosion by specifying areas under the slab where the modulus of subgrade reaction is zero. In the M-E PDG model, the extent of the void from the shoulder is predicted as a function of pavement age, percent subgrade passing the No. 200 sieve, mean annual precipitation, and a base erodibility index (Selezneva et al., 2004). Since limited erosion data exist for defining this void area and because of the complexity involved in adding this concept to the stress analysis prediction algorithms, this design framework does not include an erosion factor at this time. This will be addressed further in a subsequent study.

3.4.3 CRCP Performance Data

Calibration of the calculated damage to observed punchouts was completed in Section 3.2 for a limited number of CRCP sections. Calibration and verification of the punchout prediction models with additional Illinois performance data is needed. Surveys of crack spacing, punchouts, and estimated traffic on CRCP sections built in the last 20 years, such as I-39, I-70, and I-94 (Kennedy expressway), will increase the confidence level of the design procedure.

3.4.4 Fatigue Damage

The stresses calculated by this design procedure are extremely small and therefore, the fatigue damage is much smaller than typically seen for other rigid pavement designs. This is a further indication that detailed calibration is needed to link stresses and fatigue damage to CRCP performance. Philosophically, the magnitude of the fatigue damage raises the question as to whether a cumulative damage approach is the most efficient design method for CRCP. A future alternative approach to complement the stress and fatigue damage analysis is to check the deformation levels in the underlying support layers. High deflections can cause erosion of the base/subbase layer or permanent deformation in any of the support layers or both.

3.4.5 Reliability

A traffic multiplier is currently used to introduce reliability into the proposed design procedure, but greater justification is needed for the selection of this value. The M-E PDG uses the standard error of the measured punchouts to account for reliability. The use of field punchout data variability in determining reliability has some degree of reasonableness,

but is limited by the quality and quantity of the punchout data, and probably is not the best way to account for reliability.

3.4.6 Widened Lanes

The design procedure does not handle widened lanes. The critical tensile stresses and equivalent damage ratios obtained from the ISLAB2000 analyses assume 12-ft lanes. These analyses would need to be repeated for this design procedure to consider widened lanes. In the proposed method, the thickness design of widened lanes should be made the same as tied concrete shoulder (monolithic).

3.4.7 Crack Spacing Equation

The crack spacing equation proposed by M-E PDG can give reasonable crack spacing, assuming the correct inputs are selected. However, more work is needed in this model to better simplify the prediction. Many detailed calculations are involved in the prediction of the mean crack spacing, and these equations (e.g., bond–slip relationship, coefficient of slab–base friction, effective slab length, etc.) include numerous empirical coefficients. Research is still needed to better link field cracking patterns with theoretical models, given a limited number of user-defined inputs.

3.4.8 Controlling Stress

The tensile stresses at the bottom of the slab control for tied concrete shoulders. The bottom stresses also control for asphalt shoulders when no reduction in strength between the top and bottom of the slab is assumed. Punchouts typically occur at the edge of the slab. Based on the critical stress locations shown in Figure 3, it would be reasonable to assume that the critical tensile stresses at the top of the slab would be responsible for the majority of punchout development. The fact that the bottom stresses control in this design procedure may be related to the use of tied concrete shoulders (the standard design in Illinois). It also could be due to the way in which the critical stresses and locations were obtained from the ISLAB2000. The longitudinal contraction joint LTE and shoulder LTE likely have different values, but were assumed to be the same for this analysis. Furthermore, no erosion or permanent deformation near the edge of the pavement was assumed for the analysis, which reduces the top tensile stresses significantly.

CHAPTER 4. CONCLUSIONS AND RECOMMENDATIONS

Continuously reinforced concrete pavements (CRCP) have been used extensively in Illinois. Punchouts have been the primary structural distress for this rigid pavement type. A design framework has been developed for Illinois based on mechanistic-empirical design concepts which have been derived from other researchers and further refined in this effort. This procedure is based in large part on models contained in the M-E PDG and work done over the years by Dr. Dan Zollinger of Texas A&M University. The proposed CRCP design process can account for environmental effects and variations in traffic volume, pavement layer and slab geometry, and layer material property inputs for Illinois. This structural design procedure is based on first calculating the mean crack spacing and then conducting a cumulative fatigue damage analysis to determine the expected number of CRCP punchouts at the end of the design life.

New developments included in this proposed design procedure are the calculation of critical load stresses at the top and bottom of the CRCP slab, the determination of equivalent damage ratios for several shoulder types and crack stiffnesses, the implementation of a reduced concrete strength at the surface of the concrete, and the use of a bounded model to predict punchouts from the accumulated damage. Critical tensile stresses at the top and bottom of the slab were found using the finite element analysis program ISLAB2000 for several shoulder types, crack spacing, radius of relative stiffness, and transverse crack stiffness values. The tensile stresses at the bottom of the slab control the required slab thickness for tied concrete shoulders. The top tensile stresses control for asphalt concrete shoulders only when a reduction in strength between the top and bottom of the slab is defined. Equivalent damage ratios at both the top and bottom of the slab were used to account for wander of truck traffic within the driving lane. These equations were derived from multiple finite element runs at various lateral distributions from the lane-shoulder joint and are a function of the nondimensional slab size ratio and joint stiffness values. Two punchout prediction models are used to describe the evolution of punchouts as a function of accumulated fatigue damage, including a new logistic-type function. A limited set of CRCP field performance data with typical design inputs was used to calibrate these models for Illinois.

Design charts developed from this design procedure indicate that required slab thicknesses have limited sensitivity to shoulder type and subgrade modulus of reaction, and are instead largely controlled by traffic level and design reliability. Because the design procedure can be implemented in software such as MS EXCEL and Visual Basic, designers and future researchers have the ability to refine the assumptions and procedures detailed in this report. It is recommended that IDOT analyze additional CRCP performance data and adopt a design catalogue for the state based on design life and traffic.

REFERENCES

AASHTO (1993). *Guide for Design of Pavement Structures*. American Association of State Highway and Transportation Officials, Washington, DC.

ACI Committee 209, (1992). *Prediction of Creep, Shrinkage, and Temperature Effects in Concrete Structures*, ACI 209R-92, American Concrete Institute, Farmington Hills, MI, pp. 1-47.

Altoubat, S. A. and D. A. Lange, (2001). Creep, Shrinkage, and Cracking of Restrained Concrete at Early Age, *ACI Materials Journal*, Vol. 98, No. 4, , pp. 323-331.

ARA, (2003a *). Guide for Mechanistic-Empirical Design of New and Rehabilitated Pavement Structures*, Appendix FF, *Calibration Sections for Rigid Pavements*, NCHRP 1-37A, Report, Final draft, Applied Research Associates, Inc., Albuquerque, NM.

ARA, (2003b *). Guide for Mechanistic-Empirical Design of New and Rehabilitated Pavement Structures,* Part 2, Design Inputs, Chapter 2, *Material Characterization*, NCHRP 1-37A, Report, Final draft, Applied Research Associates, Inc., Albuquerque, NM

ARA, (2004a *).Guide for Mechanistic-Empirical Design of New and Rehabilitated Pavement Structures*, Part 3, Design Analysis, Chapter 4, *Design of New and Reconstructed Rigid Pavements*, NCHRP 1-37A, Report, Final draft, Applied Research Associates, Inc., Albuquerque, NM.

ARA, (2007). *Interim Mechanistic-Empirical Pavement Design Guide Manual of Practice*, Final draft, Applied Research Associates, Inc., Albuquerque, NM.

Barenberg, E. J., (1991). *Revised Design Curves*, Memo to Illinois Department of Transportation, University of Illinois at Urbana-Champaign, Urbana, IL,.

Beyer, M. A. and Roesler J. R. (2008a). Effective Initial Crack Depth on Concrete Surfaces, *9th International Conference on Concrete Pavements*, San Francisco, CA, Aug 17-21, International Society of Concrete Pavements.

Beyer, M. A. and Roesler, J. R , (2009). UIUC CRCP Design Software, (Version 5.5), University of Illinois at Urbana-Champaign, Urbana, IL, 2009.

Bordelon, A., Roesler, J.R., and Hiller, J.E., (2009). *Mechanistic-Empirical Design Concepts for Jointed Plain Concrete Pavements in Illinois*, Final report, Illinois Center for Transportation, University of Illinois, Urbana, IL, 252 pp.

Bradbury, R. D., (1938). *Reinforced Concrete Pavements*, Wire Reinforcement Institute, Washington, D.C..

Crovetti, J. A., (1994). *Evaluation of Jointed Plain Concrete Pavement Systems Incorporating Open-Graded Permeable Bases*. PhD dissertation, University of Illinois at Urbana-Champaign, Urbana, IL.

Darter, M. I., (1977). *Design of Zero-Maintenance Plain Jointed Pavements*, Report No. FHWA-RD-77-111, Federal Highway Administration, U.S. Department of Transportation, Washington, D.C..

ERES, (1999). ISLAB2000 Finite Element Code for Rigid Pavement Analysis, (version 3.6), ERES Consultants, Inc., Champaign, IL, 1999.

FAA, (1995). *Airport Pavement Design and Evaluation*, Advisory Circular 150/5320-6D, Federal Aviation Administration, U.S. Department of Transportation, Washington, D.C..
.

Gharaibeh, N. G., Darter, M. I. , and Heckel, L. B. , (1999). Field Performance of Continuously Reinforced Concrete Pavement in Illinois, *Transportation Research Record: Journal of the Transportation Research Board, No. 1684*, TRB, National Research Council, Washington, D.C., pp. 44-50.

Heath, A. C. and Roesler, J. R., (2000). Top-Down Cracking of Rigid Pavements Constructed with Fast Setting Hydraulic Cement Concrete, *Transportation Research Record: Journal of the Transportation Research Board, No. 1712*, TRB, National Research Council, Washington, D.C., pp. 3-12.

Huang, Y. H., (2004). *Pavement Analysis and Design*, 2nd ed., Prentice Hall, Upper Saddle River, NJ..

IDOT, (2002). Pavement Design (Chapter 54) In *Bureau of Design and Environment Manual*, , Illinois Department of Transportation, Bureau of Materials and Physical Research, Springfield.

Khazanovich, L. and Gotlif, A., (2003). *Evaluation of Joint and Crack Load Transfer Final Report*, Report No. FHWA-RD-02-088, Federal Highway Administration, U.S. Department of Transportation, Washington, D.C..

Kohler, E. and Roesler, J., (December 2006). *Accelerated Pavement Testing of Extended Life Continuously Reinforced Concrete Pavement Sections*, Final report, Transportation Engineering Series No. 141, Illinois Cooperative Highway and Transportation Series No. 289, University of Illinois, Urbana, IL, 354 pp.

Kohler, E. R., (2005). *Experimental Mechanics of Crack Width in Full-Scale Sections of Continuously Reinforced Concrete Pavements*. PhD dissertation, University of Illinois at Urbana-Champaign, Urbana, IL,.

Larson, G. E. and Dempsey, B. J. (2008). Enhanced Integrated Climatic Model Software, (Version 3.4,) [University of Illinois, Urbana, IL. .

Lee, Y. H. and Darter, M. I., (1994). *Development of Pavement Prediction Models*, Research Report FHWA/IL/UI 250, Illinois Cooperative Highway Research Program, University of Illinois at Urbana-Champaign, Urbana, IL.

McCullough, B. F. and Dossey, T. , (1999). Considerations for High-Performance Concrete Paving: Recommendations from 20 Years of Field Experience in Texas, *Transportation*

Research Record: Journal of the Transportation Research Board, No. 1684, TRB, National Research Council, Washington, D.C., pp. 17-24.

Miner, M. A.,(1945). Cumulative Damage in Fatigue, *Journal of Applied Mechanics*, Vol. 12, No. 3, pp. A159-A164.

NCHRP, (2007). Mechanistic-Empirical Pavement Design Guide Software, (Version 1.000), National Cooperative Highway Research Program, National Academy of Sciences, Washington, DC.

PCA, (1984). *Thickness Design for Concrete Highway and Street Pavements*, Report No. EB109-01P, Portland Cement Association, Skokie, IL,.

Rao, C., Selezneva, O. , Darter, M. I. , Titus-Glover, L., and Khazanovich, L., (2004). Calibration of Mechanistic-Empirical Performance Model for Continuously Reinforced Concrete Pavement Punch-Outs, *Transportation Research Record: Journal of the Transportation Research Board, No. 1896*, Transportation Research Board of the National Academies, Washington, D.C., , pp. 15-22.

Rao, S. P., (2005), *Characterizing Effective Built-in Curling and its Effect on Concrete Pavement Cracking*, PhD dissertation,.University of Illinois at Urbana-Champaign, Urbana, IL.

Rodden, R. A., (2006). *Analytical Modeling of Environmental Stresses in Concrete Slabs*, MS thesis, University of Illinois at Urbana-Champaign, Urbana, IL.

Roesler, J.R., (1998). *Fatigue of Concrete Beams and Slabs*, PhD dissertation, University of Illinois at Urbana-Champaign, Urbana, IL,.

Roesler, J. R., Popovics, J.S., and Ranchero, J.L. , (2003). *Laboratory Investigation of Longitudinal Cracking on I-57 Continuously Reinforced Concrete Slabs*, Report to Illinois Department of Transportation, University of Illinois at Urbana-Champaign, Urbana, IL.

Roesler, J. R., Hiller, J. E. , and Littleton, P. C. , (2005a). Effect of Stress State on Concrete Slab Fatigue Resistance, *8th International Conference on Concrete Pavements*, Colorado Springs, CO, Aug 14-18,, Vol. III, International Society of Concrete Pavements, pp. 67-87.

Roesler, J. R., Popovics, J. S. , Ranchero, J. L. , Mueller, M., and Lippert, D., (2005b) . Longitudinal Cracking Distress on Continuously Reinforced Concrete Pavements in Illinois, *Journal of Performance of Constructed Facilities*, Vol. 19, No. 4,, pp. 331-338.

Roesler, J., Bordelon, A., Ioannides, A., Beyer, M., and Wang, V, (2008). *Design and Concrete Material Requirements for Ultra-Thin Whitetopping*, Research Report FHWA-ICT-08-016, Illinois Center for Transportation, University of Illinois at Urbana-Champaign, Urbana, IL.

Salsilli-Murua, R. A., (1991). *Calibrated Mechanistic Design Procedure for Jointed Plain Concrete Pavements*. PhD dissertation, University of Illinois at Urbana-Champaign, Urbana, IL.

Selezneva, O., Rao, C. , Darter, M.I., Zollinger, D., and Khazanovich, L., (2004). Development of a Mechanistic-Empirical Structural Design Procedure for Continuously Reinforced Concrete Pavements," *Transportation Research Record: Journal of the Transportation Research Board, No. 1896*, Transportation Research Board, of the National Academies, Washington, D.C., pp. 46-56.

Smith, K. D. and Roesler, J. R. , (2003). Review of Fatigue Models for Concrete Airfield Pavement Design, *ASCE Airfield Pavement Specialty Conference*, Las Vegas, NV, Sept. 21-24, American Society of Civil Engineering.

Thompson, M. R. and Cation, K., (1986). *A Proposed Full-Depth Asphalt Concrete Thickness Design Procedure*, Research Report FHWA/IL/UI 213, Illinois Cooperative Highway and Transportation Research Program, University of Illinois at Urbana-Champaign, Urbana, IL, 1986.

Walpole, R. E., Myers, R. H. , Myers, S. L. , and Ye, K., (2002). *Probability and Statistics for Engineers and Scientists*, 7th ed., Prentice Hall, Upper Saddle River, NJ.

Westergaard, H. M., (1927). Analysis of Stresses in Concrete Roads Caused by Variations of Temperature," *Public Roads*, Vol. 8, No. 3, pp. 54-60.

Zollinger, D. G. and Barenberg, E.J. , (1989). *Proposed Mechanistic Based Design Procedure for Jointed Concrete Pavements*, Research Report FHWA/IL/UI 225, Illinois Cooperative Highway Research Program, University of Illinois at Urbana-Champaign, Urbana, IL.

Zollinger, D. G. and Barenberg, E. J. , (1990). *Continuously Reinforced Pavements: Punchout and Other Distresses and Implications for Design*, Research Report FHWA/IL/UI 227, Illinois Cooperative Highway Research Program, University of Illinois at Urbana-Champaign, Urbana, IL.

APPENDIX A. SEASONAL TEMPERATURE DIFFERENTIAL FREQUENCY DISTRIBUTION

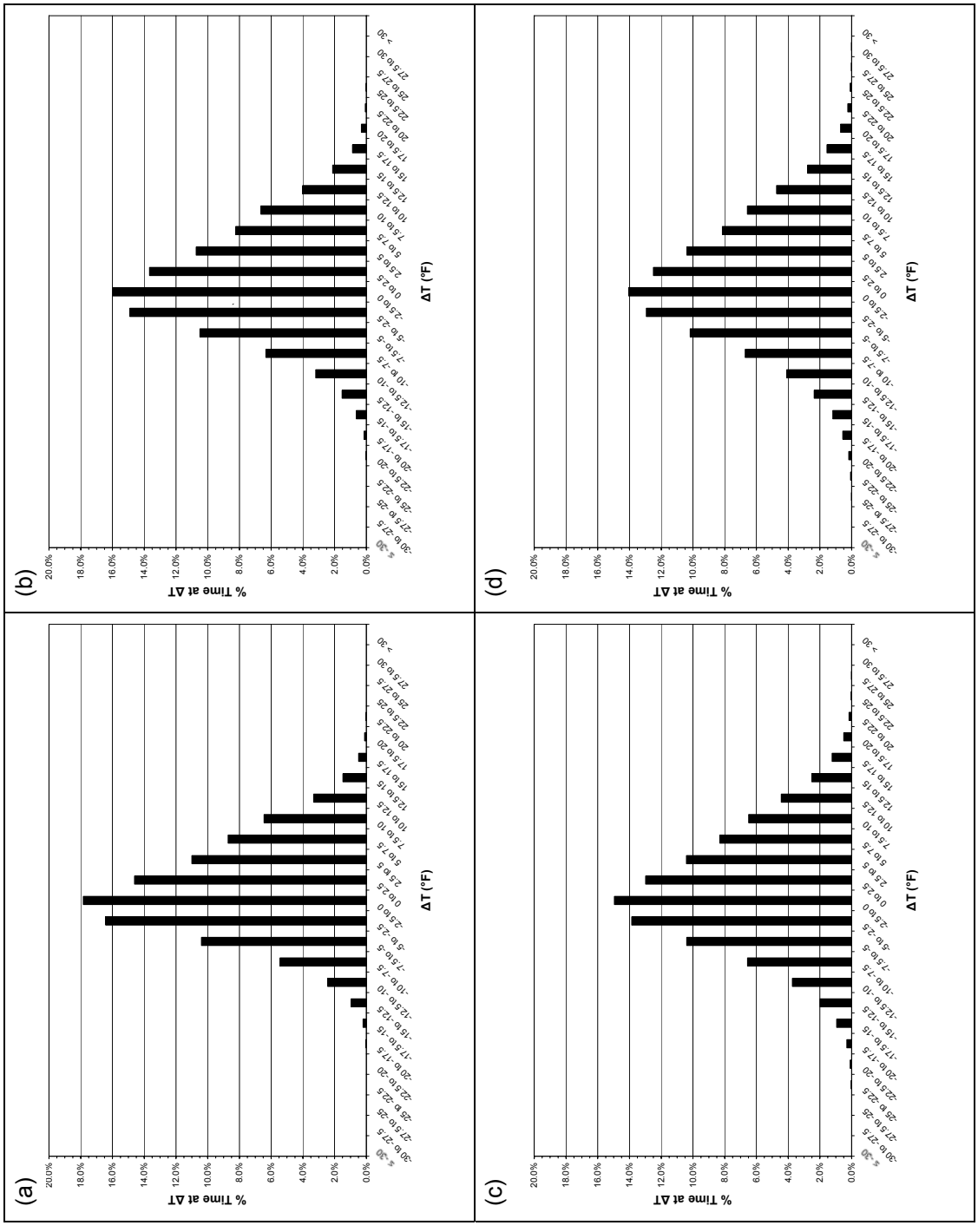

Figure A.1. Yearly temperature differential frequency distributions for concrete pavement in Champaign, Illinois with (a) 8-inch slab thickness, (b) 10 inch slab thickness, (c) 12-inch slab thickness, and (d) 14-inch slab thickness.

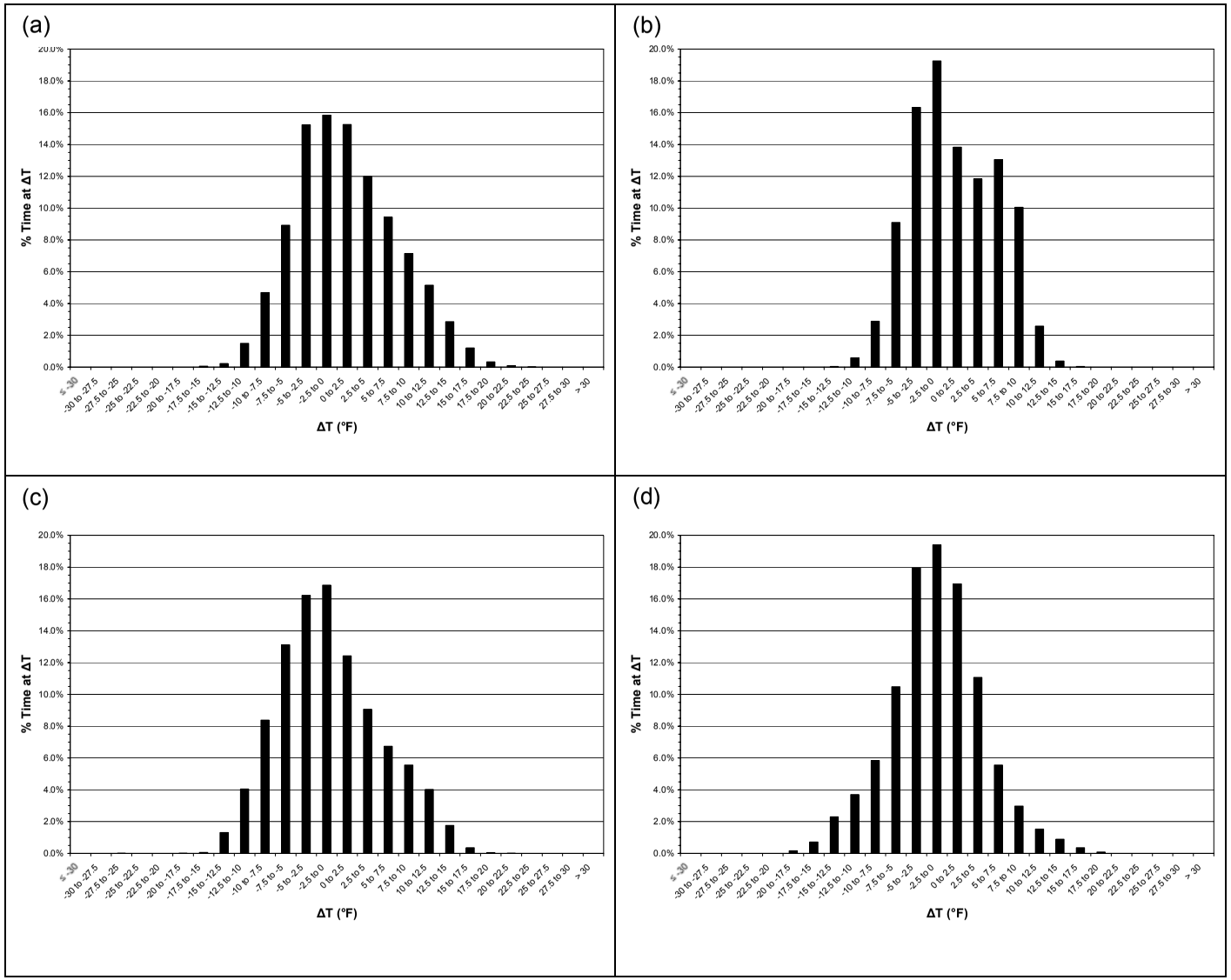

Figure A.2. Seasonal temperature differential frequency distributions for concrete pavement with 8-inch slab thickness in Champaign, Illinois for (a) spring, (b) summer, (c) fall, and (d) winter.

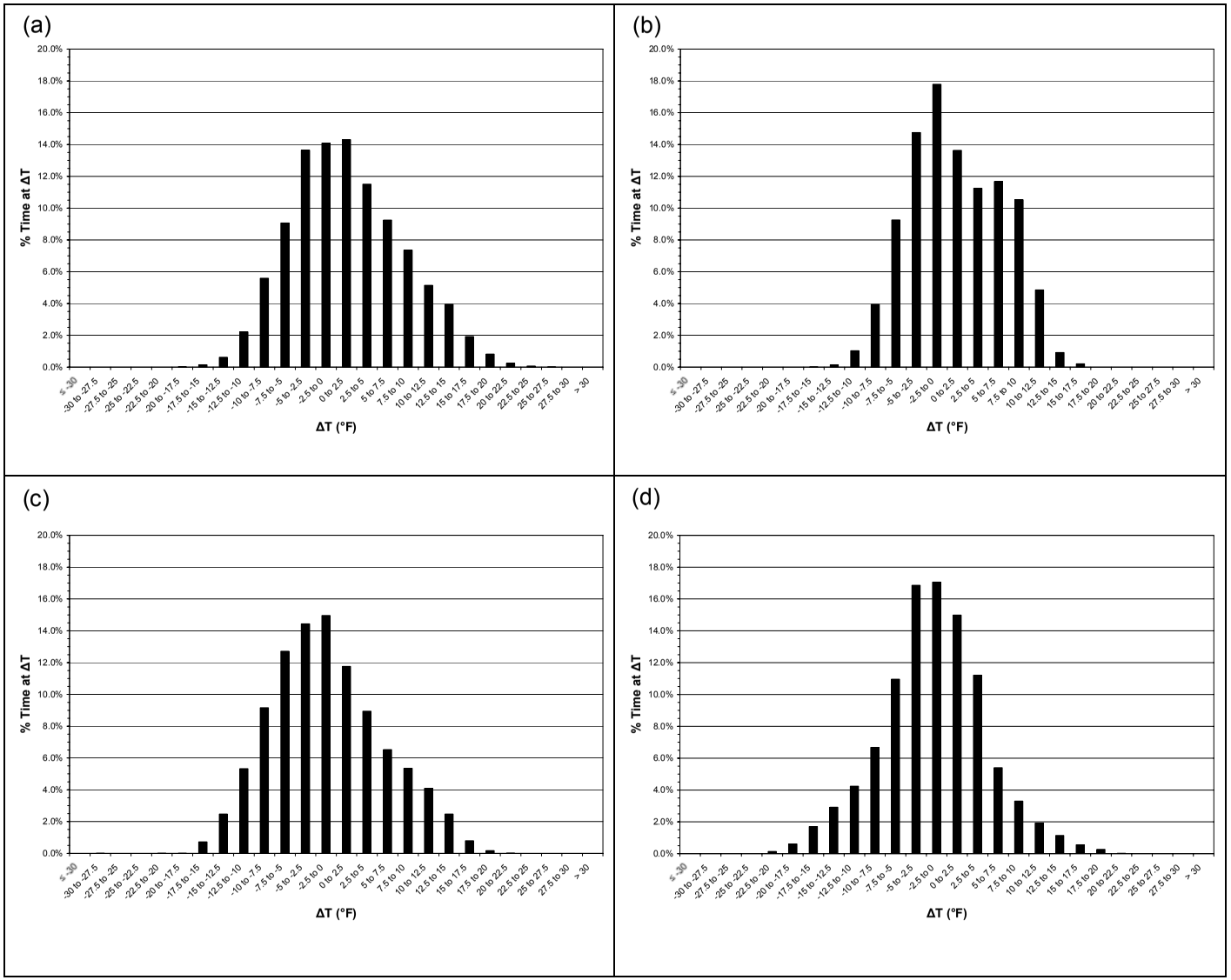

Figure A.3. Seasonal temperature differential frequency distributions for concrete pavement with 10-inch slab thickness in Champaign, Illinois for (a) spring, (b) summer, (c) fall, and (d) winter.

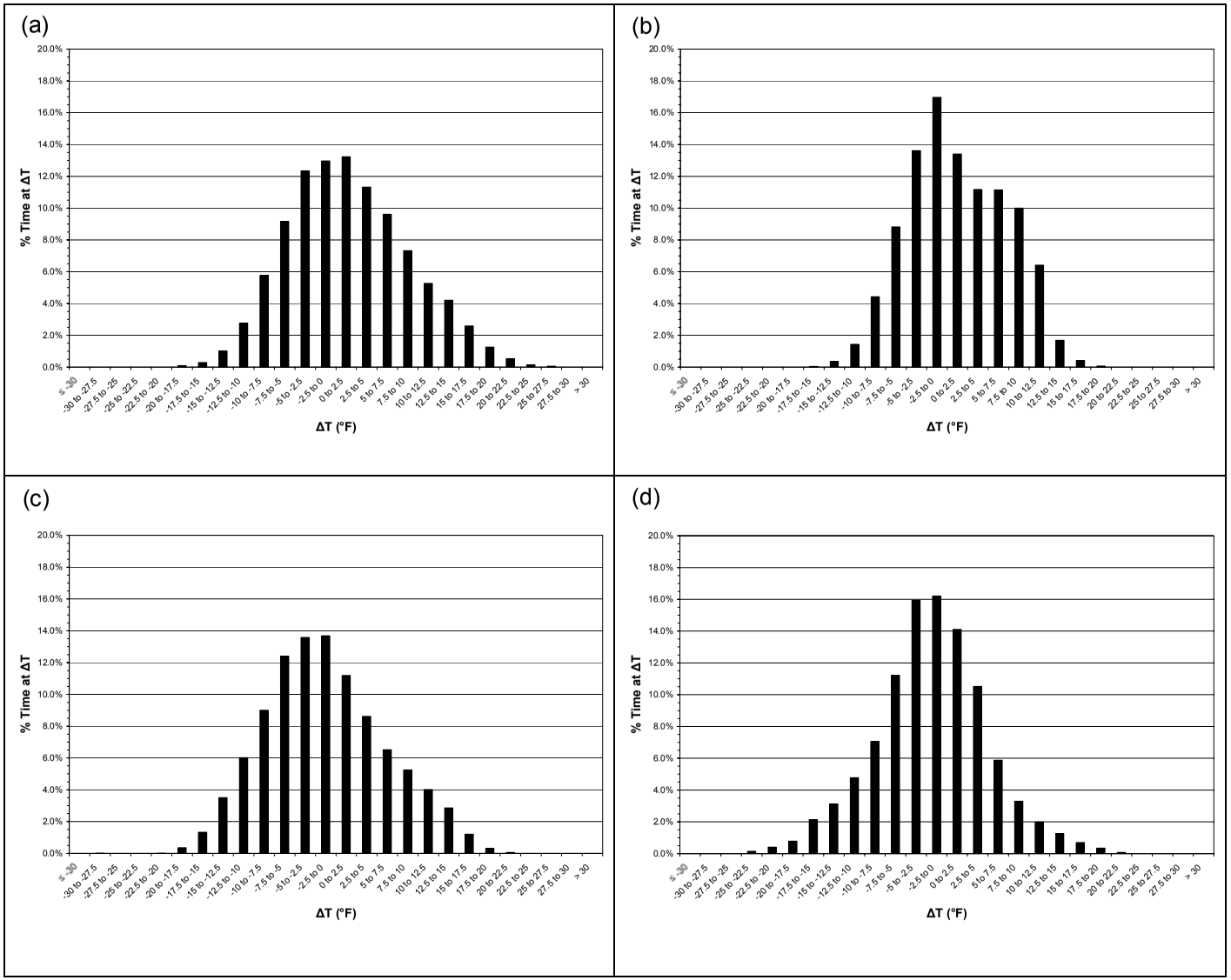

Figure A.4. Seasonal temperature differential frequency distributions for concrete pavement with 12-inch slab thickness in Champaign, Illinois for (a) spring, (b) summer, (c) fall, and (d) winter.

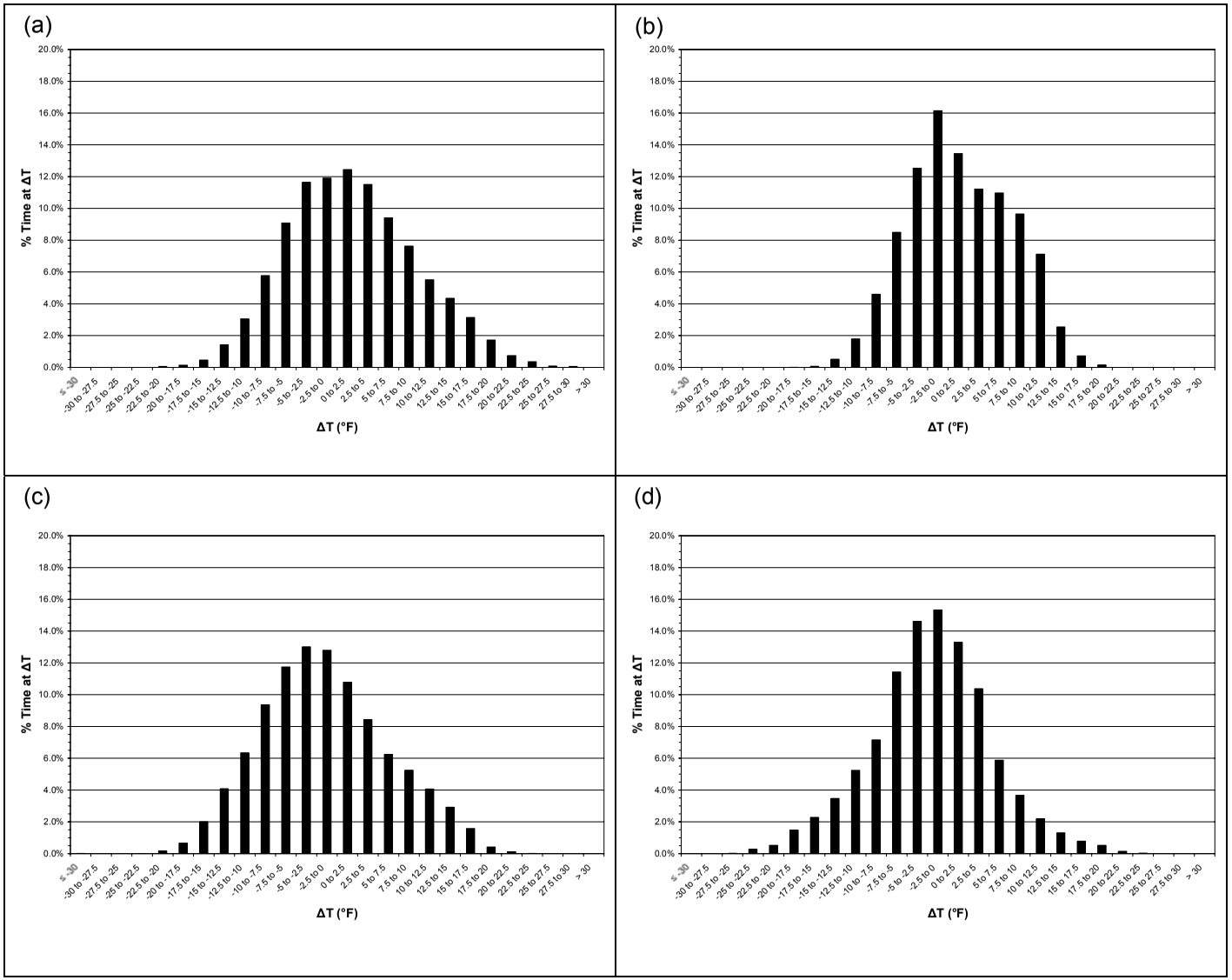

Figure A.5. Seasonal temperature differential frequency distributions for concrete pavement with 14-inch slab thickness in Champaign, Illinois for (a) spring, (b) summer, (c) fall, and (d) winter.

Table A.1. Seasonal Temperature Differential Frequencies for Concrete Pavements with 8- and 10-in.Slab Thicknesses in Champaign, Illinois

ΔT (°F)			8-inch				10-inch			
>	≤	ave.	spring	summer	fall	winter	spring	summer	fall	winter
-20.0	-17.5	-18.75	0.000	0.000	0.000	0.002	0.000	0.000	0.000	0.006
-17.5	-15.0	-16.25	0.001	0.000	0.001	0.007	0.001	0.000	0.007	0.017
-15.0	-12.5	-13.75	0.002	0.000	0.013	0.023	0.006	0.002	0.025	0.029
-12.5	-10.0	-11.25	0.015	0.006	0.040	0.037	0.022	0.010	0.053	0.042
-10.0	-7.5	-8.75	0.047	0.029	0.084	0.058	0.056	0.040	0.092	0.067
-7.5	-5.0	-6.25	0.089	0.091	0.131	0.105	0.091	0.093	0.127	0.110
-5.0	-2.5	-3.75	0.152	0.163	0.162	0.180	0.136	0.148	0.144	0.169
-2.5	0.0	-1.25	0.158	0.193	0.169	0.194	0.141	0.178	0.150	0.171
0.0	2.5	1.25	0.153	0.138	0.124	0.169	0.143	0.136	0.118	0.150
2.5	5.0	3.75	0.120	0.118	0.091	0.111	0.115	0.113	0.089	0.112
5.0	7.5	6.25	0.094	0.131	0.067	0.056	0.092	0.117	0.065	0.054
7.5	10.0	8.75	0.071	0.100	0.056	0.030	0.074	0.105	0.054	0.033
10.0	12.5	11.25	0.052	0.026	0.040	0.015	0.052	0.049	0.041	0.019
12.5	15.0	13.75	0.029	0.004	0.018	0.009	0.040	0.009	0.025	0.011
15.0	17.5	16.25	0.012	0.000	0.004	0.004	0.019	0.002	0.008	0.006
17.5	20.0	18.75	0.003	0.000	0.001	0.001	0.008	0.000	0.002	0.003
TOTAL			0.999	1.000	1.000	1.000	0.997	1.000	1.000	0.998

Table A.2. Seasonal Temperature Differential Frequencies for Concrete Pavements with 12-and 14-in.Slab Thicknesses in Champaign, Illinois

ΔT (°F)			12-inch				14-inch			
>	≤	ave.	spring	summer	fall	winter	spring	summer	fall	winter
-20.0	-17.5	-18.75	0.001	0.000	0.004	0.008	0.001	0.000	0.007	0.015
-17.5	-15.0	-16.25	0.003	0.000	0.013	0.021	0.005	0.001	0.020	0.023
-15.0	-12.5	-13.75	0.010	0.004	0.035	0.031	0.014	0.005	0.041	0.035
-12.5	-10.0	-11.25	0.028	0.014	0.060	0.048	0.031	0.018	0.063	0.052
-10.0	-7.5	-8.75	0.058	0.044	0.090	0.071	0.058	0.046	0.094	0.072
-7.5	-5.0	-6.25	0.092	0.088	0.124	0.112	0.091	0.085	0.117	0.114
-5.0	-2.5	-3.75	0.123	0.136	0.136	0.159	0.116	0.125	0.130	0.146
-2.5	0.0	-1.25	0.130	0.170	0.137	0.162	0.119	0.161	0.128	0.153
0.0	2.5	1.25	0.132	0.134	0.112	0.141	0.124	0.135	0.108	0.133
2.5	5.0	3.75	0.113	0.112	0.086	0.105	0.115	0.112	0.084	0.104
5.0	7.5	6.25	0.096	0.111	0.065	0.059	0.094	0.110	0.062	0.059
7.5	10.0	8.75	0.073	0.100	0.053	0.033	0.076	0.097	0.053	0.037
10.0	12.5	11.25	0.053	0.064	0.040	0.020	0.055	0.071	0.041	0.022
12.5	15.0	13.75	0.042	0.017	0.029	0.013	0.043	0.025	0.029	0.013
15.0	17.5	16.25	0.026	0.004	0.012	0.007	0.031	0.007	0.016	0.008
17.5	20.0	18.75	0.013	0.001	0.003	0.003	0.017	0.002	0.004	0.005
TOTAL			0.993	1.000	0.999	0.994	0.992	1.000	0.997	0.990

APPENDIX B. CRITICAL AND NONDIMENSIONAL TENSILE LOADING STRESSES FOR CRCP

The finite element analysis program ISLAB2000 (ERES 1999) was used to create a catalogue of loading stresses for the two critical tensile stresses located in the transverse direction. The critical stresses are a function of shoulder load transfer efficiency (LTE_s), transverse crack load transfer efficiency (LTE_c), and the nondimensional slab size ratio ($\overline{L}/\ell$), where ℓ is the radius of relative stiffness for load analysis. Shoulder and crack load transfer efficiencies were varied from 1 to 99% and $\overline{L}/\ell$ was varied from 0.6187 to 3.7126 (approximate crack spacings from 24 to 144 in.).

The pavement used in the ISLAB2000 analysis contained two 144-in. lane widths and an assumed 144-in.shoulder width, which is slightly larger than the typical width of 120 in. Five slabs were used in the driving lane, with a spacing of 48 in. The mesh consisted of four-in. elements. A dual wheel 18-kip single axle was used to load the pavement, as shown in Figure B.1. The dual wheels were spaced 12 in. apart, the first and third wheels on the axle were spaced 84 in. apart, and the tire pressure was 100 psi. All transverse cracks had the same load transfer efficiency. The shoulder and longitudinal contraction joint also had the same load transfer efficiency. The critical stresses were located 44 in. off the edge of the slab for top stresses and 100 in. off the edge of the slab for bottom stresses. Stresses were only calculated along the transverse crack.

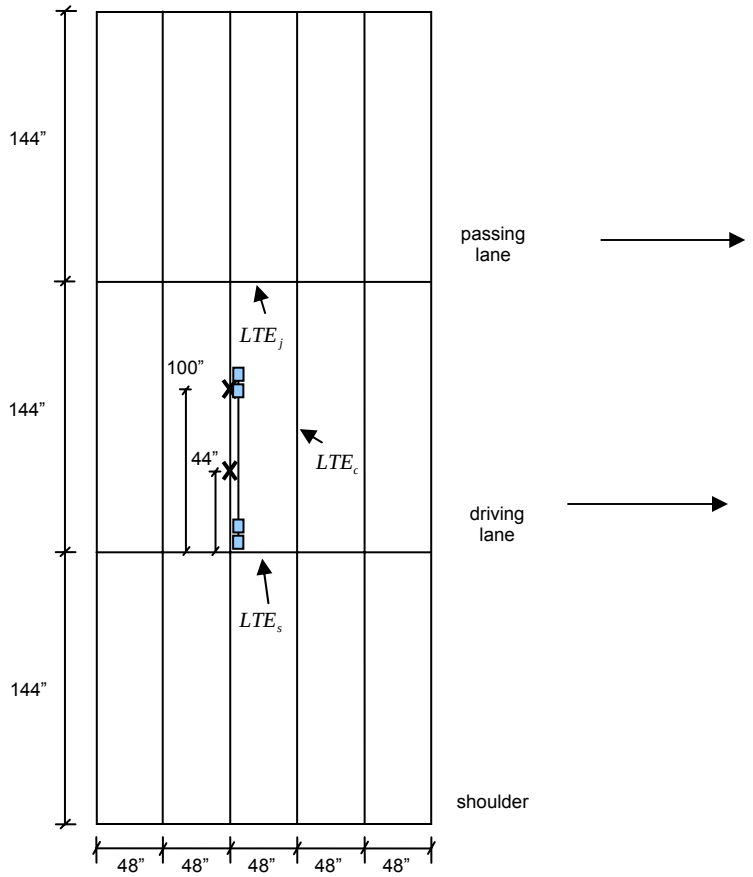

Figure B.1. Schematic of the ISLAB2000 finite element analysis pavement geometry and loading location.

Sample ISLAB2000 input and output files are shown in Figure B.2 and Figure B.3, respectively. The critical stresses were taken as the maximum positive stresses in the x-direction (tension is positive). Because the width of the slab (L) was fixed for the finite element analysis, the thickness of the slab (h_{PCC}) was varied to obtain the necessary range in $\overline{L}/\ell$ ratios. The critical stresses calculated by ISLAB2000 for one pavement thickness (h_{PCC} = 11 in.) were normalized such that the nondimensional stresses could be used for any combination of load transfer efficiency, pavement geometry, and load level. These values are reported in Table B.1. The nondimensional loading stresses (STB and STT) are shown in Table B.2.

```
*GENERAL
v1.1
crcp48111
0 0   0
0
*GEOMETRY
3 5
  37    37    37
  13    13    13    13    13
000.000 004.000 008.000 012.000 016.000 020.000 024.000 028.000
032.000 036.000 040.000 044.000 048.000 052.000 056.000 060.000
064.000 068.000 072.000 076.000 080.000 084.000 088.000 092.000
096.000 100.000 104.000 108.000 112.000 116.000 120.000 124.000
128.000 132.000 136.000 140.000 144.000 144.000 148.000 152.000
156.000 160.000 164.000 168.000 172.000 176.000 180.000 184.000
188.000 192.000 196.000 200.000 204.000 208.000 212.000 216.000
220.000 224.000 228.000 232.000 236.000 240.000 244.000 248.000
252.000 256.000 260.000 264.000 268.000 272.000 276.000 280.000
284.000 288.000 288.000 292.000 296.000 300.000 304.000 308.000
312.000 316.000 320.000 324.000 328.000 332.000 336.000 340.000
344.000 348.000 352.000 356.000 360.000 364.000 368.000 372.000
376.000 380.000 384.000 388.000 392.000 396.000 400.000 404.000
408.000 412.000 416.000 420.000 424.000 428.000 432.000
000.000 004.000 008.000 012.000 016.000 020.000 024.000 028.000
032.000 036.000 040.000 044.000 048.000 048.000 052.000 056.000
060.000 064.000 068.000 072.000 076.000 080.000 084.000 088.000
092.000 096.000 096.000 100.000 104.000 108.000 112.000 116.000
120.000 124.000 128.000 132.000 136.000 140.000 144.000 144.000
148.000 152.000 156.000 160.000 164.000 168.000 172.000 176.000
180.000 184.000 188.000 192.000 192.000 196.000 200.000 204.000
208.000 212.000 216.000 220.000 224.000 228.000 232.000 236.000
240.000
*LAYER PARAMETERS
1  1
21 4.00E+06 0.15 27.70 4.40E-06 0.087
*FOUNDATION
51 200
*PRESSURE
  100.000   144.000   150.708    96.000   102.708
  100.000   156.000   162.708    96.000   102.708
  100.000   228.000   234.708    96.000   102.708
  100.000   240.000   246.708    96.000   102.708
*YJOINT
0 0 1 8.581E+01
*XJOINT
0 0 1 8.581E+01
```

Figure B.2. Sample ISLAB2000 input file ($\overline{L}/\ell$ = 0.6187, LTE_s = 1%, LTE_c = 1%).

MAXIMUM AND MINIMUM VALUES OF STRESSES (TENSION IS POSITIVE)

LAYER No. 1 bottom surface

	stress	node	X-coord	Y-coord		stress	node	X-coord	Y-coord
Range of X-stress: from	15.8979	at 2949	244.00	96.00	to	-22.8403	at 2936	192.00	96.00
Range of Y-stress: from	6.0248	at 3035	144.00	100.00	to	-9.4219	at 3590	144.00	120.00
Maximum Principal Stress:	17.7193	at 2949	244.00	96.00					
Maximum Principal Stress Angle:	0.3195								

LAYER No. 1 top surface

	stress	node	X-coord	Y-coord		stress	node	X-coord	Y-coord
Range of X-stress: from	22.8403	at 2936	192.00	96.00	to	-15.8979	at 2949	244.00	96.00
Range of Y-stress: from	9.4219	at 3590	144.00	120.00	to	-6.0248	at 3035	144.00	100.00
Maximum Principal Stress:	24.5717	at 2934	184.00	96.00					
Maximum Principal Stress Angle:	0.2987								

Figure B.3. Sample ISLAB2000 output file ($\overline{L}/\ell$ = 0.6187, LTE_s = 1%, LTE_c = 1%).

Table B.1. Critical Tensile Stresses from ISLAB2000 Analysis (h_{PCC} = 11 inches)

LTE_s, %		1		15		40		65		90		99	
CS/RRS	**LTE_c, %**	σ_T	σ_B	σ_T	σ_B	σ_T	σ_B	σ_T	σ_B	σ_T	σ_B	σ_T	σ_B
0.6187	**1**	144.8	100.8	102.0	126.9	53.9	161.9	29.6	181.4	16.8	191.9	13.8	194.2
0.6187	**30**	145.4	101.2	114.7	121.3	71.6	151.2	44.2	170.8	25.9	184.1	20.8	187.6
0.6187	**50**	143.1	102.5	115.8	122.1	76.1	151.0	50.0	168.8	32.3	178.8	27.1	180.9
0.6187	**80**	129.9	105.2	107.5	123.0	74.8	149.9	53.5	165.5	40.0	169.5	36.9	165.0
0.6187	**95**	96.9	95.3	79.3	109.4	54.5	130.9	39.1	144.2	29.8	149.5	27.9	143.8
0.6187	**99**	63.9	71.7	48.4	83.7	27.3	102.0	14.6	113.7	7.3	120.2	6.7	119.9
1.2367	**1**	133.4	107.2	111.3	118.3	80.3	136.4	60.9	149.3	48.8	157.8	45.5	159.9
1.2367	**30**	127.3	109.0	111.6	116.5	87.1	129.1	69.8	138.8	57.0	146.4	53.0	148.5
1.2367	**50**	118.1	108.5	105.3	115.0	84.6	125.6	69.4	133.3	57.7	138.7	53.7	140.1
1.2367	**80**	90.3	96.1	80.8	101.6	65.3	111.1	53.9	117.8	45.4	121.3	42.1	121.6
1.2367	**95**	62.2	74.3	54.0	79.5	40.8	88.7	31.5	95.6	25.4	100.2	23.9	101.0
1.2367	**99**	55.2	61.9	47.3	66.9	34.6	75.9	25.5	82.8	19.5	87.6	17.8	88.8
1.8542	**1**	108.8	111.6	97.3	114.6	80.8	119.9	70.0	124.3	62.6	127.7	60.5	128.7
1.8542	**30**	98.7	108.0	90.5	109.6	77.8	112.6	68.5	115.2	61.3	117.6	59.0	118.3
1.8542	**50**	86.9	101.3	80.3	102.8	69.8	105.3	62.0	107.4	55.7	109.0	53.4	109.5
1.8542	**80**	62.6	83.3	57.6	84.9	49.6	87.7	44.0	89.9	39.8	91.5	38.4	91.9
1.8542	**95**	50.9	68.6	46.2	70.2	38.7	73.1	33.6	75.4	30.0	77.1	28.9	77.6
1.8542	**99**	49.8	61.1	45.1	62.7	37.7	65.6	32.6	67.9	28.9	69.7	27.8	70.3
2.4757	**1**	82.1	101.9	75.8	102.1	66.4	102.9	60.1	104.0	55.6	105.0	54.3	105.3
2.4757	**30**	70.3	94.1	65.9	94.0	58.9	94.3	53.8	94.7	49.8	95.2	48.5	95.4
2.4757	**50**	59.5	85.9	56.0	86.0	50.4	86.3	46.3	86.7	43.0	87.1	41.9	87.3
2.4757	**80**	44.2	71.2	41.2	71.4	36.7	71.9	33.6	72.4	31.4	72.9	30.7	73.1
2.4757	**95**	40.1	61.2	37.2	61.4	32.8	61.9	29.7	62.4	27.5	62.9	26.8	63.0
2.4757	**99**	40.0	55.4	37.1	55.7	32.6	56.2	29.6	56.7	27.3	57.2	26.7	57.3
3.7126	**1**	39.7	73.0	38.1	72.9	35.4	72.8	33.5	72.8	32.1	72.9	31.7	72.9
3.7126	**30**	30.3	64.8	29.3	64.8	27.7	64.7	26.4	64.7	25.4	64.8	25.1	64.8
3.7126	**50**	24.7	58.8	23.9	58.8	22.6	58.7	21.6	58.7	20.9	58.8	20.6	58.8
3.7126	**80**	20.3	49.7	19.5	49.7	18.2	49.7	17.2	49.7	16.6	49.7	16.3	49.7
3.7126	**95**	20.0	43.6	19.1	43.6	17.8	43.5	16.8	43.5	16.1	43.6	15.9	43.6
3.7126	**99**	20.0	38.9	19.2	38.8	17.8	38.8	16.9	38.8	16.1	38.8	15.9	38.8

*σ_T = critical top of slab tensile stress (44 inches from the edge of the slab)

*σ_B = critical bottom of slab tensile stress (100 inches from the edge of the slab)

Table B.2. Nondimensional Tensile Stresses from ISLAB2000 Analysis

LTE_s, %		1		15		40		65		90		99	
CS/RRS	LTE_c, %	STT	STB	STT	STB	STT	STB	STT	STB	STT	STB	STT	STB
0.6187	1	1.9464	1.3554	1.3720	1.7058	0.7248	2.1766	0.3973	2.4383	0.2257	2.5803	0.1861	2.6103
0.6187	30	1.9552	1.3610	1.5417	1.6307	0.9628	2.0325	0.5948	2.2963	0.3487	2.4751	0.2801	2.5218
0.6187	50	1.9235	1.3783	1.5572	1.6419	1.0235	2.0305	0.6722	2.2690	0.4345	2.4036	0.3639	2.4323
0.6187	80	1.7460	1.4143	1.4449	1.6540	1.0053	2.0150	0.7198	2.2251	0.5382	2.2794	0.4955	2.2190
0.6187	95	1.3022	1.2816	1.0657	1.4704	0.7326	1.7598	0.5251	1.9387	0.4010	2.0094	0.3754	1.9331
0.6187	99	0.8586	0.9643	0.6513	1.1255	0.3676	1.3719	0.1959	1.5280	0.0987	1.6155	0.0904	1.6117
1.2367	1	1.7940	1.4410	1.4957	1.5905	1.0789	1.8335	0.8189	2.0067	0.6566	2.1221	0.6121	2.1503
1.2367	30	1.7108	1.4651	1.5000	1.5661	1.1705	1.7359	0.9380	1.8661	0.7670	1.9676	0.7128	1.9967
1.2367	50	1.5878	1.4585	1.4158	1.5455	1.1371	1.6892	0.9330	1.7921	0.7763	1.8645	0.7220	1.8841
1.2367	80	1.2140	1.2914	1.0862	1.3664	0.8776	1.4939	0.7249	1.5833	0.6100	1.6314	0.5665	1.6351
1.2367	95	0.8363	0.9996	0.7264	1.0693	0.5491	1.1927	0.4230	1.2858	0.3409	1.3466	0.3209	1.3575
1.2367	99	0.7417	0.8318	0.6359	0.8996	0.4652	1.0208	0.3430	1.1138	0.2615	1.1775	0.2398	1.1935
1.8542	1	1.4628	1.5010	1.3078	1.5406	1.0866	1.6116	0.9413	1.6711	0.8423	1.7168	0.8128	1.7300
1.8542	30	1.3271	1.4525	1.2168	1.4741	1.0453	1.5134	0.9207	1.5490	0.8244	1.5805	0.7926	1.5904
1.8542	50	1.1686	1.3624	1.0800	1.3820	0.9391	1.4158	0.8340	1.4434	0.7482	1.4660	0.7178	1.4727
1.8542	80	0.8423	1.1200	0.7738	1.1414	0.6669	1.1789	0.5917	1.2081	0.5357	1.2299	0.5164	1.2359
1.8542	95	0.6844	0.9222	0.6207	0.9438	0.5207	0.9825	0.4512	1.0133	0.4031	1.0366	0.3892	1.0438
1.8542	99	0.6690	0.8219	0.6061	0.8436	0.5071	0.8825	0.4377	0.9135	0.3890	0.9371	0.3742	0.9445
2.4757	1	1.1040	1.3699	1.0186	1.3723	0.8926	1.3838	0.8076	1.3981	0.7476	1.4111	0.7297	1.4158
2.4757	30	0.9452	1.2647	0.8857	1.2642	0.7921	1.2673	0.7232	1.2733	0.6695	1.2800	0.6522	1.2827
2.4757	50	0.8002	1.1549	0.7526	1.1561	0.6777	1.1603	0.6226	1.1658	0.5785	1.1712	0.5638	1.1732
2.4757	80	0.5941	0.9578	0.5542	0.9605	0.4933	0.9669	0.4516	0.9737	0.4219	0.9801	0.4130	0.9825
2.4757	95	0.5397	0.8222	0.5006	0.8252	0.4404	0.8320	0.3989	0.8388	0.3692	0.8452	0.3604	0.8477
2.4757	99	0.5378	0.7454	0.4990	0.7484	0.4388	0.7553	0.3973	0.7622	0.3675	0.7686	0.3585	0.7710
3.7126	1	0.5340	0.9808	0.5119	0.9798	0.4766	0.9791	0.4509	0.9793	0.4314	0.9801	0.4256	0.9806
3.7126	30	0.4075	0.8716	0.3942	0.8709	0.3723	0.8703	0.3553	0.8703	0.3417	0.8706	0.3374	0.8708
3.7126	50	0.3325	0.7907	0.3214	0.7901	0.3037	0.7896	0.2906	0.7897	0.2806	0.7901	0.2775	0.7904
3.7126	80	0.2729	0.6688	0.2619	0.6682	0.2445	0.6676	0.2319	0.6676	0.2225	0.6680	0.2198	0.6682
3.7126	95	0.2683	0.5865	0.2572	0.5858	0.2394	0.5853	0.2265	0.5853	0.2167	0.5856	0.2137	0.5858
3.7126	99	0.2686	0.5228	0.2575	0.5221	0.2397	0.5216	0.2267	0.5216	0.2169	0.5219	0.2140	0.5221

*STT = nondimensional tensile stress at the top of the slab (44 inches from the edge of the slab)

*STB = nondimensional tensile stress at the top of the slab (100 inches from the edge of the slab)

APPENDIX C. EQUIVALENT DAMAGE RATIO

An equivalent damage ratio (EDR) is used to convert traffic that is laterally distributed across the wheel path into critical applications at the location which produces the maximum tensile stress in the slab. This concept has been used in the past in the development of the PCA method (1984), IDOT's JPCP procedure (Zollinger and Barenberg, 1989), and the FAA airfield pavement design guide (1995). Accounting for traffic wander is essential in rigid pavement design because the location of the applied load greatly influences the magnitude of the resulting stress. For this analysis, the critical location is when the 18-kip single-axle load is placed along a transverse crack, and with zero offset from the edge of the pavement.

C.1 CALCULATION PROCEDURE

The equivalent damage ratio (EDR) is calculated as:

$$EDR = \frac{n_{g=0}}{n} \tag{B-1}$$

where $n_{g=0}$ is the number of expected load repetitions at the critical position only for a fixed damage level (D), and n is the total number of expected load repetitions for damage level (D) assuming distributed traffic.

C.1.1 Expected Load Repetitions at the Critical Location

The number of expected load repetitions at the critical axle position is calculated as:

$$n_{g=0} = D \cdot N_{g=0} \tag{B-2}$$

where D is the fatigue damage accumulated at the critical location, and $N_{g=0}$ is the number of allowable load repetitions at the critical location.

C.1.1.1 Fatigue Damage at the Critical Location

The total fatigue damage accumulated at the critical location (D) on the top or bottom of the CRCP slab is calculated using the damage produced at offset positions and the Gauss quadrature weighting factors. Two- and four-point Gaussian integration is used to describe the damage at various offset distances. This process is essentially the same method used in the M-E PDG to account for wander (ARA ,2003b):

$$\begin{aligned} D = {} & 4\left(0.347855 \cdot D_{g=1} + 0.652145 \cdot D_{g=2} + 0.347855 \cdot D_{g=3} + 0.652145 \cdot D_{g=4}\right) + \\ & + 5\left(1 \cdot D_{g=5} + 1 \cdot D_{g=6}\right) \end{aligned} \tag{B-3}$$

where D_g is the fatigue damage at the critical location for an axle load located g (inches) from the edge of the pavement.

C.1.1.2 Fatigue Damage at a Point Inside the Pavement Edge

The fatigue damage at a point located g in. from the pavement edge (D_g) is calculated as follows (ARA, 2003b):

$$D_g = NORMDIST(g) \cdot \frac{n}{N_g} \tag{B-4}$$

where,

$NORMDIST(g)$ = the probability that the outer edge of the wheel will pass through the point located g in. from the pavement edge;

n = the total number of expected load repetitions; and

N_g = the number of allowable load repetitions.

C1.1.2.1 Allowable Load Repetitions

The zero-maintenance fatigue equation (Darter, 1977) was used to calculate the number of allowable load repetitions:

$$LogN = 17.61 - 17.61(SR) \tag{B-5}$$

$$SR = \sigma / MOR \tag{B-6}$$

where σ is tensile stress (psi) and MOR is the concrete modulus of rupture (750 psi).

C.1.1.2.2 Probability of coverage

The probability that the outer edge of the wheel will pass through the point g in. from the pavement edge is calculated as follows (ARA,2003b):

$$NORMDIST(g) = \frac{1}{\sigma_{wp}\sqrt{2}} e^{-\frac{1}{2}\left(\frac{g-\mu_{wp}}{\sigma_{wp}}\right)^2} \tag{B-7}$$

where,

σ_{wp} = the standard deviation of the wheel path from the lane-shoulder to the outer wheel edge (10 in.);

μ_{wp} = the mean wheel path from the lane-shoulder to the outer wheel edge (18 in.); and

g = the wheel location from the edge at each Gauss point as shown in Table C.1.

Note that four-point Gaussian integration is employed for offset distances from $g = 0$ to 8 in., and that two-point Gaussian integration is used for 8- to 18-in. offset distance.

Table C.1. Wheel Locations at Gauss Points

Gauss Point Number	Location of Gauss Point *g* (in.)
1	0.5555
2	2.6401
3	5.3599
4	7.4445
5	10.1132
6	15.8868

C.2 EQUIVALENT DAMAGE RATIO EQUATIONS

The finite element analysis program ISLAB2000 was used to investigate the effect of shoulder load transfer efficiency (LTE_s), transverse crack load transfer efficiency (LTE_c), and the nondimensional slab size ratio ($\overline{L}/\ell$) on the equivalent damage ratio. Three shoulder LTE values were examined: 65%, 40%, and 5%. These values roughly correspond to tied concrete (monolithic), tied concrete (separate), and asphalt/granular shoulders, respectively. The transverse crack LTE was varied from 50 to 99% and $\overline{L}/\ell$ was varied from 0.9966 to 1.5164. Variations in $\overline{L}/\ell$ were achieved by maintaining a 48-in.crack spacing and by varying the slab thickness from 8 to 14 in. The details of the finite element analysis and load positions are described in Appendix B.

Critical tensile stresses were calculated at two locations: 44 in. from the slab edge at the top of the slab and 100 in. offset from the edge at the bottom of the slab. Because two critical load stress locations exist, an equivalent damage ratio must be calculated for each location (STT or STB).

C.2.1 Top-of-Slab Equivalent Damage Ratio

Figure C.1 shows the effect of shoulder LTE (or shoulder type) on the top-of-slab equivalent damage ratio (EDR_{STT}) for a constant transverse crack LTE. For a given $\overline{L}/\ell$, a change in shoulder LTE results in a minor change in EDR_{STT}. Figure C.1 also shows that a decrease in $\overline{L}/\ell$ results in an increase in EDR, regardless of the shoulder LTE.

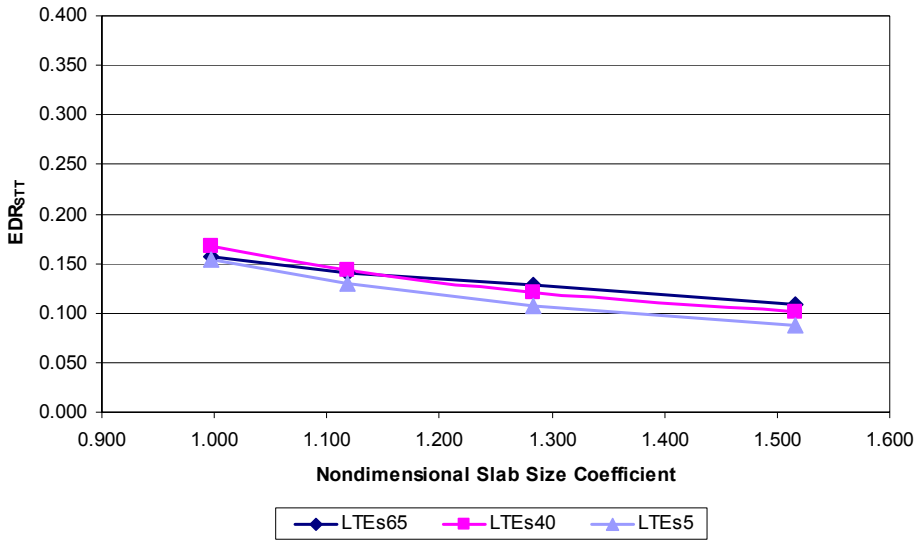

Figure C.1. Effect of slab size ($\overline{L}/\ell$) on EDR_{STT} for varying shoulder load transfer efficiencies (LTE_c = 80%).

Figure C.2 shows the effect of transverse crack LTE on the top-of-slab equivalent damage ratio (EDR_{STT}). For a given $\overline{L}/\ell$, an increase in the transverse crack LTE generally results in an increase in EDR_{STT} . The nonlinear behavior of the EDR_{STT} values when LTE_c approaches 100% is due to the shear stiffness of the aggregate interlock spring deviating from a finite value to asymptotically approaching infinity.

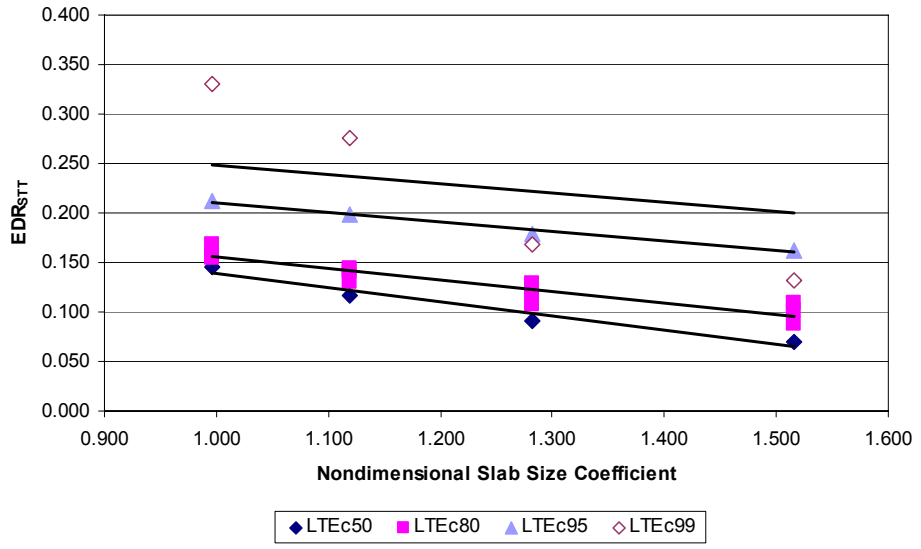

Figure C.2. Effect of slab size ($\overline{L}/\ell$) on EDR_{STT} for varying transverse crack load transfer efficiencies.

Based on the behavior shown in Figure C.2, linear trend lines were fitted to each set of equivalent damage ratio data to obtain equations for EDR_{STT}. These trend lines take the following form:

$$y = m \cdot x + b \tag{B-8}$$

where m is the slope of the line and b is the y-intercept. A slope of -0.0933 was assigned to the "LTE_c99" data set in order to obtain an equation that was roughly parallel with the equations for the remaining equivalent damage ratio data sets, as shown in Figure C.2. The regression coefficients (m and b) and squares of the correlation coefficients (R^2) for each equivalent damage ratio data set are shown in Table C.2. Each equation is a function of $\overline{L}/\ell$.

Table C.2. Top-of-Slab Equivalent Damage Ratio (EDR_{STT}) Linear Regression Coefficients

LTE_c (%)	m	b	R^2
50	-0.1424	0.2806	0.9572
80	-0.1138	0.2688	0.8716
95	-0.0965	0.3064	0.9877
99	-0.0933	0.3414	—*
*R^2 value unavailable; *s* = 0.088			

C.2.2 Bottom-of-Slab Equivalent Damage Ratio

Figure C.3 shows the effect of shoulder LTE (or shoulder type) on the bottom-of-slab equivalent damage ratio (EDR_{STB}) for a constant transverse crack LTE. For a given $\overline{L}/\ell$, a change in shoulder LTE results in a small change in EDR_{STB}. Figure C.3 also shows that a decrease in $\overline{L}/\ell$ results in an increase in EDR, regardless of the shoulder LTE.

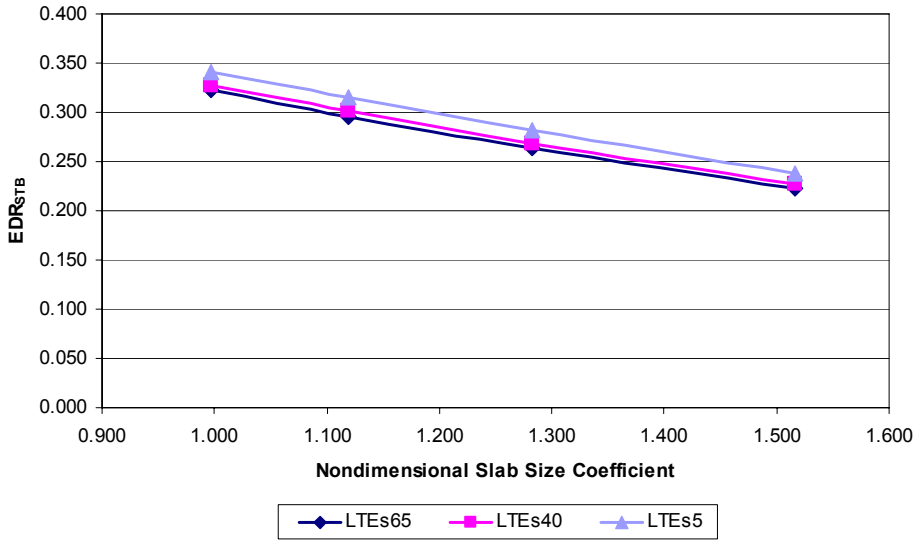

Figure C.3. Effect of slab size ($\overline{L}/\ell$) on EDR_{STB} for varying shoulder load transfer efficiencies (LTE_c = 80%).

Figure C.4 shows the effect of transverse crack LTE on the bottom-of-slab equivalent damage ratio (EDR_{STB}). The transverse crack LTE did not have a significant effect on EDR_{STB}' and therefore only a single equation is required to quantify the equivalent damage ratio for the critical bottom tensile stress location.

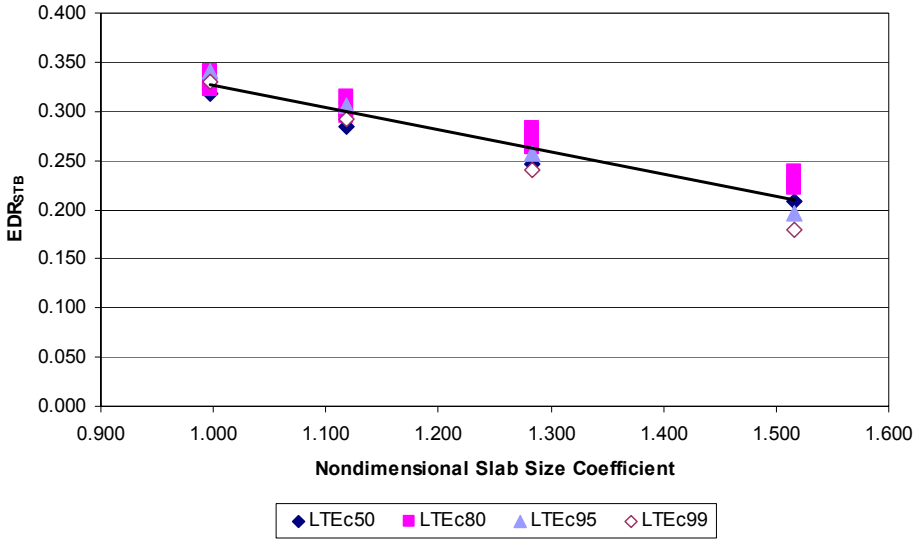

Figure C.4. Effect of slab size ($\bar{L}/\ell$) on EDR_{STB} for varying transverse crack load transfer efficiencies.

Based on the behavior shown in Figure C.4, a linear trend line was fitted to the entire equivalent damage ratio data set to obtain a global equation for EDR_{STB}. The regression coefficients (m and b) and squares of the correlation coefficients (R^2) are shown in Table C.3. This equation is a function of $\bar{L}/\ell$.

Table C.3. Bottom-of-Slab Equivalent Damage Ratio (EDR_{STB}) Linear Regression Coefficients

LTE_c (%)	m	b	R^2
50	-0.2264	0.5533	0.9085

APPENDIX D. CRCP CALIBRATION DESIGN INPUTS AND FIELD PERFORMANCE DATA

Table D.1. CRCP Calibration Design Inputs and Field Performance Data (adapted from ARA 2003a)

SHRP_ID	State	County	Functional Class	Route Signing	Route No.	Direction of Travel	Mile Point	Section Length, ft	Const. Season	Const. Year	Traffic Opening Season
I80_EB_137.65	IL	Cook	Rural Principal Arterial – Interstate	Interstate	80	East	137.65	528	summer	1968	summer
	IL	Cook	Rural Principal Arterial – Interstate	Interstate	80	East	137.65	528	summer	1968	summer
	IL	Cook	Rural Principal Arterial – Interstate	Interstate	80	East	137.65	528	summer	1968	summer
	IL	Cook	Rural Principal Arterial – Interstate	Interstate	80	East	137.65	528	summer	1968	summer
I80_EB_143.79	IL	Cook	Rural Principal Arterial – Interstate	Interstate	80	East	143.79	528	summer	1968	summer
	IL	Cook	Rural Principal Arterial – Interstate	Interstate	80	East	143.79	528	summer	1968	summer
I80_EB_151.12	IL	Cook	Rural Principal Arterial – Interstate	Interstate	80	East	151.12	528	summer	1968	summer
I80_EB_152.33	IL	Cook	Rural Principal Arterial – Interstate	Interstate	80	East	152.33	528	summer	1968	summer
	IL	Cook	Rural Principal Arterial – Interstate	Interstate	80	East	152.33	528	summer	1968	summer
	IL	Cook	Rural Principal Arterial – Interstate	Interstate	80	East	152.33	528	summer	1968	summer
I80_WB_137.65	IL	Cook	Rural Principal Arterial – Interstate	Interstate	80	West	137.65	528	summer	1968	summer
	IL	Cook	Rural Principal Arterial – Interstate	Interstate	80	West	137.65	528	summer	1968	summer
	IL	Cook	Rural Principal Arterial – Interstate	Interstate	80	West	137.65	528	summer	1968	summer
	IL	Cook	Rural Principal Arterial – Interstate	Interstate	80	West	137.65	528	summer	1968	summer
I80_WB_143.79	IL	Cook	Rural Principal Arterial – Interstate	Interstate	80	West	143.79	528	summer	1968	summer
	IL	Cook	Rural Principal Arterial – Interstate	Interstate	80	West	143.79	528	summer	1968	summer
I80_WB_148.39	IL	Cook	Rural Principal Arterial – Interstate	Interstate	80	West	148.39	528	summer	1968	summer
I80_WB_152.33	IL	Cook	Rural Principal Arterial – Interstate	Interstate	80	West	152.33	528	summer	1968	summer
	IL	Cook	Rural Principal Arterial – Interstate	Interstate	80	West	152.33	528	summer	1968	summer
	IL	Cook	Rural Principal Arterial – Interstate	Interstate	80	West	152.33	528	summer	1968	summer
	IL	Cook	Rural Principal Arterial – Interstate	Interstate	80	West	152.33	528	summer	1968	summer
I94_edens_28.46	IL	Cook	Rural Principal Arterial – Interstate	Interstate	94	East	28.46	528	summer	1980	summer
	IL	Cook	Rural Principal Arterial – Interstate	Interstate	94	East	28.46	528	summer	1980	summer
I94_edens_30.11	IL	Cook	Rural Principal Arterial – Interstate	Interstate	94	East	30.11	528	summer	1980	summer
	IL	Cook	Rural Principal Arterial – Interstate	Interstate	94	East	30.11	528	summer	1980	summer
I94_edens_32.90	IL	Cook	Rural Principal Arterial – Interstate	Interstate	94	East	32.9	528	summer	1980	summer
	IL	Cook	Rural Principal Arterial – Interstate	Interstate	94	East	32.9	528	summer	1980	summer

**Italics* indicate assumed values

Table D.1. CRCP Calibration Design Inputs and Field Performance Data (adapted from ARA 2003a)

SHRP_ID	Traffic Opening Year	Shoulder Type	Percent Steel, %	Steel Diameter	Depth to Steel, in.	Base Friction Coefficient	Base Type	PCC Thickness, in.	PCC Poisson's Ratio	PCC COTE, 1/°F	PCC Aggregate Type	MOR_{28}, psi	E_{PCC28}, psi	f'_{c28}, psi
I80_EB_137.65	1968	Asphalt	0.6	0.625	3.5	*7.5*	ATB	9	*0.15*	*5.50E-06*	*Limestone*	794	*4,400,000*	*4,500*
	1968	Asphalt	0.6	0.625	3.5	*7.5*	ATB	9	*0.15*	*5.50E-06*	*Limestone*	794	*4,400,000*	*4,500*
	1968	Asphalt	0.6	0.625	3.5	*7.5*	ATB	9	*0.15*	*5.50E-06*	*Limestone*	794	*4,400,000*	*4,500*
	1968	Asphalt	0.6	0.625	3.5	*7.5*	ATB	9	*0.15*	*5.50E-06*	*Limestone*	794	*4,400,000*	*4,500*
I80_EB_143.79	1968	Asphalt	0.6	0.625	3.5	*7.5*	ATB	9	*0.15*	*5.50E-06*	*Limestone*	794	*4,400,000*	*4,500*
	1968	Asphalt	0.6	0.625	3.5	*7.5*	ATB	9	*0.15*	*5.50E-06*	*Limestone*	794	*4,400,000*	*4,500*
I80_EB_151.12	1968	Asphalt	0.6	0.625	3.5	*7.5*	ATB	9	*0.15*	*5.50E-06*	*Limestone*	794	*4,400,000*	*4,500*
I80_EB_152.33	1968	Asphalt	0.6	0.625	3.5	*7.5*	ATB	9	*0.15*	*5.50E-06*	*Limestone*	794	*4,400,000*	*4,500*
	1968	Asphalt	0.6	0.625	3.5	*7.5*	ATB	9	*0.15*	*5.50E-06*	*Limestone*	794	*4,400,000*	*4,500*
	1968	Asphalt	0.6	0.625	3.5	*7.5*	ATB	9	*0.15*	*5.50E-06*	*Limestone*	794	*4,400,000*	*4,500*
I80_WB_137.65	1968	Asphalt	0.6	0.625	3.5	*7.5*	ATB	9	*0.15*	*5.50E-06*	*Limestone*	794	*4,400,000*	*4,500*
	1968	Asphalt	0.6	0.625	3.5	*7.5*	ATB	9	*0.15*	*5.50E-06*	*Limestone*	794	*4,400,000*	*4,500*
	1968	Asphalt	0.6	0.625	3.5	*7.5*	ATB	9	*0.15*	*5.50E-06*	*Limestone*	794	*4,400,000*	*4,500*
	1968	Asphalt	0.6	0.625	3.5	*7.5*	ATB	9	*0.15*	*5.50E-06*	*Limestone*	794	*4,400,000*	*4,500*
	1968	Asphalt	0.6	0.625	3.5	*7.5*	ATB	9	*0.15*	*5.50E-06*	*Limestone*	794	*4,400,000*	*4,500*
I80_WB_143.79	1968	Asphalt	0.6	0.625	3.5	*7.5*	ATB	9	*0.15*	*5.50E-06*	*Limestone*	794	*4,400,000*	*4,500*
	1968	Asphalt	0.6	0.625	3.5	*7.5*	ATB	9	*0.15*	*5.50E-06*	*Limestone*	794	*4,400,000*	*4,500*
I80_WB_148.39	1968	Asphalt	0.6	0.625	3.5	*7.5*	ATB	9	*0.15*	*5.50E-06*	*Limestone*	794	*4,400,000*	*4,500*
I80_WB_152.33	1968	Asphalt	0.6	0.625	3.5	*7.5*	ATB	9	*0.15*	*5.50E-06*	*Limestone*	794	*4,400,000*	*4,500*
	1968	Asphalt	0.6	0.625	3.5	*7.5*	ATB	9	*0.15*	*5.50E-06*	*Limestone*	794	*4,400,000*	*4,500*
	1968	Asphalt	0.6	0.625	3.5	*7.5*	ATB	9	*0.15*	*5.50E-06*	*Limestone*	794	*4,400,000*	*4,500*
	1968	Asphalt	0.6	0.625	3.5	*7.5*	ATB	9	*0.15*	*5.50E-06*	*Limestone*	794	*4,400,000*	*4,500*
I94_edens_28.46	1980	Asphalt	0.75	0.625	3.5	*7.5*	ATB	10	*0.15*	*5.50E-06*	*Limestone*	794	*4,400,000*	*4,500*
	1980	Asphalt	0.75	0.625	3.5	*7.5*	ATB	10	*0.15*	*5.50E-06*	*Limestone*	794	*4,400,000*	*4,500*
I94_edens_30.11	1980	Asphalt	0.75	0.625	3.5	*7.5*	ATB	10	*0.15*	*5.50E-06*	*Limestone*	794	*4,400,000*	*4,500*
	1980	Asphalt	0.75	0.625	3.5	*7.5*	ATB	10	*0.15*	*5.50E-06*	*Limestone*	794	*4,400,000*	*4,500*
I94_edens_32.90	1980	Asphalt	0.75	0.625	3.5	*7.5*	ATB	10	*0.15*	*5.50E-06*	*Limestone*	794	*4,400,000*	*4,500*
	1980	Asphalt	0.75	0.625	3.5	*7.5*	ATB	10	*0.15*	*5.50E-06*	*Limestone*	794	*4,400,000*	*4,500*

**Italics* indicate assumed values

Table D.1. CRCP Calibration Design Inputs and Field Performance Data (adapted from ARA 2003a)

SHRP_ID	f'_{t28}, psi	Ultimate Shrinkage, in./in.	Cementitious Content, lb/yd^3	RH, %	Total Stress Adjustment Factor	k-value (loading), psi	k-value (curling), psi	Fatigue Equation	PO/mile	Age, yrs	Cumulative ESALs	Age, yrs	Average Age, yrs	Design Life, yrs	Design ESALs
I80_EB_ 137.65	*566*	*7.80E-04*	*600*	*85*	*1.000*	*100*	*100*	*IDOT*	1.3	9.08	10,453,898	9	9.04	*30*	*34,350,000*
	566	*7.80E-04*	*600*	*85*	*1.000*	*100*	*100*	*IDOT*	4.2	17.08	23,408,899	17	17.04	*30*	*41,010,000*
	566	*7.80E-04*	*600*	*85*	*1.000*	*100*	*100*	*IDOT*	3.23	19.08	27,334,223	19	19.04	*30*	*42,870,000*
	566	*7.80E-04*	*600*	*85*	*1.000*	*100*	*100*	*IDOT*	10.7	21.08	31,579,851	21	21.04	*30*	*44,850,000*
I80_EB_ 143.79	*566*	*7.80E-04*	*600*	*85*	*1.000*	*100*	*100*	*IDOT*	7.1	17.08	23,408,899	17	17.04	*30*	*41,010,000*
	566	*7.80E-04*	*600*	*85*	*1.000*	*100*	*100*	*IDOT*	15.5	19.08	27,334,233	19	19.04	*30*	*42,870,000*
I80_EB_ 151.12	*566*	*7.80E-04*	*600*	*85*	*1.000*	*100*	*100*	*IDOT*	0.748	10.08	11,859,879	10	10.04	*30*	*35,140,000*
I80_EB_ 152.33	*566*	*7.80E-04*	*600*	*85*	*1.000*	*100*	*100*	*IDOT*	6.4	18.08	25,333,079	18	18.04	*30*	*41,920,000*
	566	*7.80E-04*	*600*	*85*	*1.000*	*100*	*100*	*IDOT*	11.15	20.08	29,415,415	20	20.04	*30*	*43,840,000*
	566	*7.80E-04*	*600*	*85*	*1.000*	*100*	*100*	*IDOT*	33.33	27.08	46,510,777	27	27.04	*30*	*51,440,000*
I80_WB_ 137.65	*566*	*7.80E-04*	*600*	*85*	*1.000*	*100*	*100*	*IDOT*	1.3	9.08	10,453,898	9	9.04	*30*	*34,350,000*
	566	*7.80E-04*	*600*	*85*	*1.000*	*100*	*100*	*IDOT*	6.45	17.08	23,408,899	17	17.04	*30*	*41,010,000*
	566	*7.80E-04*	*600*	*85*	*1.000*	*100*	*100*	*IDOT*	11.15	19.08	27,334,223	19	19.04	*30*	*42,870,000*
	566	*7.80E-04*	*600*	*85*	*1.000*	*100*	*100*	*IDOT*	23.7	21.08	31,579,851	21	21.04	*30*	*44,850,000*
	566	*7.80E-04*	*600*	*85*	*1.000*	*100*	*100*	*IDOT*	27	26.08	43,772,074	26	26.04	*30*	*50,260,000*
I80_WB_ 143.79	*566*	*7.80E-04*	*600*	*85*	*1.000*	*100*	*100*	*IDOT*	11.34	17.08	23,408,899	17	17.04	*30*	*41,010,000*
	566	*7.80E-04*	*600*	*85*	*1.000*	*100*	*100*	*IDOT*	50.88	26.08	43,772,074	26	26.04	*30*	*50,260,000*
I80_WB_ 148.39	*566*	*7.80E-04*	*600*	*85*	*1.000*	*100*	*100*	*IDOT*	2.26	9.08	10,453,898	9	9.04	*30*	*34,350,000*
I80_WB_ 152.33	*566*	*7.80E-04*	*600*	*85*	*1.000*	*100*	*100*	*IDOT*	0	18.08	25,333,079	18	18.04	*30*	*41,920,000*
	566	*7.80E-04*	*600*	*85*	*1.000*	*100*	*100*	*IDOT*	5.28	20.08	29,415,415	20	20.04	*30*	*42,840,000*
	566	*7.80E-04*	*600*	*85*	*1.000*	*100*	*100*	*IDOT*	23.76	22.08	33,830,866	22	22.04	*30*	*45,870,000*
	566	*7.80E-04*	*600*	*85*	*1.000*	*100*	*100*	*IDOT*	60	27.08	46,510,777	27	27.04	*30*	*51,440,000*
I94_edens_ 28.46	*566*	*7.80E-04*	*600*	*85*	*1.000*	*100*	*100*	*IDOT*	0	14.08	18,069,125	14	14.04	*30*	*38,380,000*
	566	*7.80E-04*	*600*	*85*	*1.000*	*100*	*100*	*IDOT*	1	22.08	33,830,866	22	22.04	*30*	*45,870,000*
I94_edens_ 30.11	*566*	*7.80E-04*	*600*	*85*	*1.000*	*100*	*100*	*IDOT*	0	14.08	18,069,125	14	14.04	*30*	*38,380,000*
	566	*7.80E-04*	*600*	*85*	*1.000*	*100*	*100*	*IDOT*	1	22.08	33,830,866	22	22.04	*30*	*45,870,000*
I94_edens_ 32.90	*566*	*7.80E-04*	*600*	*85*	*1.000*	*100*	*100*	*IDOT*	1	22.08	33,830,866	22	22.04	*30*	*45,870,000*

**Italics* indicate assumed values

Table D.2. CRCP Design Inputs and Performance Data for ATREL CRCP Test Sections (Kohler and Roesler 2006)

Section_ID	State	County	Functional Class	Section Length, ft	Construction Month	Construction Season	Construction Year	Traffic Opening Month	Traffic Opening Season	Traffic Opening Year	Shoulder Type	Percent Steel, %	Steel Diameter, in.	Depth to Steel, in.	Base Friction Coefficient	Base Type	PCC Thickness, in.
ATREL-1	IL	Champaign	CRCP Test section	125	12	Fall	2001	5	spring	2002	Granular	0.55	0.625	3.5	8	ATB	10
ATREL-2	IL	Champaign	CRCP Test section	125	12	Fall	2001	5	spring	2002	Granular	0.80	0.75	3.5	8	ATB	10
ATREL-3	IL	Champaign	CRCP Test section	125	12	Fall	2001	5	spring	2002	Granular	1.09	0.875	3.5	8	ATB	10
ATREL-4	IL	Champaign	CRCP Test section	125	12	Fall	2001	5	spring	2002	Granular	0.78	0.875	4.5	8	ATB	14

Section_ID	Poisson's Ratio	PCC COTE, in./in./°F	PCC Aggregate Type	PCC MOR 28 days, psi	PCC E 28 days, psi	PCC f'c 28 days, psi	PCC f't 28 days, psi	Ultimate Shrinkage	Cementitious Content, lb/yd^3	RH, %	Total Stress Adjustment Factor	k-value (loading), psi	k-value (curling), psi	Age, yrs	PO/mile	Age, yrs	Cumulative ESALs
ATREL-1	0.15	3.54E-06	Limestone	745	6,890,000	5,680	522	780.0E-6	605	85	1	100	100	30	50	30	511,000,000
ATREL-2	0.15	3.54E-06	Limestone	745	6,890,000	5,680	522	780.0E-6	605	85	1	100	100	30	50	30	230,000,000
ATREL-3	0.15	3.54E-06	Limestone	745	6,890,000	5,680	522	780.0E-6	605	85	1	100	100	30	50	30	548,000,000
ATREL-4	0.15	3.54E-06	Limestone	745	6,890,000	5,680	522	780.0E-6	605	85	1	100	100	30	50	30	764,000,000

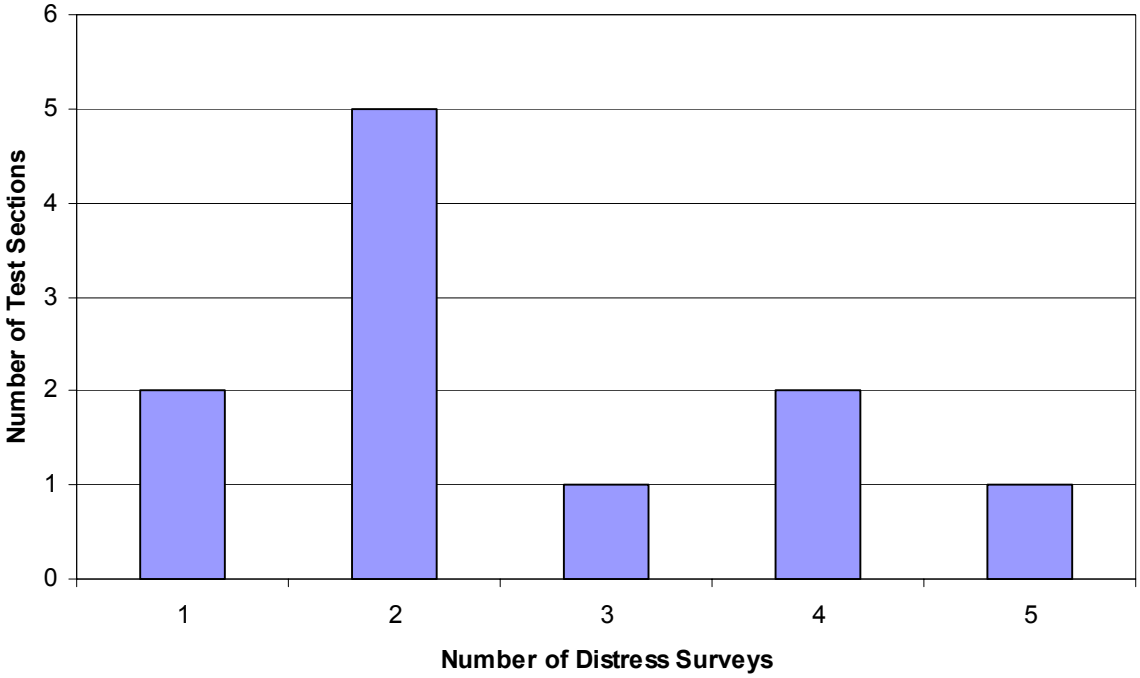

Figure D.1. Distribution of I-80 and I-94 (Edens Expressway) CRCP test sections by number of distress surveys.

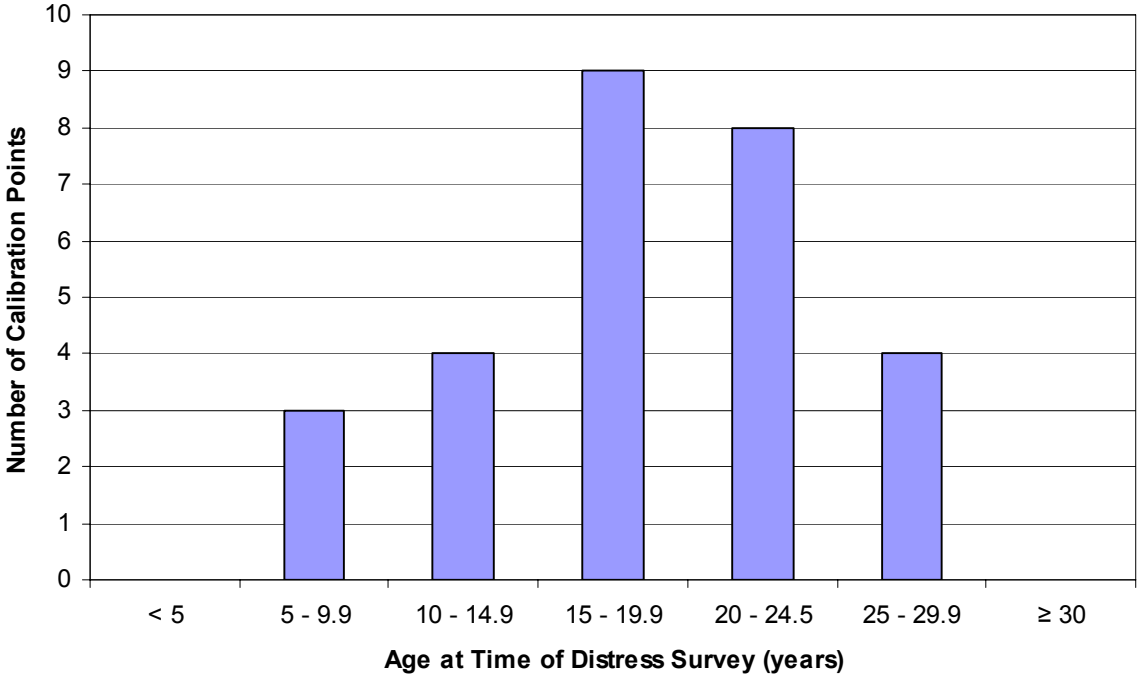

Figure D.2. Distribution of I-80 and I-94 (Edens Expressway) CRCP calibration points by age at time of distress surveys.

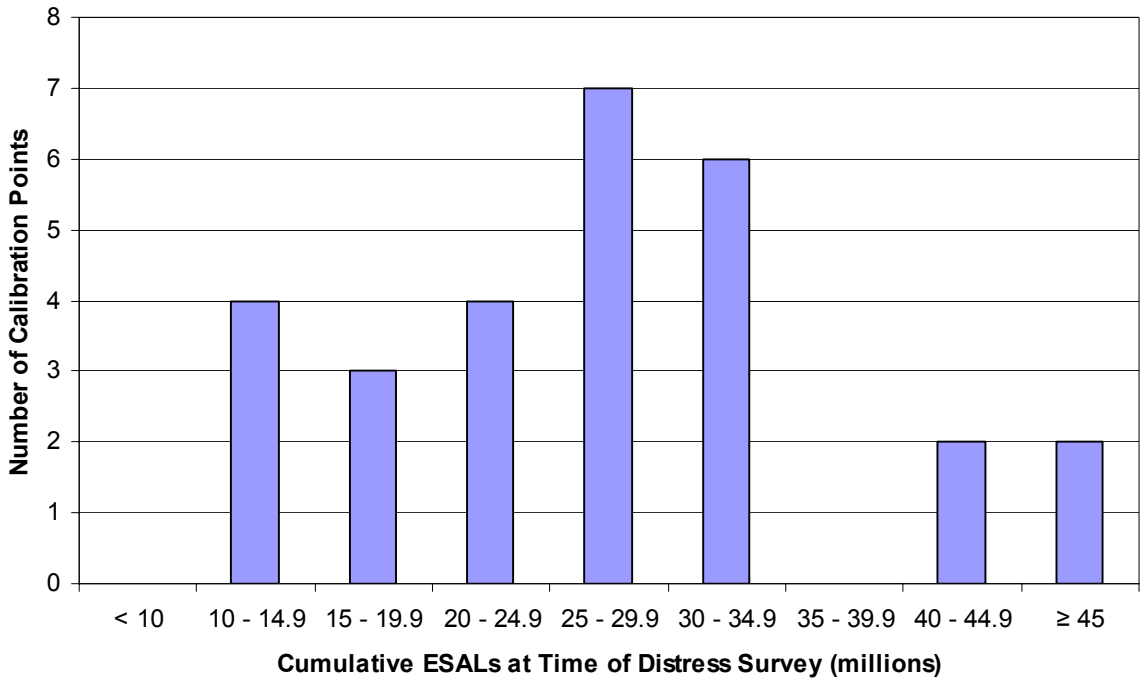

Figure D.3. Distribution of I-80 and I-94 (Edens Expressway) CRCP calibration points by cumulative ESALs at time of distress surveys.


Illinois Department
of Transportation


ILLINOIS
UNIVERSITY OF ILLINOIS AT URBANA-CHAMPAIGN